



Identification and characterisation of
novel chemical scaffolds active against
Mycobacterium tuberculosis

By

Ramon Soto

A thesis submitted to the University of Birmingham

for the degree of

DOCTOR OF PHILOSOPHY

Institute of Microbiology and Infection, School of Biosciences, College of Life and
Environmental Sciences, University of Birmingham

March 2018

UNIVERSITY OF
BIRMINGHAM

University of Birmingham Research Archive

e-theses repository

This unpublished thesis/dissertation is copyright of the author and/or third parties. The intellectual property rights of the author or third parties in respect of this work are as defined by The Copyright Designs and Patents Act 1988 or as modified by any successor legislation.

Any use made of information contained in this thesis/dissertation must be in accordance with that legislation and must be properly acknowledged. Further distribution or reproduction in any format is prohibited without the permission of the copyright holder.

Declaration

The work presented in this thesis was carried out in the School of Biosciences at the University of Birmingham, U.K., B15 2TT and in GlaxoSmithKline, Tres Cantos, Spain, 28662 during the period August 2014 to August 2017. The work in this thesis is original, except where acknowledged by reference.

No part of the work is being, or has been, submitted for a degree, diploma or any other qualification at any other University.

Acknowledgements

I would like to thank all those people that have made this dream possible. First of all, I would like to thank my supervisors Professor Gurdyal S. Besra and Dr. Luke J. Alderwick for their mentoring and scientific support throughout these three years. I would like to thank them directly for having shared their passion for science and allowing me to think critically; skills that I want to highlight as the most important learning experience in my PhD. I would also like to express my gratitude to GSK for allowing me to spend a very fruitful stay and for kindly providing me with the necessary resources and expertise to succeed in my PhD. Special thanks to Usha Veeraghavan and Beatriz Rodriguez and their mentoring in biochemistry, protein purification and high-throughput screening techniques that I have passionately learned and mastered over this period. Among all those people that I have met in GSK I would like to extend my gratitude to Alfonso Mendoza and Ruben Gonzalez for listening and helping me when necessary and to the malaria guys (Lydia, Sara, etc.) for making me feel welcome. A special mention to Cristian Varela not only for his constant advice in the lab with patience and tolerance, but also for becoming such a good friend.

To my family, thanks for all these years of support. However, I would like to dedicate this thesis to Mariela, a person whom I admire and a far better individual than I am.

Abstract

Mycobacterium tuberculosis (*M.tb*), the causative agent of tuberculosis (TB), is the leading cause of death amongst bacterial infections worldwide, with drug resistance strains potentially killing more than 10 million people by 2050. TB infection is associated with poverty and poor healthcare access in low-income countries; note therefore that drug development can only contribute to its final eradication only if access to medicines is improved. The identification of the mechanism of action of hit and lead molecules, *in vivo* efficacy and toxicity issues are the biggest bottlenecks observed in drug discovery. Therefore, the validation of new pathways targeted by novel chemical entities is essential to ensure success in the early stages of drug discovery. In this context, the aspartyl-tRNA synthetase of *M.tb* (Mt-AspS) represents an attractive target since very few approved inhibitors target aminoacyl-tRNA synthesis, decreasing the likelihood of drug resistance. We have identified a number of inhibitors in a phenotypic screen that have been further validated in several biochemical assays and investigated the chemical space around these molecules through a structure activity relationship (SAR) map. Moreover, we have explored the *Mb3185c* gene as a potential resistance mechanism against antitubercular compounds. The results of my thesis will set out future guidelines for the discovery of novel protein synthesis inhibitors against the other eighteen tRNA-synthetases of the *M.tb* proteome.

Table of Contents

List of Figures	9
List of Abbreviations	13
1. Chapter I. Introduction	17
1.1 Immunopathogenesis of <i>Mycobacterium tuberculosis</i>	18
1.2 Epidemiology and socioeconomic factors for TB drug discovery	24
1.3 Detection methods of TB infection: current systems and future prospects.....	28
1.3.1 Sputum smear microscopy (SMM)	29
1.3.2 Culture	30
1.3.3 Tuberculin skin test (TST)	30
1.3.4 Chest X-ray	31
1.3.5 Nucleic acid amplification test (NAAT)	31
1.3.6 Antibody-based diagnostic assay	32
1.3.7 IFN- γ -release assays (IGRA)	32
1.3.8 Summary and future prospects	33
1.4 The threat of drug resistance	33
1.4.1 Molecular mechanisms of drug resistance	36
1.4.2 Spread of drug resistant strains	41
1.5. TB drug discovery	42
1.5.1 Introduction	42
1.5.2 <i>De novo</i> drug discovery approaches	43
1.5.3 Drug repurposing.....	46
1.5.4 Target de-convolution strategies.....	47
1.5.5 Novel emerging drug targets in the drug discovery pipeline	52
Aims and Objectives	56
2. Chapter II. Identification and characterisation of new chemical scaffolds targeting Mt-AspS	57
2.1 Introduction	58
2.1.1 Role of aminoacyl tRNA synthetases in protein biosynthesis	58
2.1.2 Aminoacyl-tRNA synthetases as potential targets for antibiotic development.....	62
2.1.3 <i>M.tb</i> aspartyl-tRNA synthetase as potential target for the development of small molecule inhibitors	65

2.2 Results	69
2.2.1 <i>M.tb</i> AspS protein purification	69
2.2.2 Enzyme activity confirmation by a tRNA-independent biochemical assay	71
2.2.3 Identification of novel <i>M.tb</i> AspS inhibitors by a target-based tRNA-independent biochemical assay	72
2.2.4 Counter-screening assay against an HK/GLC6PDH coupled reaction	75
2.2.5 Mechanistic characterisation of PWS/700/1, ST/476208 and ST/476208, the three screening hits identified from the 177 TB set	76
2.2.6 <i>In vitro</i> profiling (SAR) of a series of GSK3448232A analogues	81
2.2.7 Mechanistic studies of the hit compound against <i>M.tb</i> AspS	86
2.2.8 Purification of recombinant <i>Homo sapiens</i> mitochondrial Hs-AspS	90
2.2.9 Biochemical characterisation of the human mitochondrial Hs-AspS in the tRNA-independent biochemical assay	91
2.2.10 Compound selectivity assessment against the human mitochondrial aspartyl-tRNA synthetase	95
2.2.11 Identification of novel antitubercular hits targeting Mt-AspS through a whole-cell target-based high-throughput screening assay	97
2.2.12 Development of a tRNA-based biochemical assay	100
2.2.13 Biochemical validation of screening hits in a tRNA-based biochemical assay	104
2.2.14 Mechanistic studies of validated hits against Mt-AspS	107
2.2.15 Medium-throughput target-based screening assay of a series of analogues of whole-cell validated hits against Mt-AspS	111
2.3 Discussion	113
3. Chapter III. Identification of new targets and resistance mechanisms in <i>M.tb</i>	118
3.1 Introduction	119
3.2 Results	120
3.2.1 Generation of <i>M. bovis</i> BCG resistant isolates against GSK756354A and confirmation of their resistance phenotype	120
3.2.2 Cross-resistance of GSK756354A-resistant strains to GSK756354A analogues	122
3.2.3 Whole-genome sequencing studies of spontaneous resistant isolates against GSK756354A	123
3.2.4 Mechanism of action studies: effect of Mb3185c overexpression on resistance/sensitivity against GSK756354A	124
3.2.5 Overexpression studies with pMV261-Mb3185c	128
3.3 Discussion	130
4. Chapter IV. Conclusions	133
5. Chapter V. Materials and Methods	143
5.1 General chemical and media preparation	144
5.1.1 Luria-Bertani (LB) Broth	144
5.1.2 Luria-Bertani (LB) Agar	144
5.2 Transformation Buffers	144

5.3 Lysis Buffer	144
5.4 Dialysis Buffer	144
5.5 Mt-AspS coupled Reaction Buffer.....	144
5.6 tRNA-based Mt-AspS Reaction Buffer	144
5.7 HK/GLC6PDH Reaction Buffer	145
5.8 Human mitochondrial AspS Reaction Buffer	145
5.9 Bacterial Strains and Conditions.....	145
5.10 Preparation of competent cells.....	145
5.10.1 <i>E. coli</i> chemically competent cells.....	145
5.10.2 <i>M. bovis</i> BCG electrocompetent cells.....	145
5.11 Transformation of bacterial cells	146
5.11.1 Transformation of <i>E. coli</i> cells by heat shock method.....	146
5.11.2 Transformation of <i>M. bovis</i> BCG cells by electroporation.....	146
5.12 DNA work.....	147
5.12.1 Polymerase Chain Reaction (PCR) amplification of Mb3185c	147
5.12.2 Agarose gel DNA electrophoresis.....	147
5.12.3 DNA extraction from agarose gel	147
5.12.4 PCR clean up.....	148
5.12.5 Genomic DNA extraction.....	149
5.12.6 Plasmid DNA extraction	149
5.13 Mt-AspS recombinant protein purification.....	150
5.14 SDS-PAGE	151
5.15 Mt-AspS-based screening of the GSK TB set compound library	151
5.16 HK/GLC6PDH-based TB set screening.....	152
5.17 Whole-cell compound potency determination (MIC)	153
5.17.1 Solid MIC determination	153
5.17.2 Liquid MIC determination	153
5.18 Compound profiling studies.....	154
5.18.1 Time-course dependence	154
5.18.2 Substrate competition studies.....	154
5.18.3 DTT dependence.....	155

5.19 Biochemical characterisation of human mitochondrial Hs-AspS & assay development for selectivity assessment	155
5.19.1 Recombinant protein purification	155
5.19.2 Substrate dependence of human mitochondrial AspS.....	156
5.19.3 Compound selectivity assessment.....	156
5.20 Whole-cell target-based high throughput screening assay	157
5.21 tRNA-based biochemical assay.....	158
5.21.1 Filtration assay.....	158
5.21.2 Scintillation Proximity Assay (SPA)	160
5.22 Medium-throughput screening assay of a series of analogues in a tRNA-independent biochemical assay.....	160
5.23 Generation of spontaneous resistant isolates against GSK756354A	161
5.23.1 Confirmation of the resistant phenotype.....	161
5.23.2 Genome extraction from resistant strains	162
5.23.3 Genomic DNA whole-genome sequencing of <i>M. bovis</i> BCG resistant isolates.....	162
6. Chapter VI. References	164
7. Supplementary information	185

List of Figures

Figure 1. Host-pathogen interactions during <i>M.tb</i> infection by human alveolar macrophages	19
Figure 2. Comparison of granulomas of immunocompetent and immunosuppressed infected individuals	21
Figure 3. Worldwide TB incidence rates in 2014	27
Figure 4. Evolution in TB prevalence from 1990 to 2015 in different world regions	28
Figure 5. Ziehl-Neelsen acid-fast staining of <i>M.tb</i> clinical specimens from a sputum sample	29
Figure 6. Chest X-ray scan of a TB patient	31
Figure 7. Different ELISAs types for the detection of TB antigens	32
Figure 8. Antibacterial discovery timeline and first-ever reported cases of clinical resistance	35
Figure 9. Catalytic mechanism of class A β-lactamases	39
Figure 10. Crystal structure of MtrD in the open state, a multidrug efflux pump in <i>Neisseria gonorrhoeae</i>	41
Figure 11. The two historical drug discovery strategies in TB: target-to-drug versus drug-to-target approach	45
Figure 12. Affinity-based methods for the identification of compound targets	49
Figure 13. Schematic representation of the ABP structure	50
Figure 14. BTZ043 and DNB1 structures, two main chemical scaffolds in development against <i>M.tb</i> DprE1	53
Figure 15. Several chemical scaffolds in development mapping to MmpL3 in WGS of <i>in vitro</i> <i>M.tb</i> resistant isolates	54
Figure 16. New chemical scaffolds targeting QcrB	55
Figure 17. Catalytic mechanism of aminoacyl-tRNA synthetases	59

Figure 18. Active site topologies in class I (a) e.g. GlnRS and II (b) tRNA synthetases.....	60
Table 1. Eighteen aminoacyl-tRNA synthetases (aaRS) of <i>M.tb</i> and their corresponding gene names.....	61
Table 2. Reported inhibitors against tRNA synthetases.....	64
Figure 19. <i>M. smegmatis</i> AspS crystal structure.....	66
Figure 20. Structure of the rhodanine parent compound.....	66
Figure 21. Effects of <i>M. bovis</i> Mt-AspS overexpression on cell growth on 7H11 agar plates.....	67
Figure 22. Dose-response <i>in vitro</i> activity curve of the effect of a rhodanine scaffold against Mt-AspS in a tRNA-independent coupled reaction.....	68
Figure 23. Schematic representation of a tRNA-independent coupled reaction.....	68
Figure 24. Identification of relevant fractions containing Mt-AspS using Bio-Rad pre-cast SDS (10%) Tris-Glycine PAGE gels.....	70
Figure 25. Dose-response <i>in vitro</i> Mt-AspS activity at several protein amounts in order to establish assay quality and sensitivity.....	72
Figure 26. Structure and batch identification codes of the newly identified anti-mycobacterial compounds that target the essential aspartyl-tRNA synthetase Mt-AspS.....	73
Figure 27. Dose-response <i>in vitro</i> activity curves of the effect of several anti-mycobacterial compounds against Mt-AspS in the tRNA-independent	74
Figure 28. Effect of PWS/700/1 on HK and GLC6PDH activity at 100, 300 and 500 μ M	75
Figure 29. Reversible, non-competitive mode of inhibition of several Mt-AspS screening hits...	77
Figure 30. Time-dependence assessment of Mt-AspS inhibition in the presence of ST/476208..	78
Figure 31. Dose-response <i>in vitro</i> assay of ST/476208 at 0.5 and 5 μ M Mt-AspS for promiscuity assessment.....	79
Figure 32. <i>In vitro</i> dose-response activity curves of ST/476208 in the presence and absence of 1mM DTT	80
Table 3. Summary of the SAR map of the parent compound GSK3448232A.....	82
Figure 33. Whole-cell <i>in vitro</i> potency assays of two analogues of the parent compound GSK3448232A against a <i>M. bovis</i> BCG pMV261-AspS overexpressor strain and an empty pMV261-containing <i>M. bovis</i> BCG strain	83

Figure 34. Promiscuous activity of a series of analogues of the parent compound GSK3448232A against the HK/GLCPDH coupled reaction at two different concentrations (100 and 300 μ M)....	85
Figure 35. Time course assessment of GSK3449228A.....	88
Figure 36. Reversible non-competitive mode of inhibition of GSK3449228A as shown by a decrease in V_{max}	89
Figure 37. Bio-Rad pre-cast SDS Tris-glycine (10%) PAGE gel showing the approximate 67 KDa band of the polyhistidine-tagged human mitochondrial Hs-AspS.....	91
Figure 38. Effect of the pH on the activity of the human mitochondrial Hs-AspS.....	92
Figure 39. Substrate dependence of human mitochondrial Hs-AspS activity.....	93
Table 4. Apparent K_M and R^2 values for the three substrates used by the human mitochondrial Hs-AspS enzyme.....	94
Table 5. Inhibitory values of parent compound analogues and screening hits against the human mitochondrial Hs-AspS at three increasing concentrations (100, 300 and 500 μ M)	96
Table 6. Whole-cell target engagement of several GSK whole-cell screening hits.....	99
Figure 40. Whole-cell target engagement of two chemical entities against a <i>M. bovis</i> BCG pMV261-AspS overexpressor strain (solid squares) and an empty pMV261-containing <i>M. bovis</i> BCG strain (solid circles)	100
Figure 41. Time-course of the aminoacylation activity monitored using the standard TCA precipitation method at several AspS concentrations: 0.2 (triangles), 0.5 (circles) and 1 μ M (inverted triangles)	102
Figure 42. Substrate dependence of Mt-AspS activity in a tRNA-based assay.....	103
Table 7. Summary of the reported apparent K_M values for Mt-AspS determined under Michaelis-Menten conditions.....	104
Figure 43. Dose-response <i>in vitro</i> activity curves of the effect of several screening hits in the amino acylation reaction.....	105
Table 8. IC50 values of the three screening hits validated against Mt-AspS in the aminoacylation reaction.....	106
Figure 44. Structure and GSK identification codes of the newly identified anti-mycobacterial chemical families that target the essential aspartyl-tRNA synthetase Mt-AspS	106
Figure 45. Reversible, non-competitive mode of inhibition of two chemical entities targeting Mt-AspRS.....	108
Figure 46. Time-dependence assessment of GSK445893A and GSK2198097C inhibition	109

Figure 47. <i>In vitro</i> dose-response activity curves of GSK445893A in the presence and absence of 1 mM DTT	110
Figure 48. <i>In vitro</i> potency of newly identified antitubercular analogues of GSK1568097A targeting Mt-AspS.....	112
Figure 49. Structures of several antitubercular analogues of GSK1568097A targeting Mt-AspS	112
Figure 50. Whole-cell <i>in vitro</i> potency assessment of GSK756354A against several <i>M. bovis</i> strains	121
Figure 51. Whole-cell <i>in vitro</i> dose-response activity curves of GSK756354A analogues against several <i>M. bovis</i> strains.....	122
Table 9. Structure-activity relationship map of several GSK756354A analogues	123
Figure 52. Agarose gel (1%) showing the amplified <i>Mb3185c</i> gene product at 1.15 Kb	125
Figure 53. Agarose (1%) gel showing the digested products of the BamH1 and HindIII reaction	126
Figure 54. Restriction analysis of recombinant <i>E. coli</i> DH5α colonies transformed with pMV261-<i>Mb3185c</i>.....	128
Figure 55. Dose-response <i>in vitro</i> activity curves of the effect of GSK756354A on <i>M. bovis</i> BCG pMV261-<i>Mb3185c</i> (solid squares) and <i>M. bovis</i> BCG pMV261 strains (solid circles)	129

List of Abbreviations

%	Percentage
aaRS	Aminoacyl-tRNA synthetase
aatRNA	Aminoacyl-tRNA
ABP	Activity-based probes
ADPCP	β - γ -methyladenosinetriphosphate
AM	Alveolar Macrophages
AMO	Aspartyladenylate intermediate
ATP	Adenosin triphosphate
ATP	Adenosintriphosphate
AU1235	Adamantyl urea
BCG	Bacille Calmette Guerin
BLAST	Basic Local Alignment Search Tool
Bp	Base pair
BTZ043	Benzothiazinone 043
CHAPS	3-[(3-cholamidopropyl)dimethylammonio]-1-propanesulfonate
CLND	Chemiluminiscent Nitrogen Detection
DAPI	4',6-diamidino-2-phenylindole
DARTs	Drug-Affinity Responsive Target Stability
DC	Dendritic Cells
DMSO	Dimethylsulfoxide
DNA	Deoxyribonucleic acid
DNB1	Dinitrobenzamide 1
DTT	Dithiotreitol

E.g	Exempli gratia
ELISA	Enzyme-Linked Immunosorbent Assay
ESBLs	Extended-Spectrum Beta-Lactamases
FI	Fluorescence intensity
Fig.	Figure
G6P	Glucose-6-phosphate
GFP	Green Fluorescence Protein
GLC6PDH	Glucose-6-phosphate dehydrogenase
GSK	GlaxoSmithKline
HDT	Host Directed Therapies
HEPES	(4-(2-hydroxyethyl)-1-piperazineethanesulfonic acid
HIV	Human Immunodeficiency Virus
HK	Hexokinase
Hs-Asps	Human mitochondrial aspartyl-tRNA synthetase
HTS	HighThroughputScreening
IC50	Inhibitory Concentration 50
IFN α	Interferon-alpha
IFN γ	Interferon-gamma
IGRA	Interferon-gamma Release Assays
IMAC	Immobilized Metal Ion Affinity Chromatography
INH	Isoniazid
IP	Imidazopyridine
IPTG	Isopropyl β -D-1-thiogalactopyranoside
KDa	Kilodaltons
K _M	Michaelis-Menten affinity constant

KMSKS	Catalytic triad
L-Asp	L-aspartic acid
LM	Lipomannan
logP	Partition coefficient
LTBI	Latent Tuberculosis Infection
<i>M.tb</i>	<i>Mycobacterium tuberculosis</i>
mCi	Millicuries
MDR	Multidrug-resistant
MHC	Major Histocompatibility Complex
MIC	Minimum Inhibitory Concentration
mL	Mililiters
mM	Milimolar
mRNA	Messenger ribonucleicacid
MRSA	Methicillin-resistant <i>Staphylococcus aureus</i>
Mt-AspS	<i>M.tb</i> aspartyl-tRNA synthetase
NAAT	Nucleic Acid Amplification Test
NaCl	Sodium chloride
NADPH	Nucleotideadenindiphosphate
nm	Nanometers
ORF	Open Reading Frame
PBMC	Peripheral Blood Monocuclear Cells
PK/PD	Pharmacokinetics/Pharmacodynamics
PPi	Pyrophosphate
PRR	Pattern Recognition Receptor
PZA	Pyrazinamide

REMA	Resazurin Emission Microplate Assay
RM	Resistant Mutant
RNS	Reactive Nitrogen Species
SAR	Structure-Activity Relationship
SD	Standard deviation
SDS-PAGE	Sodium Dodecyl Sulfate Polyacrylamide Gel Electrophoresis
SPR	Surface Plasmon Resonance
SSM	Sputum Smear Microscopy
TB	Tuberculosis
TCA	Trichloroacetic acid
TDR	Total drug-resistant
TLR	Toll-like receptor
TMM	Trehalose monomycolate
TNF α	Tumor necrosis factor alpha
TRIS	Tris(hydroxymethyl)aminomethane
tRNA	Transfer ribonucleic acid
TST	Tuberculin Skin Test
V _{max}	Maximum velocity
WGS	Whole-genome sequencing
WHO	World Health Organisation
WT	Wilde-type
WW2	World War II
XDR	Extensively drug-resistant
μL , μM	Microliters, micromolar

CHAPTER I

INTRODUCTION

1. Introduction

1.1 Immunopathogenesis of *Mycobacterium tuberculosis*

Mycobacterium tuberculosis (*M.tb*), the causative agent of tuberculosis (TB), is an aerobic-airborne pathogen. Discovered by Robert Koch in 1882, its pathogenic hallmark is the formation of granulomas within the lungs in which it remains latent (non-pathogenic) for a period of time that can vary from months to even years, depending on strain virulence and immune factors of the infected individual (Corbett et al., 2003). The granuloma represents a convergent point of contradictory theories that try to explain its development, from a host perspective the granuloma represents a confinement of the bacteria that prevents spreading within the lungs, whilst conferring a protective environment for the pathogen from host immune responses, while remaining virulent (Silva Miranda et al., 2012). Either way, in 5-10% of individuals infected with *M.tb* will break through the granuloma and develop active disease (O'Garra et al., 2013). Amongst the reasons for this event are a number of potential factors, including host genetics and strain virulence, although the exact molecular mechanisms remain unclear. Malnutrition is a socioeconomic factor that has also been linked to the development of active disease: besides the expected impact of malnutrition on immune function (Macallan, 1999), a more recent link between vitamin C deficiency and tuberculosis development has been discovered (Vilcheze et al., 2013).

What are the molecular mechanisms driving granuloma formation that promotes *M.tb* survival within the lungs? We will describe later how different *M.tb* researchers have tried to target these molecular events in order to stop infection. The first step after an infective dose, a 10 bacilli-containing aerosol is inhaled, is the recruitment of alveolar macrophages (AM) and dendritic cells (DC) to the site of infection as a first innate immune response barrier. The Pattern Recognition Receptors (PRRs) are molecules on

the surface of AM and DCs that recognise mycobacterial ligands embedded in the highly complex structure of the cell wall, such as lipoarabinomannan (LAM) and lipomannan (LM). Amongst, the most important PRRs are the Toll-like receptors (TLRs), believed to play an essential role in the phagocytosis of the bacilli. Upon binding with these bacilli membrane-embedded molecules a series of intracellular phosphorylation events mediated by kinases leads to the production and release of pro-inflammatory cytokines such as IFN γ and TNF α , which in turn recruit and activate other macrophages, monocytes and CD4 $^{+}$ lymphocytes to the site of infection (Fig. 1). It is this release of cytokines that is ultimately responsible for the development of the granuloma, a compact and organised structure of layers of CD4 $^{+}$ T cells and macrophages that confine bacilli that could escape intracellular macrophage-mediated molecular events, such as phagolysosome fusion and the production of reactive nitrogen species (RNS).

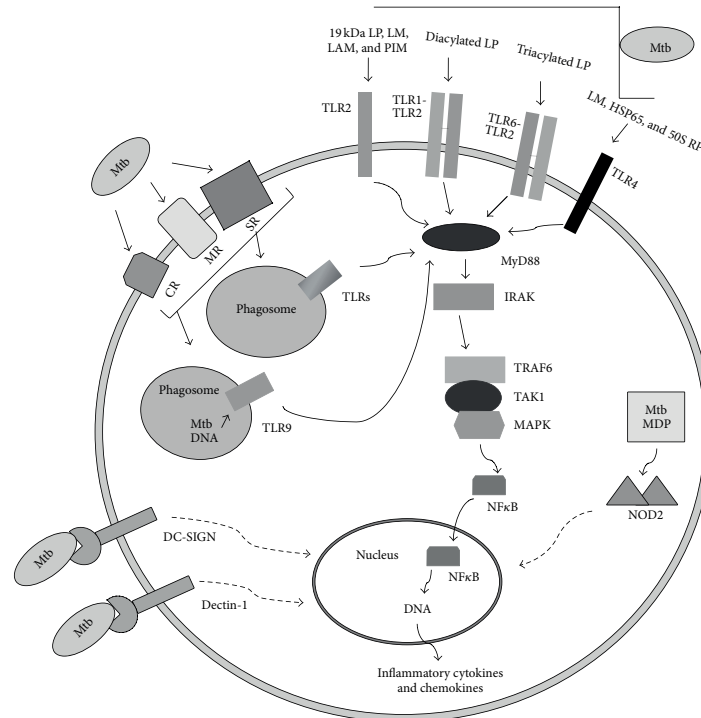


Figure 1. Host-pathogen interactions during *M.tb* infection by human alveolar macrophages. Figure reproduced from (Hossain and Norazmi, 2013) under the Creative Commons attributions licence.

As will be described later, one of the biggest challenges of TB drug discovery is to find drugs compatible with anti-HIV medication. In 2014, deaths from TB infection in Africa followed an alarming trend among HIV-infected individuals, representing an overall 68% rate of the total number of TB deaths in Africa. Avoiding drug-to-drug interactions with anti-HIV retrovirals is therefore essential for the successful treatment outcome in HIV patients.

Why are HIV patients so susceptible to develop active TB? The answer resides in the poor capacity of the immune system of these patients to form a compact granuloma in the lungs. Amongst other HIV-triggered mechanisms (Pawlowski et al., 2012), a depletion of CD4⁺ T-cells (HIV target) would promote the development of thin, easy-to-break granulomas instead of the highly compact ones of immunocompetent individuals (Fig. 2). Bacilli contained in these weak granulomas find it easier to break it open and infect the rest of the lungs, developing active disease faster than non-HIV co-infected patient

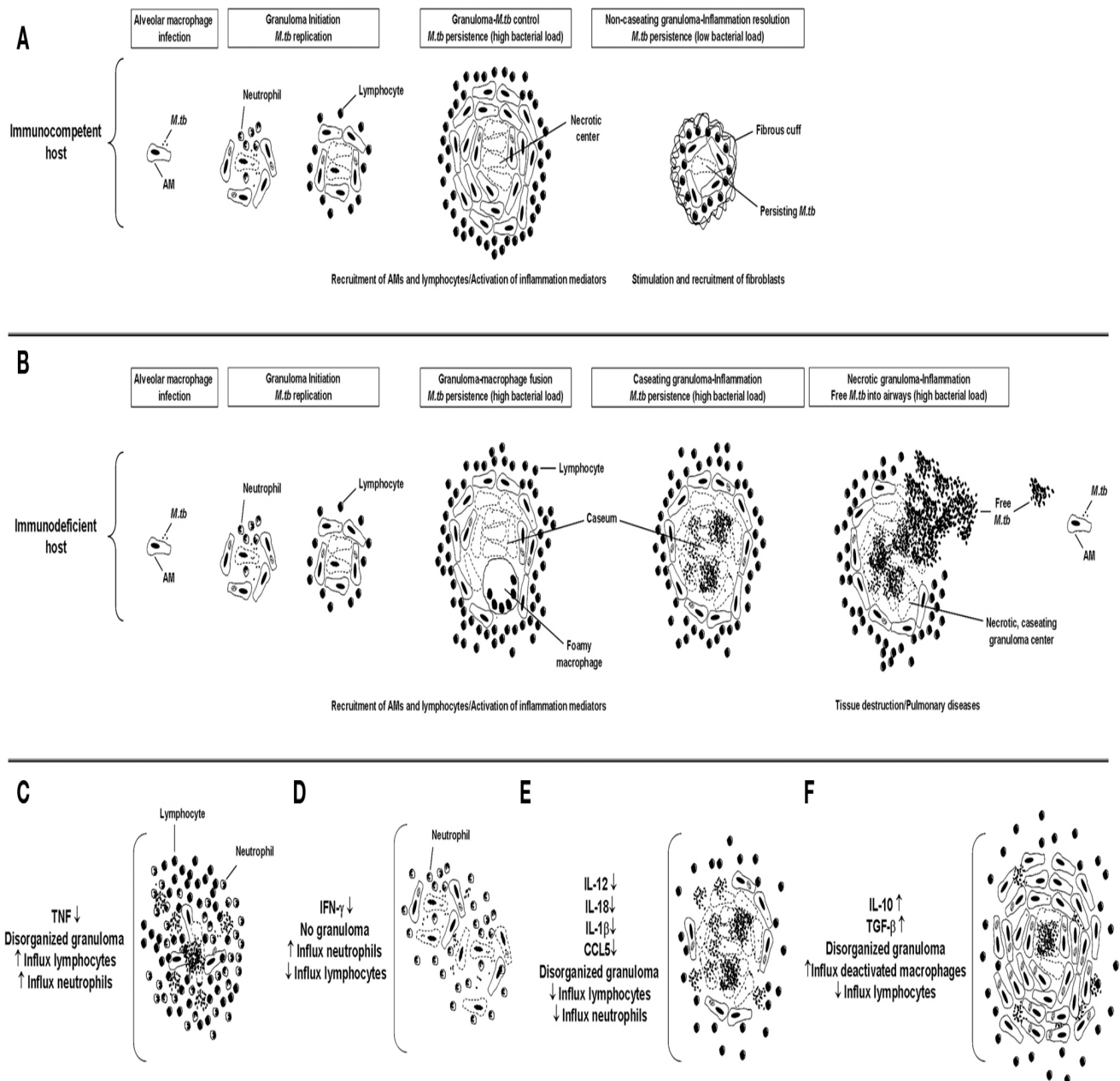


Figure 2. Comparison of granulomas of immunocompetent and immunosuppressed infected individuals. Whilst non-HIV infected patients have small and compact granulomas (A), those of immunosuppressed patients are large and lack the CD4+ T cells layer (B), representing an easy barrier for *M.tb* to break free into the airways. (C-F) Impact of the absence of several cytokines on the structure and appearance of the tubercular granuloma. The importance of IFN-gamma and TNF-alpha for the maintenance of a compact structure and bacilli confinement is shown. Figure obtained from (Sasindran and Torrelles, 2011) under the Creative Commons attribution licence.

It is also of interest to know what are the main factors behind the loss of host immune competency in non-HIV infected TB patients. Even though an effective immune response either leads to the complete elimination or confinement of tubercle bacilli in granulomas, in 5% of cases *M.tb* escapes this confinement, developing active disease and completing the infection cycle. It has been proven from latently infected individuals that bacilli remain alive within the granulomas, therefore managing to survive after the acute phase of infection. The pathogen makes use of several molecular mechanisms, such as blocking the fusion of the phagolysosome (Deretic et al., 2006), diminished macrophage presentation to T-cells by down-regulating MHC class II expression (Harding and Boom, 2010), the secretion of *Mycobacterium* protein tyrosine phosphatase (Zhou et al., 2010) and the protection against oxidative species such as ROS and RNI produced by IFN-gamma activated macrophages (Pieters, 2008), mainly mediated by KatG (Ng et al., 2004). These mechanisms not only prevent bacteria from being destroyed by the macrophage or T-cells, but also promote host cell survival and formation of the granuloma to develop persistent infections. Under these stressful conditions, (hypoxia, nutrient starvation and immune attack) the bacteria down-regulates several signalling pathways, such as DNA replication and mycolic acid biosynthesis to save on energy cost, switching to the low-power mode, allowing survival and persistent infection (Ng et al., 2004).

In this latent state, *M.tb* becomes phenotypically resistant to many antibiotics (e.g. isoniazid) (Karakousis et al., 2008). Under this condition, cell wall biosynthetic and DNA replication enzymes are non-essential, rendering their drug counterparts inactive. In order to gain more understanding on the complex host-pathogen interaction during latent infection more relevant *in vivo* models are needed, since a low oxygen-containing environment cannot mimic the stress conditions under which bacteria remain latent *in vivo*. An important advancement in the study of virulence factors was made possible by

the availability of the *M.tb* genome (Cole et al., 1998) and the development of genetic tools, which allowed the study of how these virulence factors contribute to all kinds of aspects of pathogenesis, from bacterial internalisation to the establishment of latency. For example, studies on KasB led to the discovery of this particular protein was not only involved in mycolic acid biosynthesis, but also played an important role in the pathogenesis of the organism. A $\Delta kasB$ strain was unable to cause infection in a murine animal model of TB-infection up to 600 days, suggesting a likely role in pathogenicity (Bhatt et al., 2007).

In this sense, targeting host-pathogen interactions (also known as Host Directed Therapies, or HDTs) using small molecules represents an alternative strategy for the development of TB inhibitors (Zumla et al., 2015). This approach focuses on either increasing the effectiveness of the host immune response or direct drug therapy against host-pathogen interactions. One of the potential advantages of incorporating HDTs in treatment regimens is that it can reduce the risk of drug-drug interactions with anti-virals in patients co-infected with HIV. Another interesting aspect of exploiting these treatment opportunities is, as expected with any potential new drug, shortening the current treatment duration of 6-9 months with drug-sensitive TB and 18 months of drug-resistant strains. Shortening treatment regimens reduces pill burden, minimising potential side effects derived from the use of other more toxic and less effective drugs.

An example of how targeting host-pathogen interactions can lead to the development of inhibitors of TB infection. (Zhou et al., 2010). *Mycobacterium* protein tyrosin phosphatase B (MptpB), a virulence factor secreted into the cytoplasm of the macrophage when bacilli are taken up, blocks the immune response by reducing IL-6 production in IFN γ -activated macrophages, as well as promoting their survival by down-regulating caspase 3, essential for the successful development of the granuloma and establishment of latency. An MptpB

inhibitor was able to reverse the blocking of the immune system by MtpB, preventing mycobacterial growth in macrophages (Zhou et al., 2010). Another strategy yet to be exploited is the development of compounds that enhance the effectiveness of the immune system against *M.tb* infection. In this sense, a high content screening assay using 4'6-diamidino-2-phenylindole (DAPI) and green fluorescent protein (GFP) as reporter systems showed *in vitro* activity of several non-TB related inhibitors (fluoxetine and gefitinib) due to an increased production of TNF α and increased autophagy (Stanley et al., 2014).

All in all, much remains to be discovered about the molecular mechanisms involved in host-pathogen interactions that drive evasion of the immune response, formation of the granuloma and reactivation. It has been shown that bacterial populations are not uniform, but rather heterogenic, in response to stressful conditions, such as antimicrobial therapy or host niche (Manina et al., 2015). It is therefore of global interest to discover the underlying mechanisms for this phenotypic heterogeneity which allows for a better adaptation of the population in the host.

1.2 Epidemiology and socioeconomic factors for TB drug discovery

Despite the global threat of antibiotic resistance, bacterial infections don't represent the main focus of research in the portfolio of pharmaceutical companies. With global recession and debt crisis hitting hard on governments budgets, together with an ageing population and consequent increased healthcare costs, government funding for not-for-profit research topics is thought to shrink in the next decade. Antimicrobials are not that profitable either for pharmaceutical companies due to: 1) the nature of the disease: if the infection disappears, so the need for antibiotics does, and 2) the regulatory landscape. Cuts in drug pricing due to increased healthcare costs potentially discourages investors

worldwide to invest in new antibacterial treatments. In this infertile environment there is a way forward. Firstly, in order to encourage private investments economic incentives need to be granted, either by patent extension, drug priority review by regulatory agencies, or easier access to funding from not-for-profit institutions or governments. Secondly, in order to speed up the drug discovery pipeline, close collaboration between pharmaceutical companies and Universities worldwide is needed, outsourcing tasks where appropriate. In this sense, not-for-profit organisations, such as the Stop TB partnership (Stoptb.org, 2017) or the More Medicines For TB consortium (Mm4tb.org, 2017) have taken over in order to provide new drugs and diagnostic tools to help improve healthcare access in under developed countries.

Despite all this joined-up effort, antibacterial research is not that attractive when compared to research in therapies for chronic diseases, such as diabetes, cancer or Alzheimers. Just as an example to illustrate what costumers need worldwide, here there is the list of the top-selling drugs in 2015 (List taken from Blake, et al 2018).

- 1) Humira (adalimumab), \$8.2 billion
- 2) Abilify (aripiprazole), \$7.9 billion
- 3) Sovaldi (sofosbuvir), \$6.9 billion
- 4) Crestor (rosuvastatin), \$5.9 billion
- 5) Enbrel (etanercept), \$5.9 billion
- 6) Harvoni (ledipasvir and sofosbuvir), \$5.3 billion
- 7) Nexium (esomeprazole), \$5.3 billion
- 8) Advair Diskus (fluticasone), \$4.7 billion
- 9) Lantus Solostar (insulin glargine), \$4.7 billion
- 10) Remicade (infliximab), \$4.6 billion

Since, the first anti-infective on the list is Sofosbuvir for the treatment of chronic Hepatitis C, it becomes evident that antimicrobials are not in demand in societies in developed countries. Since antimicrobials are only high on demand in under-developed countries these don't represent big markets for industry. The only way drugs can be accessible to these patients is by cutting drug pricing, which of course is not a big incentive for pharmaceutical companies. Here is where the above-mentioned economic incentives can boost research on antimicrobials and eventually bring new drugs onto the market.

In the case of TB, as mentioned earlier, despite the punctual cases of multidrug-resistant strains in developed countries, it still remains a disease associated with poverty and poor healthcare access. It is remarkable that countries ranking 7th and 9th on the top ten list of most powerful economies worldwide (Brazil and India, respectively) have 110,000 and 2,500,000 TB cases in 2014, respectively (<http://www.tbfacts.org>). Poverty in this case, unlike in African countries, is not a generalised problem among Society. Instead, it is more likely to be related to a massive income gap between social classes, poor social welfare and political corruption.

According to the WHO in its annual report, the global targets for TB burden reduction and eventual eradication have not been met yet (WHO, 2015). Despite an important advance in the reduction of TB deaths (47%) and incidence and prevalence rates (Figs. 3 and 4) in the 2000-2014 period, with new cases of active TB lowering by a 1.4% rate annually, there are still 1.1 million deaths. Amongst the 9.6 million new TB cases, MDR-TB accounted for 480,000 cases, with a cure rate of 50% globally, still far from the 75% cure rate expected by the WHO in 2015. Amongst the cases for MDR-TB, 9.7% were reported to be XDR-TB, for which poor treatment outcomes have been reported (Pietersen et al., 2014). Moreover, among 1.1 million TB deaths, 360,000 were HIV positive, confirming HIV co-infection as an important risk factor to develop active TB. More importantly, there

is still a 1.3 USD billion funding gap that needs to be filled to meet global targets. There are new treatment regimens being tested in clinical trials and drugs in the pipeline that together with inexpensive, quick *in situ* diagnostic tools will help manage TB patients more effectively and reduce TB prevalence worldwide. There is still a long way ahead, since developing new antibiotics is as important as adequately administering them. Patient adherence to treatment is essential to prevent sub-optimal drug concentrations that are responsible for drug resistance (Andersson and Hughes, 2014). Also important is the need to improve healthcare access to people living in poor economic areas, as well as developing a strong healthcare system that can provide patients with novel diagnostic and treatment tools.

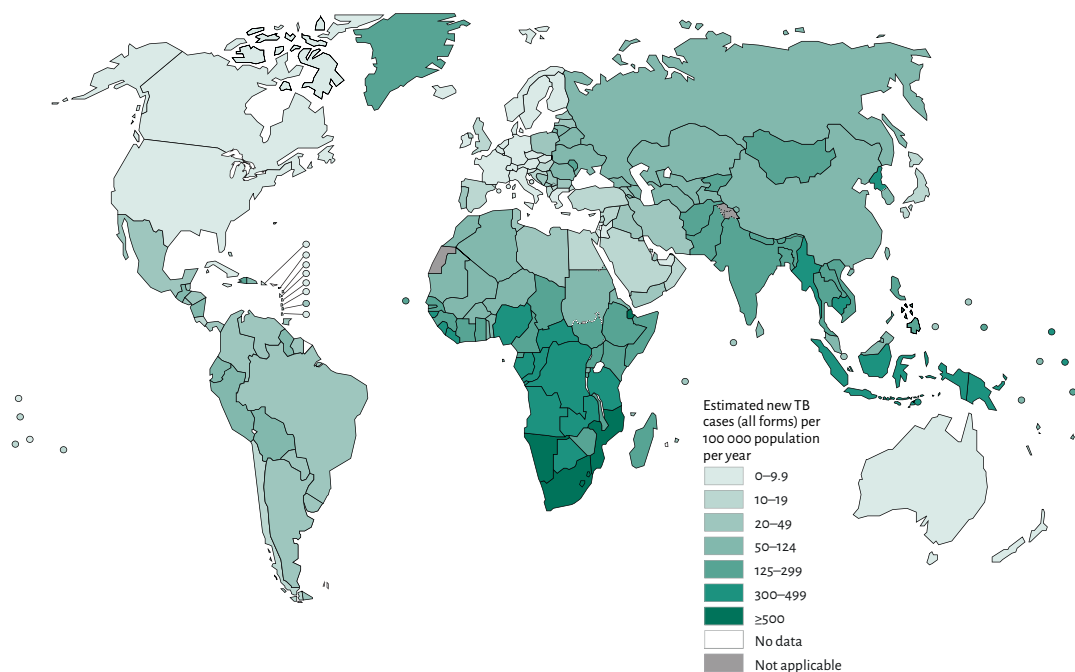


Figure 3. Worldwide TB incidence rates in 2014. Figure taken from the WHO report on tuberculosis (WHO, 2015).

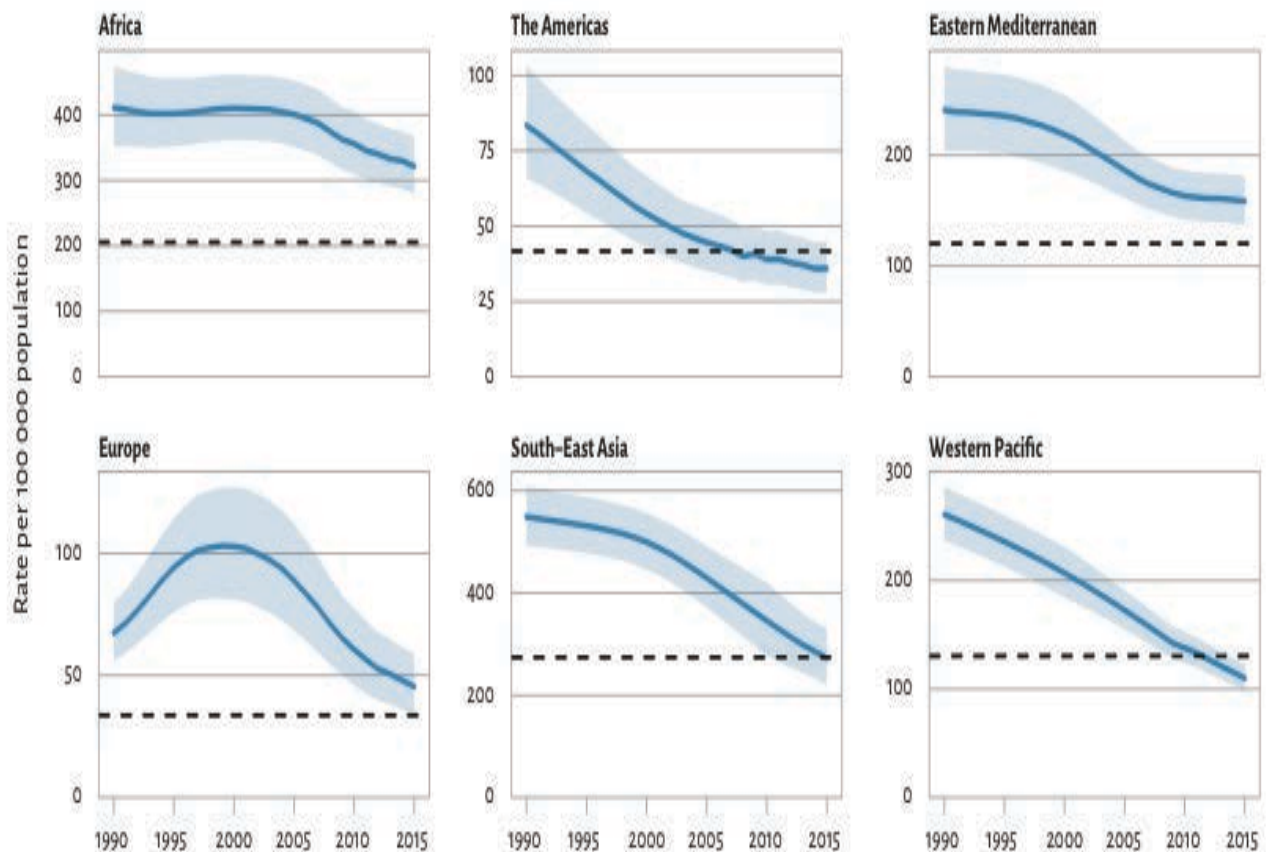


Figure 4. Evolution in TB prevalence from 1990 to 2015 in different world regions. It is evident the success in the implementation of TB containment strategies as shown by the decrease in prevalence worldwide. Figure taken from the WHO report on tuberculosis (WHO, 2015).

1.3 Detection methods of TB infection: current systems and future prospects

Detecting TB infection is essential in order to provide quick and effective treatment to cure patients and prevent spreading of the disease. We describe herein the most common diagnostic methods with their respective ups and downsides and outline what still

remains to be done to develop a quick, cost-effective and reliable tool for the early detection and diagnosis of *M.tb*.

1.3.1 Sputum smear microscopy (SMM)

Acid-fast staining is a rapid and inexpensive method for the detection of bacilli in the sputum of TB patients. The clinical sample is treated with a dye that stains the *M.tb* cell wall, even after an ethanol-based decolourisation step using hydrochloric acid. Bacilli will appear red when observed under a bright field microscope (Fig. 5), while the rest of cells or debris appear in blue when the counter-stain is added. Despite its relative specificity and inexpensiveness, this technique has a high false-negative rate, since at least 10,000 bacilli/mL of sputum are needed for an accurate detection (Dorman, 2010). It can also stain other microorganisms that are not mycobacteria, therefore also affecting its false-positive rate.

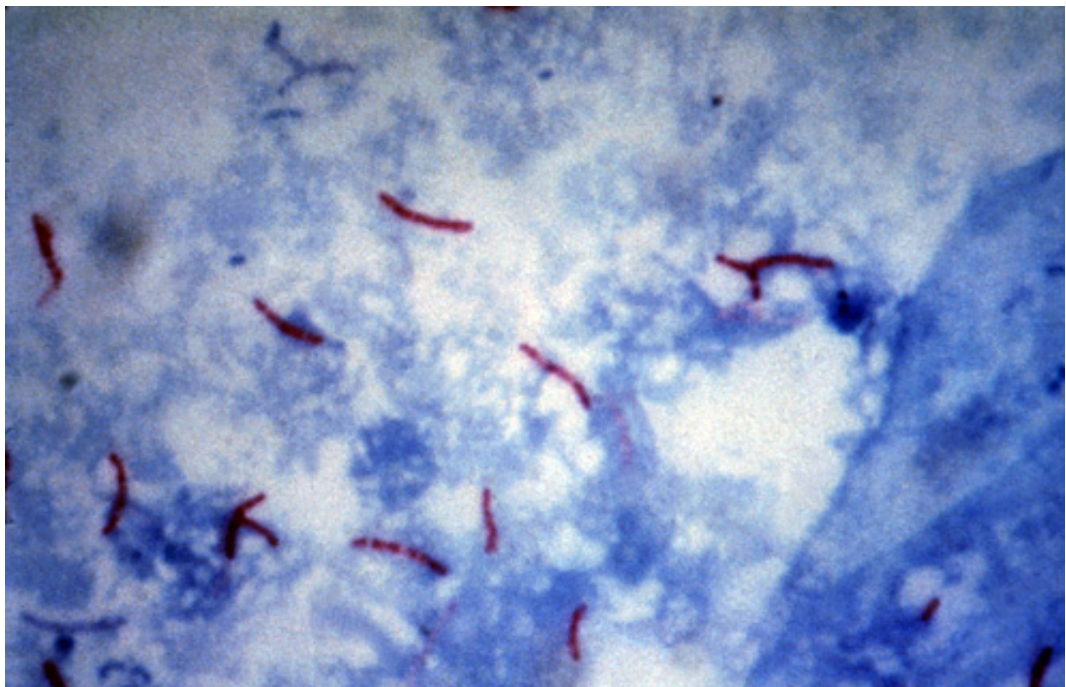


Figure 5. Ziehl-Neelsen acid-fast staining of *M.tb* clinical specimens from a sputum sample. Figure reproduced from (Acharya, 2017). Permission for reproduction granted by phil.cdc.com. No copyright restrictions apply.

1.3.2 Culture

Isolation and growth of *M.tb* in the laboratory is also a good method for the detection of bacilli from clinical samples since it detects live (but only viable) bacilli, but this technique is hampered by its inherent slow growth rate (3 weeks at least) and laboratory contamination can also increase the number of false positives of this technique (Ruddy et al., 2002). Moreover, cases of extra-pulmonary TB won't be detected or even cases of pulmonary TB in children, who do not usually produce enough sputum. Overall, it is considered that up to 81% of all TB cases are confirmed with this technique.

1.3.3 Tuberculin skin test (TST)

Also called the Mantoux test, this method is based on the generation of immunological memory following TB infection, which allows the estimation of the current 2 billion worldwide cases of latent TB infection (Dye et al., 1999). The patient to be tested is administered a shot with around 200 TB antigens under the skin of the forearm, and results are taken 48-72h post-administration. If the person has ever been infected with TB, a red indent will appear. Although quick, the drawback of this method is the high rates of false-positives. Some patients without prior exposure to TB have tested positive for this method, in particular those that have been vaccinated with BCG (Wang et al., 2002). Moreover, this method cannot discriminate *M.tb* infection from non-TB environmental mycobacteria, since they contain many of the antigens administered in the TST (Huebner et al., 1993).

1.3.4 Chest X-ray

This technique is based on the detection of pulmonary lesions caused by TB infections (Fig. 6). Although, in most of the cases bacilli cause lung damage, these can also be related to other health problems affecting the lungs (Al-Zamel, 2009). Moreover, in the early stages of TB infection, lung damage has not become apparent yet, therefore increasing the false-negative rates. This technique should be complemented by other detection methods in order to precisely diagnose TB.



Figure 6. Chest X-ray scan of a TB patient. TB creates visible cavities as pointed by the arrow
Figured extracted from (Emedicine.medscape.com, 2017). No copyright permissions apply.

1.3.5 Nucleic acid amplification test (NAAT)

The amplification of specific sequences of DNA material is relatively specific and a sensitive TB detection method (Noordhoek et al., 1995). Although, it is reported to be more sensitive than SSM but less than culturing, it still requires a high number of bacilli to obtain workable amounts of genomic material. Laboratories compensate for this by growing more bacteria, but this requires several weeks. Costs are also a drawback of this

method, preventing its implementation in under-developed countries and impeding *in situ* TB detection, an essential feature for effective patient management.

1.3.6 Antibody-based diagnostic assay

TB detection methods using enzyme-linked immunosorbent assay (ELISA) (Fig. 7) have been developed that allow a rapid, inexpensive and easy-to-setup serological detection of *M.tb* antigens, such as purified glycolipids or pools of mycobacterial antigens after sonication and filtration. The use of recombinant TB antigens has also been reported (Daniel et al., 1986). One of the big problems associated with ELISA is the difficulty to achieve high sensitivity (Chiang et al., 1997), which makes this method not suitable as a single diagnostic method for TB infection.

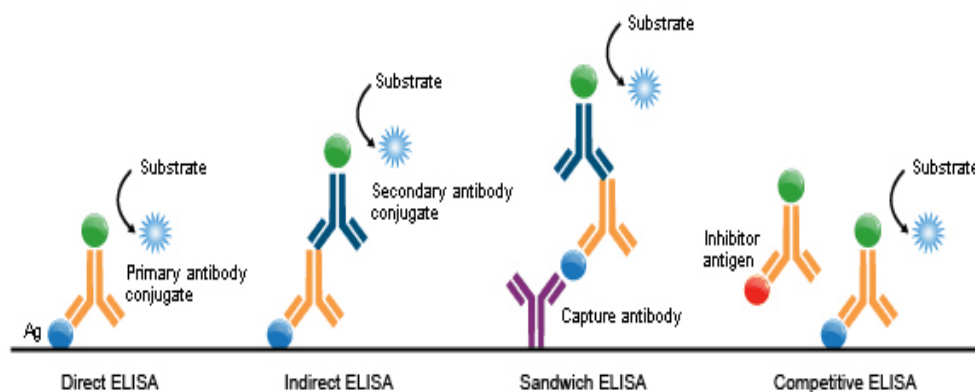


Figure 7. Different ELISAs types for the detection of antigens . Figure courtesy of the antibody provider Abnova (Abnova.com, 2017).

1.3.7 IFN- γ -release assays (IGRA)

This method provides an accurate and sensitive detection for active TB. It is based on the secretion of IFN- γ by peripheral blood mononuclear cells (PBMC) upon interaction with mycobacterial antigens. The main advantage of this detection system is IFN- γ secretion is entirely dependent on the recognition of *M.tb* bacilli, therefore making this assay insensitive to exposure to other environmental bacteria or the BCG vaccine, and it has

proven to be more specific and sensitive than TST in the detection of latent tuberculosis infection (LTBI) (Pai et al., 2004). There are two kits available: QFT-G and T-SPOT.TB for IGRA. The former one detects the release of IFN- γ by PBMC whereas the latter one detects the number of IFN- γ producing PBMC. Both kits have great specificities (over 95%) and sensitivities (89% for QFT-G and up to 97% for T-SPOT.TB) making this detection method a suitable choice for the early detection of *M.tb* infection.

1.3.8 Summary and future prospects

Although, the suitability of IGRA for effective TB detection is clear over other detection methods, the need for rapid detection of drug-resistant strains has accelerated the development of platforms, such as GeneXpert MTB-RIF, a rapid molecular diagnostic tool for the detection of rifampicin-resistant mutations in two hours (User, 2017). The WHO has recommended its implementation worldwide, but due to its cost, SMM is still the method of choice for *M.tb* detection in middle and low-income countries (WHO, 2015).

1.4 The threat of drug resistance

The discovery of penicillin by Alexander Fleming in 1928 marked the beginning of the golden antibiotic age (Fig. 8), which posed a significant improvement in the treatment of bacterial infections that consequently brought along a better life quality and increased life expectancy worldwide. The impact of the discovery of penicillin went far deeper than just the elimination of bacterial infections, not only playing an important role in WW2 for the treatment of wounded soldiers in the Allied Forces, but also boosting productivity in companies and decreasing healthcare costs. Due to its widespread use, resistance was first detected in 1942, therefore diminishing its potential and enhancing the need for

more potent antibiotics. Despite the availability of other antibiotics discovered and introduced throughout the golden antibiotic era, drug resistance has been reported for virtually every bacterial infection only a few years after their introduction, rendering drugs ineffective for the treatment of bacterial infections.

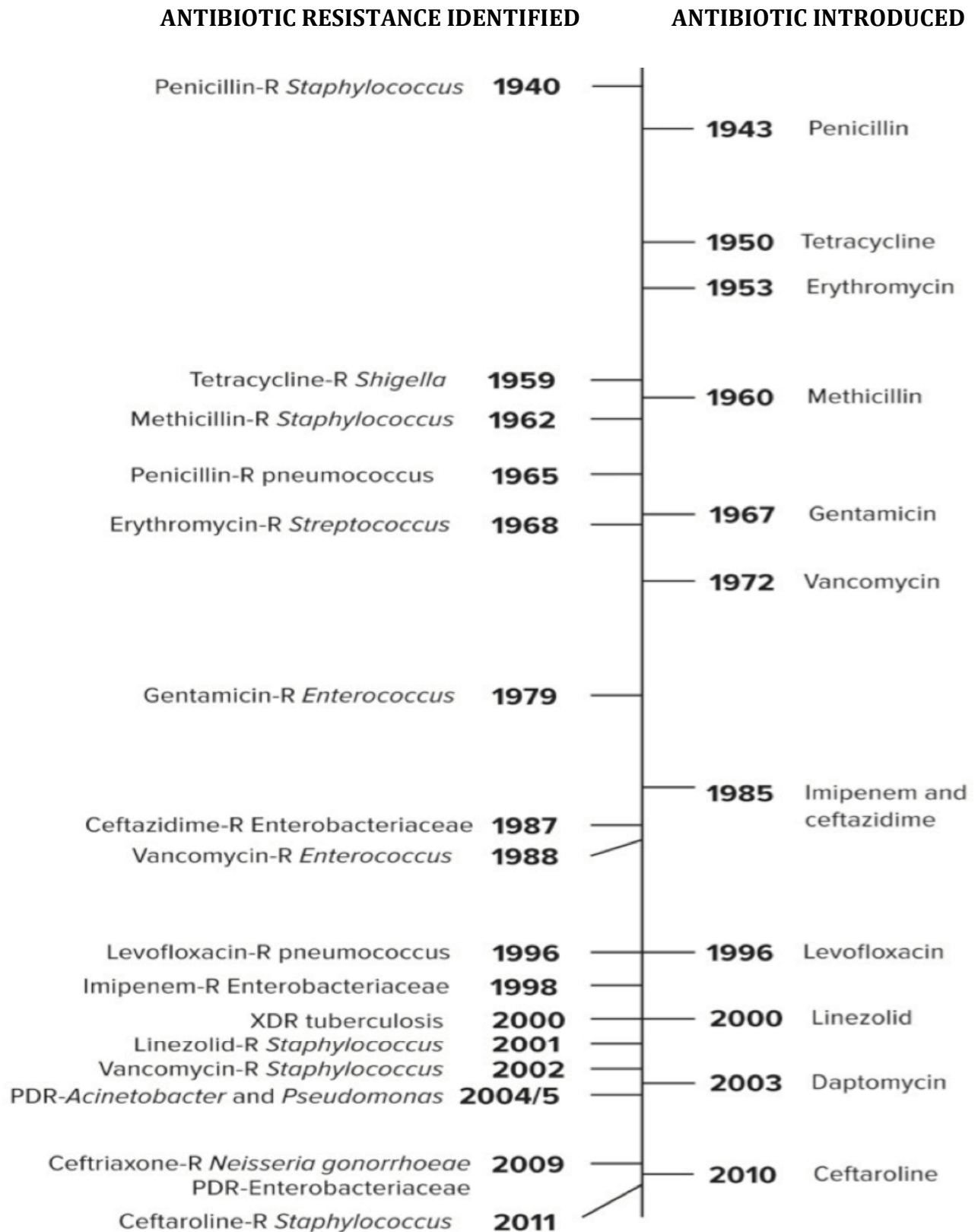


Figure 8. Antibacterial discovery timeline and first-ever reported cases of clinical resistance. Figure obtained from the Centre of Disease control and Prevention (Cdc.gov, 2017). No copyright restrictions apply.

Antibiotic resistance has become a major health concern due to the low availability of effective treatments. Investment in bacterial drug development decreased substantially after the golden antibiotic era due to its low profitability for pharmaceutical companies, decreasing the rate of introduction of new antibiotics on the market (Aminov, 2010). The front-line antibiotics used for the treatments of life-threatening infections caused by Gram negative bacteria such as *Klebsiella pneumoniae*, *Staphylococcus aureus* and are now ineffective due to the appearance and spread of resistance mechanisms caused by an excess use of antibiotics (Ventola, 2015). Therefore, a better use of drugs is needed to decrease bacterial burden among patients worldwide. In particular, more than 50 years after the introduction of isoniazid as the first treatment option for TB, MDR and XDR *M.tb* clinical isolates have been detected virtually worldwide. MDR-TB is defined as resistance to the front-line antitubercular agents, rifampicin and isoniazid, whereas XDR is described as resistance to the front-line TB drugs (isoniazid and rifampicin) and at least one fluoroquinolone agent, and to either of the following aminoglycosides: kanamycin, amikacin or capreomycin (Migliori et al., 2007). Even though some physicians have reported the existence of totally resistant TB (TDR-TB) in India (Velayati et al., 2013), the WHO does not recognise this definition. An extensive description of antibacterial resistance mechanisms will be given to further understand the molecular basis of stress response to antibiotic exposure that triggers the resistance phenotype.

1.4.1 Molecular mechanisms of drug resistance

Adaptive evolution of infectious pathogens to antibiotics and other stress conditions demand increased genetic diversity. Transcriptional regulation allows bacterial populations to adapt to changing environmental conditions and to promote survival of bacteria and therefore evolution. Antibiotics induce the expression of mutagenesis that

promotes the appearance of “fitter” mutants capable of adapting and thriving under selective pressure (Galhardo et al., 2007), such as the upregulation of an error-prone DNA polymerase (Boshoff et al., 2003).

1.4.1.1 Appearance and evolution of β -lactamases.

β -lactams have been the most common antibiotic of choice for the treatment of infections caused by Gram-negative bacteria, such as *Klebsiella pneumoniae* and *E. coli*. There are several classes of β -lactams, including monobactams, penicillins, cephalosporins and carbapenems (Demain and Elander, 1999). As stated above, the first ever reported case of clinical resistance was in penicillin. Chemists have introduced structural modifications in order to overcome resistance and enhance the activity spectrum, leading to the creation of a wide range of β -lactam antibiotics (Kong et al., 2010). Despite the availability of more potent compounds, resistance has proven to be unavoidable, with β -lactamases responsible for the development of resistance against broad-spectrum antibiotics. These enzymes have the ability to hydrolyse the β -lactam ring upon compound binding. The first cases of β -lactamase-producing *Staphylococcus aureus* date just a few years later after the use of penicillin became widespread, and methicillin was synthesised to overcome resistance, but in 1961, the first-ever case of methicillin-resistant *S. aureus* (MRSA) was reported (Singh Lubana et al., 2015). The origin of the molecular mechanism for methicillin resistance is well characterised and a transposon acquired from a different organism seems to be the most convincing explanation (Chambers, 1997). As pharmaceutical companies developed more potent compounds to overcome β -lactamase-mediated resistance, so their spectrum did, developing mutations in the β -lactam binding site that increased affinity for other substrates, widening the range of β -lactam antibiotics prone to hydrolysis (Medeiros, 1997). These so-called extended-spectrum β -lactamases

(ESBLs) produced by species of *Enterobacteriaceae* and *Klebsiella* can hydrolyse penicillins, first-, second-, and third-generation cephalosporins and aztreonam, but not carbapenems or cephamycins (Malloy and Campos, 2011, Falagas and Karageorgopoulos, 2009). Their catalytic mechanism involves the hydrolysis of the β -lactam ring through an activated water molecule (Fig. 9). Since, most β -lactamases are plasmid-encoded and due to horizontal gene transfer, the spread of antibiotic resistance continues unabated, with such cases confirmed in *K. pneumoniae* and *E. coli* (Harris et al., 2015). The use of β -lactams for the treatment of *M.tb* infections has never been systemically established due to inherent β -lactamases. However, β -lactam/ β -lactamase inhibitor combinations have strong potency *in vitro* due to the irreversible inhibition of the extended-spectrum β -lactamase BlaC by clavulanate (Hugonnet and Blanchard, 2007) (Hugonnet et al., 2009). These findings have led the TB community to develop extended-spectrum β -lactamase inhibitors that can be used in combination with β -lactams for the treatment of MDR and XDR-TB (Dincer et al., 2004).

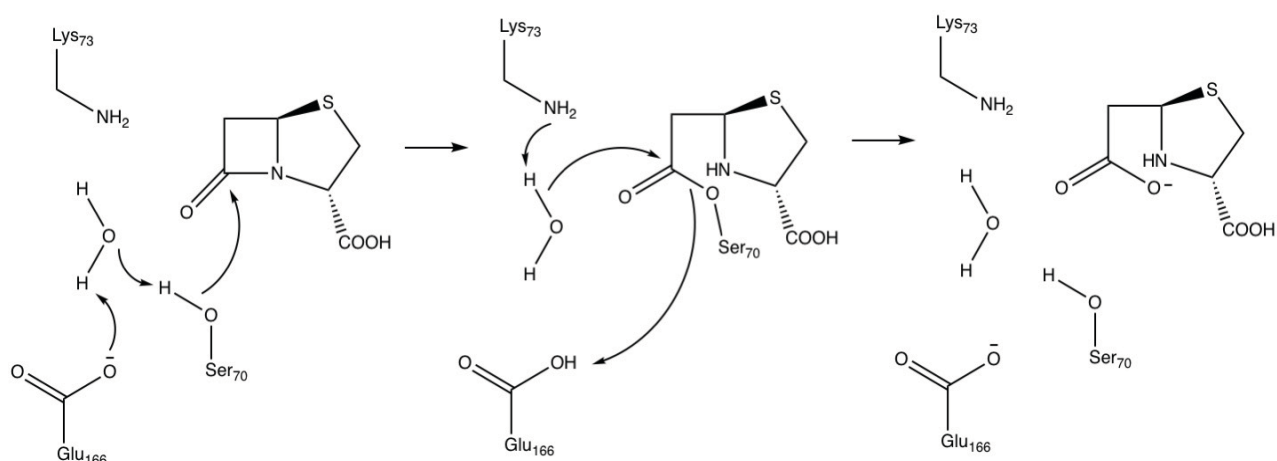


Figure 9. Catalytic mechanism of class A β -lactamases. Aminoacylation of Ser70 with the consequent opening of the β -lactam ring and slow deacylation upon attack of the activated water molecule by Lys73 releasing the inactive opened product. Figure obtained from (Hugonnet and Blanchard, 2007), cleared for reproduction under copyright 2007, American Chemical Society.

1.4.1.2 Mutations in drug targets.

A very common mechanism of resistance in bacteria is the disruption of the drug-target interaction by spontaneous mutations in residues in close contact with the drug. This mechanism drives target identification efforts after the *in vitro* isolation of spontaneous-resistant mutants and further whole-genome sequencing. Examples of mutations in drug targets have been extensively reported in the literature, (Grzegorzewicz et al., 2012) (Koul et al., 2007). There appear to exist some indicator about the molecular mechanisms driving the generation of spontaneous-resistant isolates, suggesting the up-regulation of the error-prone DNAE2 polymerase under antibiotic pressure (Boshoff et al., 2003). Further studies are needed to elucidate the molecular mechanisms involved in the appearance of spontaneous mutations that a compound selects.

1.4.1.3 Mutations in drug-activating enzymes.

Resistance can also be driven by mutations in prodrug-activating enzymes, such as KatG or PnaC (Cade et al., 2010) (Scorpio and Zhang, 1996). In order to investigate the molecular basis for pyrazinamide (PZA) resistance, the functional locus of PnaC was cloned into a multi-copy plasmid that was used to transform genetically confirmed resistant strains harboring mutations in PnaC. Susceptibility was restored to that of wild-type strain levels, therefore proving PnaC as a PZA-activating enzyme. Moreover, cell-free based assays showed a decrease in PnaC activity in *M.tb* resistant strains, clearly linking this enzyme to PZA activity. Mutations in KatG are more frequent than in InhA, the isoniazid target (90% vs. 10% in clinical isolates) therefore confirming the importance of these enzymes in the mode of action of these compounds.

1.4.1.4 Efflux pumps.

Another common mechanism of resistance in bacteria is the presence of efflux pumps (Fig. 10). Many potent enzyme inhibitors lack whole-cell activity and together with the highly impermeable cell wall of *M.tb*, efflux pumps are believed to play a major role in this regard. Many have been characterised and well known efflux pump inhibitors have been reported, such as Verapamil (Ainsa et al., 1998). Even though resistance-conferring mutations in clinical isolates is mainly driven by mutations in either drug targets or drug-activating enzymes (Jagielski et al., 2015), efflux-pump mediated resistance to rifampicin has also been observed (Louw et al., 2011). Overall, the use of efflux pump inhibitors could increase the susceptibility of MDR and XDR-TB clinical isolates to front-line TB agents. In order for this strategy to be successful, structural characterisation of validated efflux pumps is needed in order to design inhibitors to diminish drug efflux (Pule et al., 2016). In an ideal scenario, an efflux pump of front-line anti-tubercular agents is induced

in vivo as a response to antibiotic stress and can be targeted with inhibitors that have been found to significantly block drug efflux (Grossman et al., 2015). These drugs should also be non-toxic, show no drug-to-drug interactions in combination with front-line TB drugs, and of course help reduce bacterial burden in patients with MDR and XDR-TB.

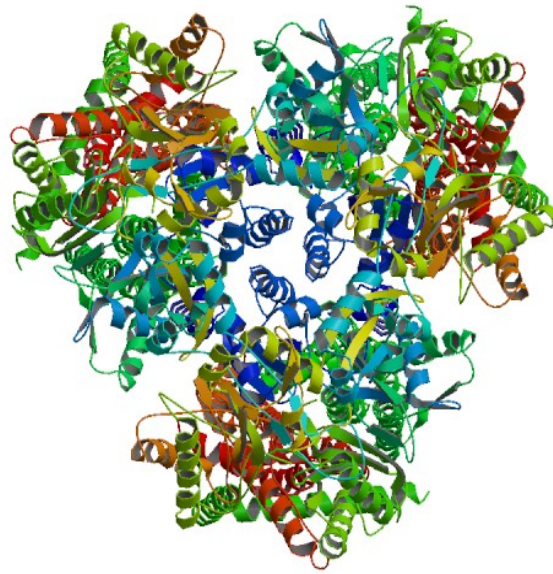


Figure 10. Crystal structure of MtrD in the open state, a multidrug efflux pump in *Neisseria gonorrhoeae*. The central pore is open to allow the export of compounds outside the cell. Reproduced from (Bolla et al., 2014) under the Creative Commons Attribution licence.

1.4.2 Spread of drug resistant strains

The appearance of drug resistant mutations is a natural process. Environment adaptation is essential in order to survive with the transfer of genetic material to the offspring. In

bacterial infections, genetically acquired resistance occurs randomly at a very low frequency (1×10^{-7} , depending on the gene in question). Once mutated, bacterial cells are now adapted to the new environmental conditions and will transfer this genetic trait to their daughter cells. The molecular basis for the generation of these mutations has already been discussed in some cases (Boshoff et al., 2003), although further understanding is needed to better understand these events. Since *M.tb* is an airborne pathogen, the mode of transmission of drug-resistant strains and the lack of effective treatments available make them even more dangerous than other communicable diseases. Even though the eventual appearance of resistance is unavoidable, it can still be minimised through the proper use of antibiotics. Overuse and sub-inhibitory concentrations of antibiotics due to lack of patient adherence are very good examples of induced drug resistance (Davies and Davies, 2010).

Old antibiotics can still be used for the treatment of multi-drug resistant infections but higher concentrations are needed to achieve the same levels of clinical efficacy. This practice carries along the possibility of drug-induced toxicity due to interactions with human targets other than its own (off-target effects) and that would not happen if the drug weren't administered at lower concentrations (Guengerich, 2006). Therefore the adherence to good clinical practices, as well as an increased control in patient management, is needed in order to minimise the development of drug resistance.

1.5. TB drug discovery

1.5.1 Introduction

Whilst treatment of drug-susceptible TB involves 6 months of daily administration of isoniazid (INH), rifampicin (INH), ethambutol and pyrazinamide (PZA) plus 3 months of daily isoniazid and rifampicin, the WHO recommends a combination of front- and second-

line drugs including high-dose isoniazid, clofazimine, pyrazinamide, kanamycin, gatifloxacin, ethambutol and prothionamide, for the treatment of patients with MDR and XDR-TB. The downside of using second-line drugs is the appearance of side-effects, poor effectiveness and their high cost. In this case, physicians have issued some guidelines on the rationale drug administration for MDR-TB patients. More effective and less toxic drugs are needed to shorten treatment regimens and achieve better outcomes. In this case, different strategies for TB drug discovery can be followed. Repurposed chemical scaffolds (e.g. moxifloxacin), the use of drugs initially approved for other infectious diseases, such as clofazimine for inclusion in TB chemotherapy regimens, (which was initially used for the treatment of leprosy (Tyagi et al., 2015)), and the discovery and development of new chemical scaffolds from *de novo in vitro* drug discovery efforts, opening up unexplored areas of druggable biological space.

1.5.2 *De novo* drug discovery approaches

Several compounds have already been tested in both pre-clinical and clinical trials to assess their potency and toxicity as therapeutic agents. As discussed above, amongst the strategies employed in TB drug discovery, the use of repurposed drugs, such as gatifloxacin and moxifloxacin is promising. However, the use of entirely new novel compounds with innovative mechanisms of action has the potential to discover unexplored areas of biology and chemical space, such as benzothiazinones that target DprE1, an epimerase involved in arabinan synthesis (Makarov et al., 2009). In order to highlight the success of *de novo* TB drug discovery approaches, a new drug that has recently been FDA-approved is Bedaquiline (branded as Sirturo™) for the treatment of both susceptible and drug-resistant TB, which targets the subunit C of the ATP-synthase,

blocking metabolism and causing cell death (Koul et al., 2007). One of the main mechanisms of resistance to drugs, amongst others, is driven by compound induced-resistant mutations in the drug target that disrupt compound binding and therefore inhibition. In fact, this mechanism of resistance drives one of the current target identification approaches. Once a compound is identified as a promising hit from a high throughput screening campaign, resistant colonies are isolated under high selective pressure. When these strains are confirmed for their resistant phenotype, genomic DNA is then extracted and sequenced in order to identify single nucleotide polymorphisms (SNPs) in genes whose coded proteins are presumably involved in compound binding (Andries et al., 2005) (Makarov et al., 2009). The suspected target is then cloned and overexpressed in *M. bovis* BCG for subsequent target validation. If the overexpressor strain titrates the compound when compared to the WT strain (as shown by the Minimum Inhibitory Concentration (MIC) shift of at least 4-fold) and the gene is essential then the encoded protein is thought to be the target of that particular compound (Gurcha et al., 2014). Further validation studies include biochemical-backed evidence showing correlation between whole-cell and enzymatic inhibition (MIC and IC₅₀, respectively). Due to its phylogenetic proximity to *M.tb*, the use of BCG as an effective surrogate for certain studies, such as target identification, rewash proved useful (James et al., 2012). The global TB community has therefore adopted whole-cell screening followed by target identification approaches to discover compounds with new mechanisms of action that are likely to avoid drug-resistance in the short term. Although, it is acknowledged that resistance will eventually occur. Target-based screening campaigns require the prior purification of the protein, which is not always achievable, has had little or no success due to the lack of potency of these hits in whole-cell assays. As an example, nearly 70 biochemical screening campaigns at GlaxoSmithKline against targets from many bacterial

species have generated many hit compounds with good on-target activities but very few of them have showed whole-cell potency in phenotypic assays, hampering the effectiveness of this approach and explaining the shift towards phenotypic screens as the source of initial hits (Fig. 11) (Lechartier et al., 2014). Attrition in this case is due to the lack of correlation between target-based inhibition and whole-cell activity, mainly due to the low permeability of the bacterial cell wall to many compounds. Moreover, other factors such as intracellular target location, protein folding and off-target mechanisms can also affect compound-protein interaction, proving this approach as a too simplistic version of the actual environment within the cell. Whole-cell screening, however represents a holistic approach that considers all these factors.

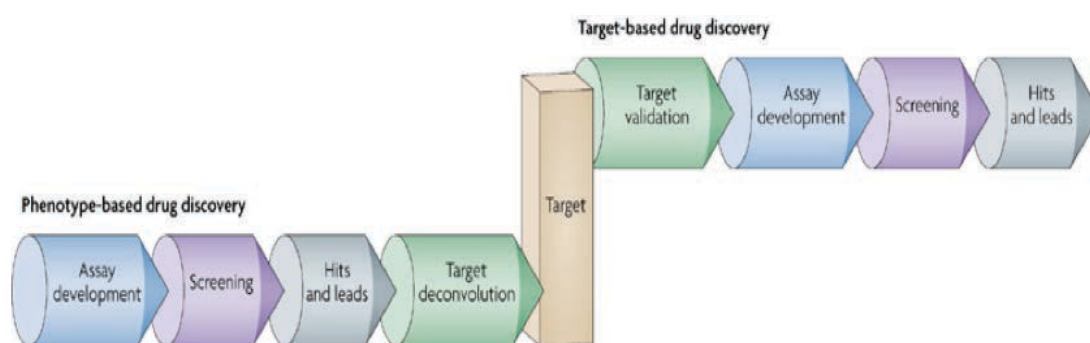


Figure 11. The two historical drug discovery strategies in TB. Target-to-drug versus drug-to-target approach. Figure reproduced from (Terstappen et al., 2007).

Consent for reproduction granted by Springer Nature under licence number 4312650568120.

Although presenting some clear advantages, such as the lack of knowledge of the mechanism of action, target identification remains challenging in the drug-to-target approach, with very few pharmacologically validated targets available according to the TB

drug accelerator program (Bill & Melinda Gates Foundation, 2017). The aim of the Foundation is to provide funding to pharmaceutical companies and research institutions for the discovery of new chemical entities that act through novel signaling pathways. In this case, the discovery of new targets remains essential to guide structure-activity relationship (SAR) in medicinal chemistry programmes aimed at improving their overall properties during the hit-to-lead generation phase, such as solubility, activity and toxicity. Given a known and validated target, biochemical and crystallography assays can be set up once the protein is successfully expressed and purified to confirm on-target inhibition and therefore compound binding. Subsequently, a new validated target can be used for further screening using a whole-cell target-based approach to identify new chemical scaffolds or even guide structure-based drug design for the same purpose. Biochemical and ligand binding assays are then essential during early-phase drug discovery, however it can be concluded that they are not appropriate for the primary identification of active chemical matter.

1.5.3 Drug repurposing

Medicinal chemistry on approved drugs has several advantages over *de novo* drug discovery efforts. First, the availability of a known and validated target of interest can help streamline medicinal chemistry efforts if its structure and a biochemical assay are readily available for further evaluation. Second, approved drugs have a well-characterised PK/PD profile that helps for a starting point for further optimisation. The main drawback of this approach is the presence of resistance mechanisms already described in bacterial systems. Drug repurposing may be seen as a quick drug resistance by-pass in the short term but the presence of well-described resistance mechanisms may render this approach ineffective in

the longer run.

1.5.4 Target de-convolution strategies

Before going deep into the description of the project, let's review the main target identification approaches used by drug discovery researchers to gain more insight into the mechanism of action of chemical entities. Despite target identification still being challenging the overall advantages of the drug-to-target approach render this strategy more suitable for the discovery of active chemical entities. It is therefore important to keep in mind that target identification has to be dealt with in a case-by-case manner, since some compounds with unspecific mechanisms of action may not be amenable to identification by whole-genome sequencing following-up resistant mutant generation studies, since it is more difficult to develop resistance in multiple targets (Li et al., 2014). Another reason behind the absence of resistant colonies can include intolerance to target overexpression (Zimhony et al., 2000). In this case increased resistance to the drug *in vitro* was found when a genomic library cloned in multicopy plasmids was screened in *Mycobacterium smegmatis*. The isolated gene was identified to be FASI, but no transformants were able to grow when slow growing mycobacteria were transformed, suggesting intolerance to FASI overexpression. Therefore, other target identification strategies need to be exploited in order to streamline the drug discovery pipeline. A description of the main target identification approaches is given below with their respective advantages and disadvantages.

1.5.4.1 Chemical proteomics approaches

1.5.4.1.1 Label-based techniques

The availability of label and label-free techniques coupled to mass spectrometry can greatly enhance target identification (Loo et al., 1999). Within compound-labelled techniques, the compound is immobilised onto a solid support with an affinity tag and is then exposed to the proteome (Fig. 12) (Lomenick et al., 2011). This strategy relies on the affinity of the compound for its target(s) and after several washing steps aimed at removing unspecific binders, the compound-target interaction is weakened by the addition of denaturising agents/conditions (urea, acidic pH). Bands from an SDS-PAGE protein gel are then excised out and subjected to mass spectrometry studies. The protein sequenced is then BLAST-analysed against protein databases for final target identification. Further studies require ligand-binding experiments to assess compound-target interaction, such as surface plasmon resonance (SPR) or tryptophan fluorescence assays. Even though the idea is simple, the immobilisation onto a solid support requires the chemical modification of the compound, which can result in a decrease in affinity for its target, therefore requiring prior extensive SAR knowledge of the molecule. This can be overcome by the introduction of a small azide or alkyne group following extensive SAR knowledge of the structure of the compound in order not to interfere with on-target activities. The well-known copper-catalysed click-chemistry reaction will allow the clickable group to be linked onto a solid support. As it will be shown later on, the introduction of an azide group on different structural sites can have a significant impact on the inhibitory action of the hit compound against the enzyme. This approach has been successfully used for the identification of kinases as the target of several inhibitors in mammalian cells (Shi et al., 2011, Shi et al., 2012).

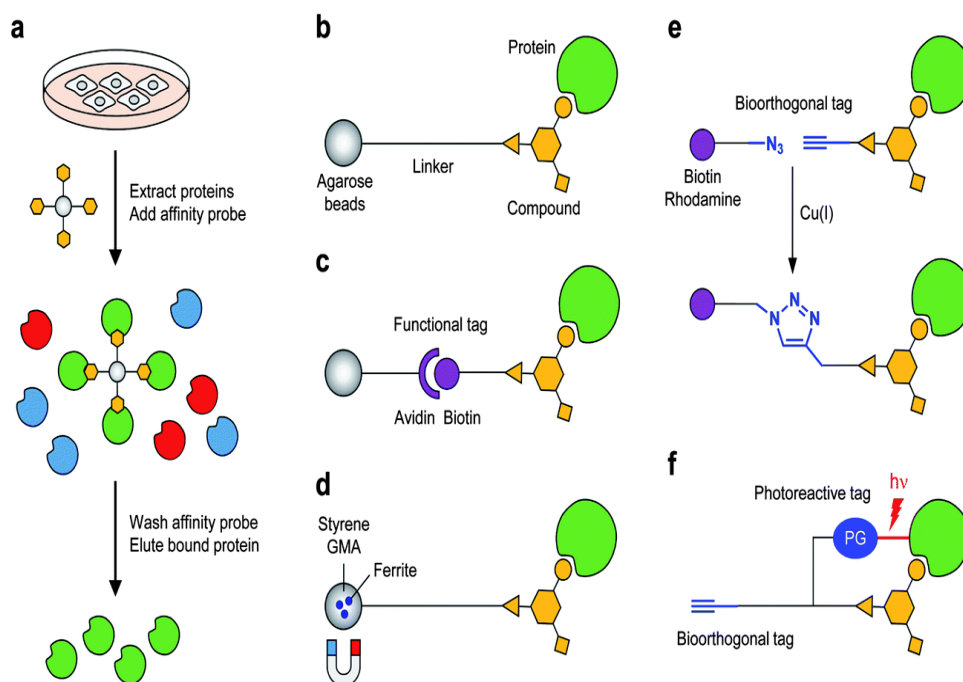


Figure 12. Affinity based methods for the identification of compound targets. (A) Generic pull down assay procedure: the cell extracts are incubated with the probes to allow protein target binding and after washing and elution steps the sample is subject to mass spectrometry identification studies. (B-F) Types of functional probes employed in pull down assays. Figure extracted from (Titov and Liu, 2012) with permission granted by Springer Nature under license number 43126500568120.

Another strategy using labeled compounds is the introduction of a photoreactive group such as a benzophenone, diazirine, or arylazide to induce covalent cross-linking between the compound and its target, plus a reporter group for its isolation. This approach has been successfully implemented for the identification of the γ -secretase activating protein (gSAP) as the target of the marketed drug, imatinib when the drug was modified with an arylazide (He et al., 2010).

1.5.4.1.1.1 Activity-based probes (ABPs)

Activity-based probes (ABPs) have also been used for target identification. These are small molecules with three different components: (i) an electrophile group for the induction of covalent linking to the protein target, (ii) specific groups for the interaction with the enzyme and (iii) a reporter group for target isolation (Fig. 13). Although, some groups have reported their successful application the introduction of an electrophile group on the structure of the compound may not be a specific strategy for protein detection, since covalent modification of cysteines or serines could occur with off-target proteins (I.Hall, 2011). Moreover, this approach relies on the presence of either cysteines or serines (reactive nucleophile-containing residues) in the compound-binding site, which is entirely dependent on the mode of inhibition of the compound in question, i.e. reversible inhibitors do not covalently modify proteins, therefore the addition of a reactive electrophile will not help if there are not cysteines around the binding site. However, this approach is applicable to the simultaneous screening and target identification of a library of ABPs (Arastu-Kapur et al., 2008).

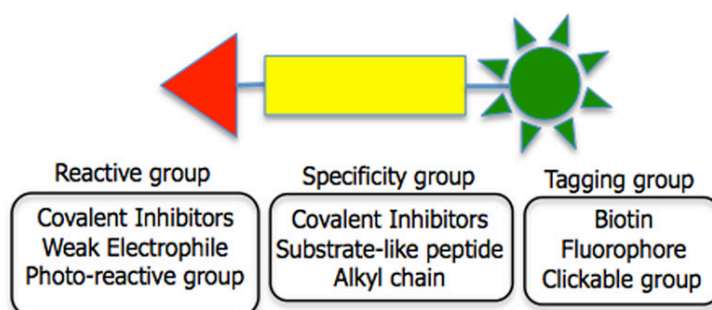


Figure 13. Schematic representation of the ABP structure. Figure obtained from (Lee and Boggyo, 2013) with permission for reproduction granted by Elsevier under license number 4312660045883 .

1.5.4.1.2 Label-free techniques

This chemical proteomics-based approach is based on the changes of thermodynamic stability upon compound binding. Compound-target interaction can decrease the susceptibility to proteolysis (Fontana et al., 2004). A technique called DARTS (Drug Affinity Responsive Target Stability) was used to identify targets of resveratrol and rapamycin (Pai et al., 2015). Unlike affinity chromatography approaches, this technique does not require the chemical modification of the compound, therefore the loss of activity disappears.

1.5.4.2 Expression cloning techniques

A gene library can be cloned into plasmids that are transformed (in bacteria) or transfected (in mammalian cells) and will then express a representative fraction of the proteome. The compound will therefore select for a particular transformant/transfectant since target overexpression will confer resistance. This strategy was used to identify the target of the anti-TB agent ethambutol EmbAB (Belanger et al., 1996) and also for pyrazinamide, which targets FASII in *M.tb* (Zimhony et al., 2000).

1.5.4.3 Microarrays

Gene expression profiles can be useful to predict the mechanism of action of a given chemical entity. Compounds with similar transcription profiles are clustered and assigned to those with similar transcriptional responses (Boshoff et al., 2004). In fact, this strategy has been effectively used to elucidate the mechanism of action of new chemical entities. Promoter regions in common upregulated genes in response to inhibitors with a given mechanism of action have been fused to reporter genes so that a compound with similar mechanism of action will trigger the expression of the reporter gene (King et al.,

2009). The mechanism of action is further validated biochemical assays.

1.5.4.4 Metabolomics

Whole-cell metabolic profiling can also help elucidate the mechanism of action of a hit compound (Creek and Barrett, 2014, Beyoglu and Idle, 2013). Cell cultures are typically incubated at compound concentrations below the MIC and then subjected to mass spectrometry analysis for metabolite profiling (Birkenstock et al., 2012). The full metabolic profile is then compared to control cultures without compound and those metabolites over and underrepresented can potentially represent substrates and products of an inhibited enzymatic activity, respectively. The compound target can be inferred from this enzymatic activity and further confirmed using genetic or biochemical tools.

1.5.5 Novel emerging drug targets in the drug discovery pipeline

1.5.5.1 DprE1

The importance of the discovery of new targets is such that in the past few years we have seen a substantial increase in the identification and validation of novel emerging targets for several compounds. The most promising of all has received the so-called “magic bullet”, DprE1, due to its high apparent druggability by different chemical scaffolds (Fig. 14) (Manina et al., 2010). Amongst them, benzothiazinones (BTZs) have shown great potency in whole-cell assays (MIC of 1 ng/mL) and whole-genome sequencing studies of resistant isolates have shown missense mutations in cysteine residues of DprE1 (Makarov et al., 2009). This enzyme catalyses the epimerisation reaction of decaprenylphosphorylribose (DPR) into decaprenylphosphorylarabinose (DPA), the

sugar donor for the arabinan component of arabinogalactan (AG) (Mikusova et al., 2005). BTZ binds DprE1 in an irreversible manner. The crystal structure of DprE1 in complex with a BTZ derivative shows a covalent bond as expected with the cysteine residue change (Batt et al., 2012). Additional DprE1 inhibitors have been discovered (Christophe et al., 2009) (Liu et al., 2017), suggesting DprE1 as a highly attractive target from a druggability point of view, encouraging further whole-cell target-based screening against this particular target.

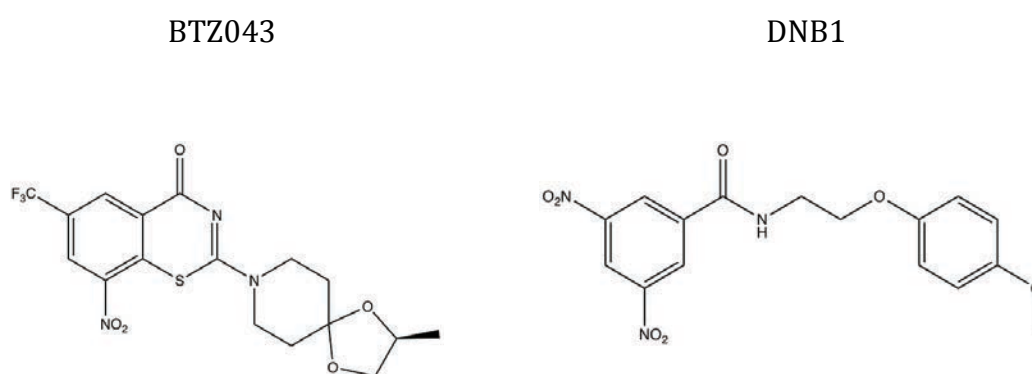


Figure 14. BTZ043 and DNB1 structures, two main chemical scaffolds in development against *M.tb* DprE1.

1.5.5.2 MmpL3

Several inhibitors have been shown to target MmpL3, such as AU1235 (Grzegorzewicz et al., 2012), SQ109 (Tahlan et al., 2012) and the tetrahydropyrazolopyrimidine (THPP) family (Remuinan et al., 2013), a series of compounds synthesized by GSK (Fig. 15). Questions have arisen as to whether these compounds actually target this protein considering the fact that SQ109 is also active against other bacteria that do not have

MmpL3 orthologous proteins (Makobongo et al., 2013). In the absence of a crystal structure of MmpL3 with any of the mentioned compounds, much needs to be done with regard to MmpL3 function and its role in drug resistance. Some researchers regard the fact that many inhibitors map to this protein as an artifact due to an increased hydrophobicity that would lead to compound accumulation in the membrane and therefore a higher likelihood of interaction with the protein (Goldman, 2013). Our group has recently shown how whole-genome sequencing (WGS) of spontaneous resistant isolates can mask the actual target of small molecules that apparently target MmpL3, by revealing the actual target of THPP inhibitors by a pull-down approach (Cox et al., 2016).

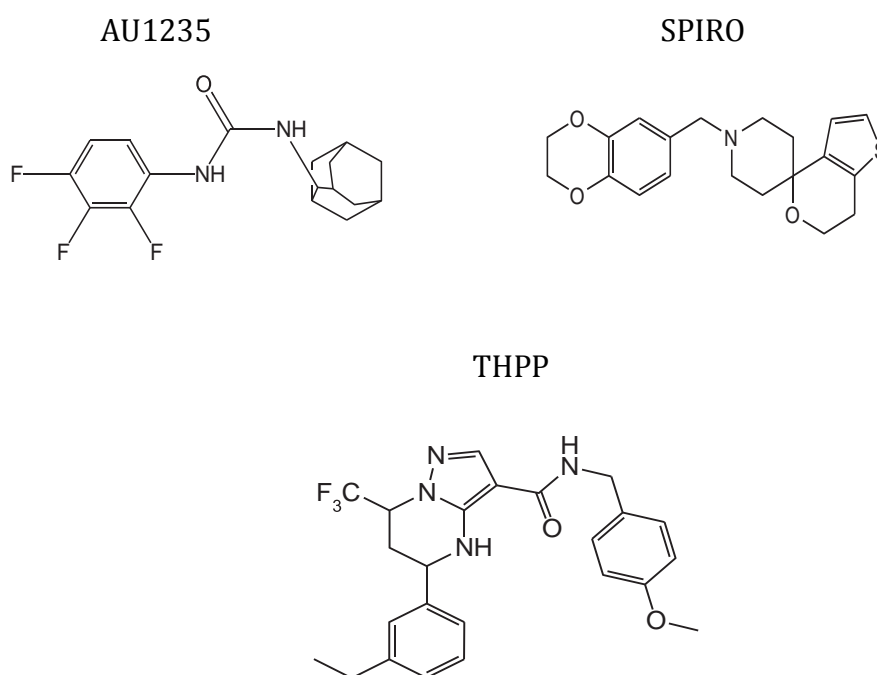


Figure 15. Several chemical scaffolds in development mapping to MmpL3 in WGS of *in vitro* *M.tb* resistant isolates. Among these, AU1235 was shown to cause an accumulation of the mycolic acid precursor trehalose monomycolate (TMM) due to inhibition of MmpL3 (Grzegorzewicz et al., 2012). It remains to be validated whether the other compounds also inhibit MmpL3 function and its role in drug resistance.

1.5.5.3 QcrB

SNPs have been identified in this subunit B of the cytochrome C reductase involved in respiration. Overexpression of QcrB and the entire cytochrome complex QcrCAB have conferred resistance to imidazopyridine (IP) inhibitors and the novel imidazopyridine amide Q203 (Abrahams et al., 2012, Pethe et al., 2013) and several other compounds have been reported to map to this protein (Chandrasekara et al., 2017) (Fig. 16).

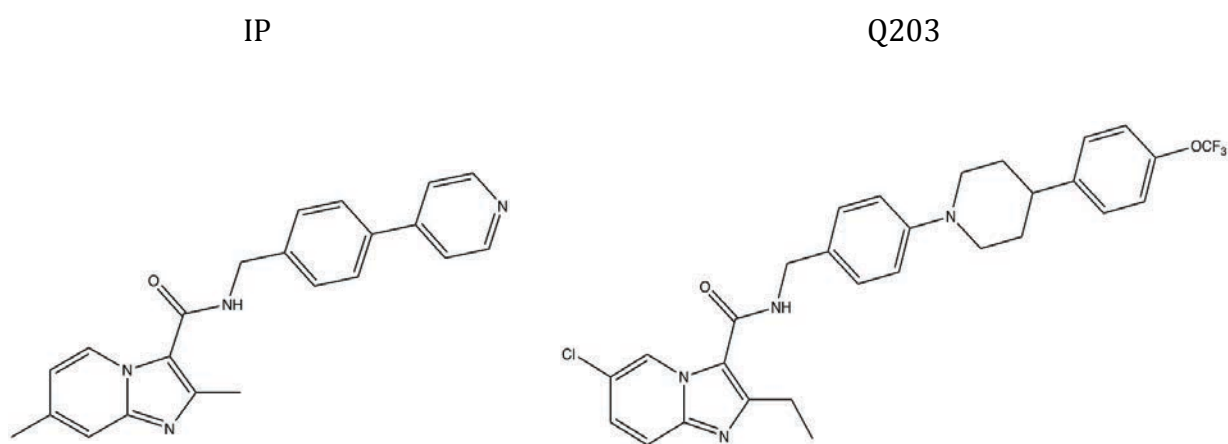


Figure 16. New chemical scaffolds targeting Mt-QcrB.

Aims and Objectives

The main aims and objectives of this thesis can be divided into two main chapters. First, the identification and characterisation of new chemical entities targeting the aspartyl-tRNA synthetase of *M.tb* through a combination of biochemical and phenotypic screens. The identified and validated screening hits will be further optimised through medicinal chemistry efforts in an iterative approach by constructing SAR with on-target, whole-cell and physicochemical data. As part of the biochemical characterisation of these hits and their further progression in the hit-to-lead phase, a selectivity assay with a human mitochondrial AspS will be performed to assess their selectivity against the TB enzyme. Second, we have selected a few chemical entities from the GSK TB set collection to identify novel potential targets and resistance mechanisms through the generation of spontaneous resistant isolates, whole-genome sequencing studies and functional genetic approaches in *M. bovis BCG*.

Chapter II

IDENTIFICATION AND CHARACTERISATION OF NEW CHEMICAL Scaffolds TARGETING

***M.tb* ASPARTYL-tRNA SYNTHETASE**

(Mt-AspS)

2.1 Introduction

2.1.1 Role of aminoacyl tRNA synthetases in protein biosynthesis

Aminoacyl-tRNA synthetases (aaRS) have been widely studied across species due to their essential role in protein biosynthesis (Ibba and Soll, 2000). Their main function is the catalysis of tRNA charging reactions with cognate amino acids prior to an activation step with adenosine triphosphate (ATP) (Fig. 17). There are eighteen tRNA synthetases in *M.tb* clustered in two groups, class I and II, which differ structurally despite sharing a conserved catalytic mechanism. Class I tRNA synthetases contain a Rossmann dinucleotide-binding domain in the active site, whereas class II contains an antiparallel β -fold (Fig. 18). Once the aspartyl-tRNA is formed, the complex is transferred to the A site of subunit 30S of the ribosome where codon-anticodon recognition between mRNA and tRNA avoids translation errors during elongation (Laursen et al., 2005). The protein complex in the ribosome then catalyses the formation of peptide bonds between the peptide being formed and the newly incorporated amino acid. The ribosome complex then moves along the mRNA, shifting the free tRNA to the E site, allowing the entrance of a new aa-tRNA into the protein synthesis machinery and therefore the elongation of the nascent peptide.

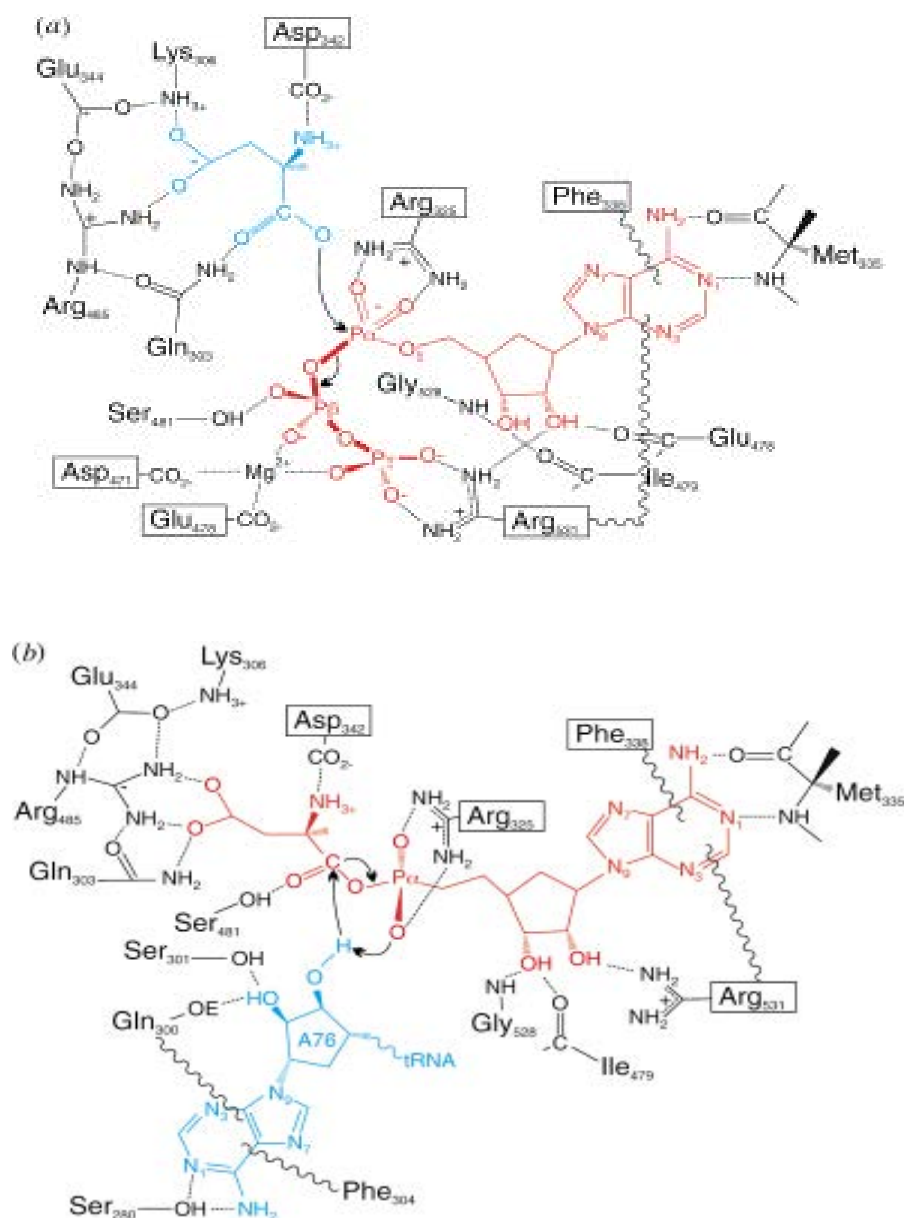


Figure 17. Catalytic mechanism of aminoacyl-tRNA synthetases. A) Activation of the amino acid with ATP releasing inorganic pyrophosphate. The negative charge is delocalised around the carboxylic acid of the L-Asp molecule, preventing the 3'-hydroxyl group of the tRNA from attack, therefore requiring prior activation with ATP before charging. B) Upon formation of the aspartyl-adenylate intermediate, the carbon group of the ester group is susceptible to nucleophilic attack by the 3' hydroxyl group of the tRNA, allowing the formation of the final aspartyl-tRNA product that is released by the enzyme. Figure reproduced from (Ibba and Soll, 2000) with permission granted by Annual Reviews under license number 43126600993263.

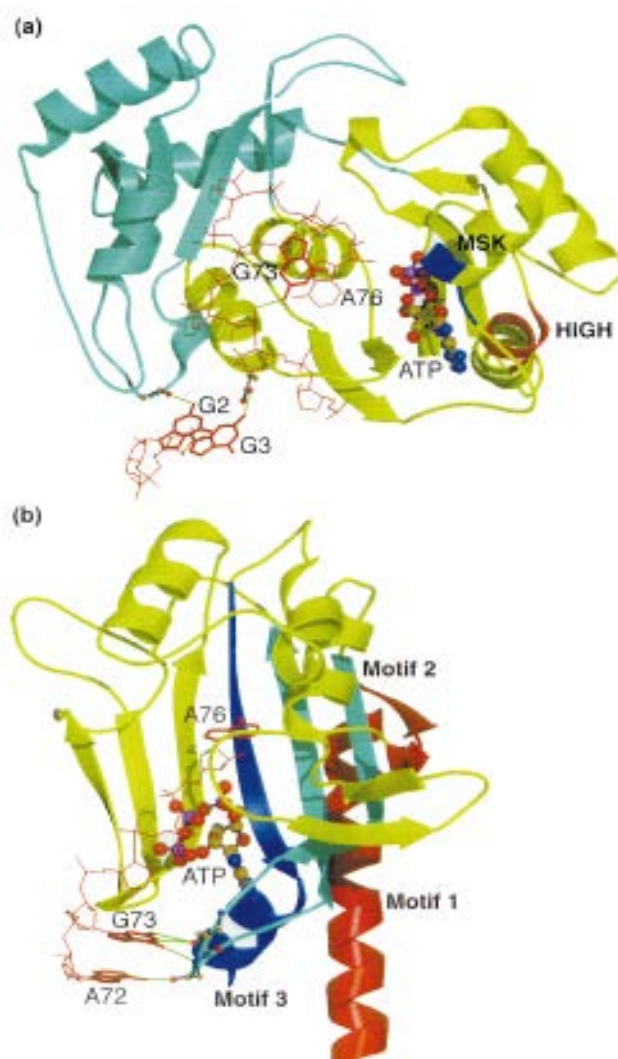


Figure 18. Active site topologies in (a) class I (GlnRS) and (b) class II (AspRS) tRNA synthetases. Shown are the acceptor stem of the tRNA and ATP Figure reproduced from (Ibba and Soll, 2000) with permission granted by Annual Reviews under license number 43126600993263..

A number of structural features allow each tRNA to be recognised by its cognate tRNA synthetase amongst a large pool of similar molecules. Nucleotides playing an important role in tRNA recognition comprise not only the anticodon-binding region but also the 3' acceptor stem, the inside of the L-shaped tRNA, the D-stem and the phosphate backbone (Ibba and Soll, 2000). These identity sets have been determined through site-directed

mutagenesis experiments and the resulting tRNA has been assessed for its competence in the amino acylation reaction. Despite the widespread notion of 20 existing tRNA synthetases in cells and organisms, only eighteen aaRS catalyse the aminoacylation reaction of each of the 20 tRNA expressed in bacteria (Fig. 19). As a result two of them, namely AspS and GluRS, have so-called “relaxed specificity”, which allows them to recognise non-cognate tRNAs (tRNA^{Asn} and tRNA^{Gln}) synthesizing the mis-aminoacylated intermediates Asp-tRNA^{Asn} and Glu-tRNA^{Gln}. The final synthesis of glutamyl-tRNA and asparaginyl-tRNA is tRNA-dependent and catalysed through a transamidation reaction from glutamate and aspartate, respectively (Becker and Kern, 1998).

aa-tRNA synthetase	Gene name
AlaRS	Rv2555c
GlyRS	Rv2375c
ValRS	Rv2448c
LeuRS	Rv0041
IleRS	Rv1536
SerRS	Rv3834c
ThrRS	Rv2614c
ProRS	Rv2845c
TrpRS	Rv3336c
TyrRS	Rv1689
PheRS	Rv1649, Rv1650
MetRS	Rv1007c
CysRS	Rv3580c, Rv2130c
AspS	Rv2572c
GluRS	Rv1992c
LysRS	Rv3598c, Rv1640c
HisRS	Rv2580c
ArgRS	Rv1292

Table 1. Eighteen aminoacyl-tRNA synthetases (aaRS) of *M.tb* and their corresponding gene names.

Initial biochemical characterisation of tRNA synthetases aimed to study the concentration of total active enzyme and the kinetic constants of the first step of the aminoacylation reaction e.g. amino acid and ATP binding to the active site (Francklyn et al., 2008). Other

biochemical studies on tRNA synthetases have focused on the flexibility of the catalytic KMSKS loop during substrate binding and on the editing domain of LeuRS during misaminoacylation (Hu et al., 2013), (Mykuliak et al., 2014). In order to achieve high fidelity protein translation (only 1 in 10000 tRNA^{-Leu} molecules are mischarged with isoleucine), key residues on LeuRS play an essential role for the proofreading activity of misaminoacylated tRNA. The studies have used misaminoacylated tRNA and assessed their competence for a deacylation reaction with several LeuRS mutants in the C-terminal binding domain. These experiments involve the use of alanine-scanning mutagenesis as a source of tRNA synthetase mutants. Other proof-reading mechanisms by LeuRS occur during amino acid pre-transfer onto the tRNA (pre-transfer editing) further ensuring fidelity during protein translation.

2.1.2 Aminoacyl tRNA synthetases as potential targets for antibiotic development

From a biomedical perspective, aaRS represent a highly valuable target for TB drug discovery because of the following reasons (Hurdle et al., 2005). Firstly, the divergence between eukaryotic and prokaryotic aaRS allows for target specificity, reducing potential off-target effects. Secondly, aaRS are phylogenetically conserved in bacteria, which could widen their spectrum of activity. Thirdly, each aaRS represents an independent target for TB drug discovery, which in turn opens up possibilities for drug development for each of the eighteen tRNA synthetases in the *M.tb* proteome. Fourthly, the essentiality of these targets due to the lack of alternative aaRS makes these proteins attractive targets for drug development.

To date there is only one commercially available antibiotic that targets isoleucine-tRNA synthesis, mupirocin, a bifunctional inhibitor with respect to isoleucine and ATP, consistent with structural similarities to isoleucyl-AMP, the aminoacyl-adenylate

intermediate (Yanagisawa et al., 1994) (Nakama et al., 2001). However, its use is restricted to topical infections caused by *S. aureus* and other Gram positive bacteria due to the poor instability of the antibiotic (Sutherland et al., 1985). A number of preclinical candidates that are currently under development targeting LeuRS have shown good biochemical and whole-cell potency (Palencia et al., 2016), but clinical trials are yet to validate their safety and effectiveness. The most promising preclinical candidate, GSK070, developed by Anacor Pharmaceuticals in conjunction with GSK, inhibits LeuRS through a tRNA-trapping mechanism in the editing domain of the enzyme in such a way that prevents leucine from being transferred onto the 3' hydroxyl group of the A76 of the tRNA (Zhao et al., 2015). A few other natural products inhibiting tRNA synthetases, including ThrRS, TrpRS, PheRS, IleRS, ProRS and LeuRS have been discovered (Hurdle et al., 2005) (Fig. 20). However, lack of whole-cell potency and poor selectivity over the human enzyme counterparts has rendered these inhibitors ineffective as chemotherapeutic agents for bacterial infections (Chopra et al., 2002). Despite considerable divergence between prokaryotic and eukaryotic tRNA synthetases are able to predict selectivity and therefore clinical safety, a selectivity assessment needs to be performed on a case-by-case scenario. It is important to consider that each particular tRNA synthetase recognises the same ATP molecule and amino acid side chain regardless of the origin of the organism. Therefore a certain degree of sequence similarity on the aminoacyladenylate-binding pocket is expected. The current development of inhibitors against kinases in cancer (Zhang et al., 2009) highlights the need for a thorough assessment of selectivity over orthologous proteins to evaluate potential off-target effects in downstream studies. If selective inhibition of the target of interest is not achieved the hit-to-lead development of such an inhibitor should be abandoned and the target used to screen for other selective molecules that can pharmacologically validate the target (Davis et al., 2011).


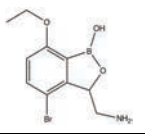
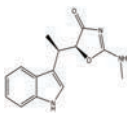
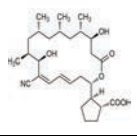
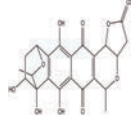
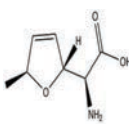
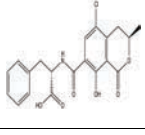
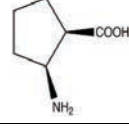
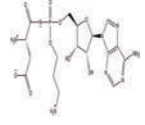
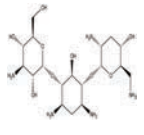
Inhibitor	Structure	aaRS targeted	Binding mechanism	Species (<i>spp</i>)	Aspects
Mupirocin		IleRS	Bifunctional inhibitor	<i>S.aureus</i> and other Gram + bacteria	Restricted to topical infections
GSK070		LeuRS	Trapping mechanism (covalent)	<i>M.tuberculosis</i> (including MDR and XDR)	Investigational
Indolmycin		TrpRS	Tryptophan competitive	Inactive	Poor permeability
Borrelidin		ThrRS	Unknown	<i>P.falciparum</i>	Inactive against bacteria
Granaticin		LeuRS	Leucine competitive	Gram + bacteria	Toxic
Furanomycin		IleRS	Isoleucine competitive	Inactive	Poor permeability
Ochratoxin A		PheRS	Unknown	Unknown	Carcinogenic
Cispentacin		ProRS	Proline competitive	<i>C.albicans</i>	Unkown potency against bacterial infections
Microcin C		AspRS	ATP competitive	Inactive	Poor permeability
Tobramycin		AspRS	tRNA competitive	Inactive	Poor permeability

Table 2. Reported inhibitors against tRNA synthetases. Note the lack of whole-cell activity due to poor permeability across bacterial membranes and the high toxicity for some entities, presumably due to a conserved binding mechanism across orthologous tRNA synthetases.

2.1.3 *M.tb* aspartyl-tRNA synthetase as potential target for the development of small molecule inhibitors

M.tb aspartyl-tRNA synthetase (Mt-AspS) belongs to the class II series of tRNA synthetases that catalyse the aminoacylation of tRNA with aspartic acid (L-Asp) (Fig. 19). Predicted to be essential since unique structural features of aminoacyl-tRNA synthetases do not allow recognition of non-cognate amino acids, its inhibition would block protein synthesis, leading to an accumulation of free L-Asp and tRNA molecules, and eventually cell death. Target identification studies looking at non-synonymous single nucleotide polymorphisms (SNPs) identified mutations in Mt-AspS (D179A, F521A, T570A) in resistant isolates against a thiazolidinone-core containing compound (Fig. 20) (Ioerger et al., 2013). In the same study, mutations in Mt-AspS were transferred back into wild type *M. bovis* BCG by recombineering and colonies were able to grow up to a compound concentration of 32 μ M, suggesting a direct role in resistance. Using similar functional genetic studies, our group showed that overexpression of Mt-AspS in BCG conferred resistance to GSK3448232A up to 13 μ M in solid plates (Fig. 21) (Gurcha et al., 2014). Biochemical evidence of Mt-AspS inhibition and therefore target validation of the rhodanine scaffold GSK3448232A was also shown by a tRNA-independent biochemical assay (Fig. 22). Taken together, a high level of resistance conferred by spontaneous mutations, an overexpression assay and biochemical inhibition confirmed Mt-AspS as the target of this series of compounds that could potentially be optimised through medicinal chemistry efforts during a hit-to-lead optimisation phase. Furthermore, the availability of a tRNA-independent biochemical assay permits biochemical validation of screening hits against an Mt-AspS-overexpressor *M. bovis* BCG strain and a subsequent mechanistic characterisation to determine reversibility type and time/enzyme dependence, etc.

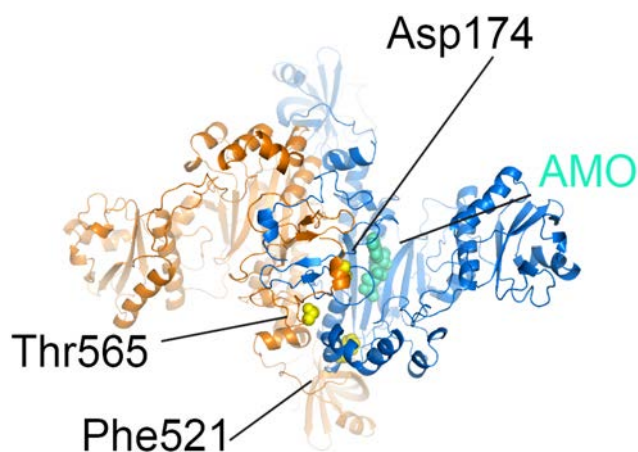


Figure 19. *M. smegmatis* AspS crystal structure. Resistance-conferring mutations are highlighted in yellow spheres. These residues fall into close proximity of the aspartyl-adenylate binding site, the reaction intermediate (AMO, green spheres), suggesting that the compound interferes with aspartate transfer onto the tRNA (Gurcha et al., 2014).

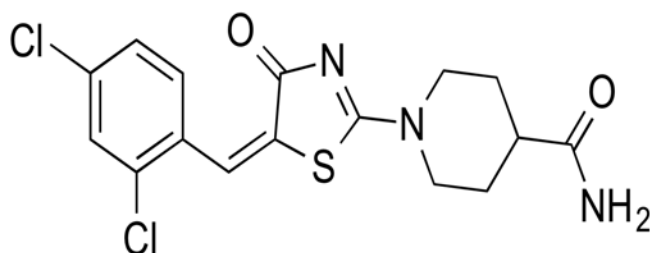


Figure 20. Structure of the rhodanine parent compound GSK3448232A The drug-to-target approach was followed to identify AspS as the target of this series of chemical entities (Ioerger et al., 2013).

The assay used for the biochemical validation of Mt-AspS the target of these series is a tRNA-independent pyrophosphate exchange protocol (Lloyd et al., 2013) adapted to a 96-well-format that consists of a three-enzyme coupled reaction (Mt-AspS, hexokinase and

glucose 6 phosphate dehydrogenase) using nicotinamide adenine dinucleotide phosphate (NADPH) fluorescence as a readout, avoiding therefore the technical and spatial requirements needed in radioactive assays (Fig. 23). The first enzymatic step is the formation of an aminoacyl-adenylate intermediate (AMP-L-Asp) from β - γ -methyleneadenosine 5-triphosphate (ADPCP) and L-Asp (L-Asp) that is subsequently cleaved with inorganic pyrophosphate (PPi) to release adenosine triphosphate (ATP), which is coupled to hexokinase (HK) phosphorylation of glucose to glucose-6-phosphate (G6P) which is then oxidised by glucose-6-dehydrogenase (GLC6PDH) to gluconate as NADP is reduced to NADPH, that finally emits fluorescence when excited at 350nm (Fig. 23). Having a biochemical assay set up enables not only hit optimisation during the lead generation phase, but also allows target validation of Mt-AspS inhibitors that may have been previously screened in a whole-cell target-based assay.

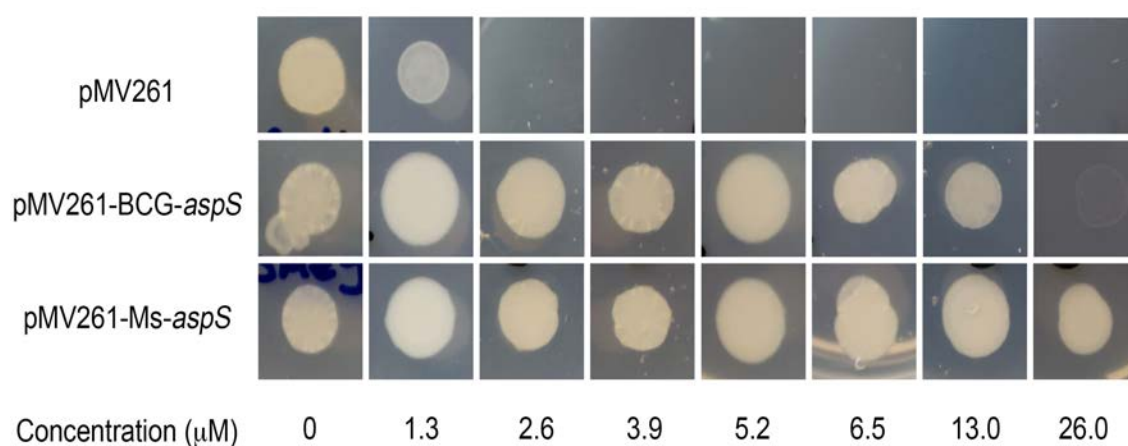


Figure 21. Effects of *M. bovis* AspS overexpression on cell growth on 7H11 agar plates. Strains harbouring pMV261-AspS from both *M. bovis* BCG and *M. smegmatis* grew up to a compound concentration >4-fold higher than the empty pMV261-plasmid containing control strain, confirming whole-cell target engagement. Figure reproduced from (Gurcha et al., 2014), free for distribution under the Creative Commons Attribution licence.

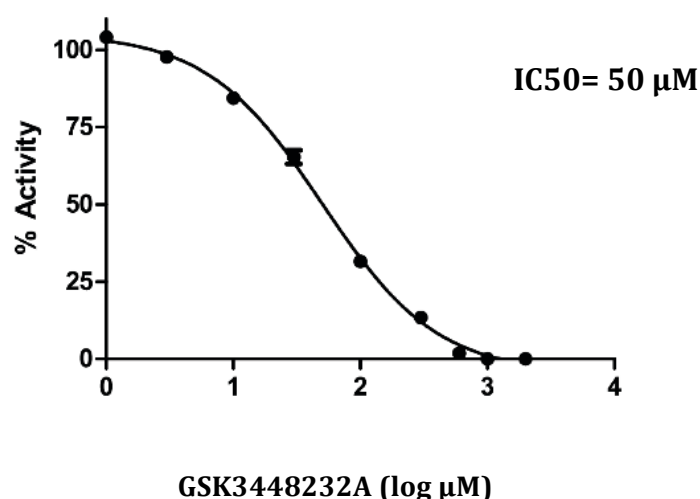


Figure 22. Dose-response *in vitro* activity curve of the effect of a rhodanine scaffold (Fig. 20) against Mt-AspS in a tRNA-independent coupled reaction. GSK3448232A (0.1-100 μM in a 1/3 dilution fashion) was pre-plated into a 96-well plate containing 190 μL of assay mixture and 500 μM PPi was used to trigger the reaction in a Pherastar plate reader. Slopes (FI/s) were standardised to percentage enzyme activity values and plotted against the logarithm of inhibitor concentration on Prism 6.0 for the determination of the IC₅₀. Figure obtained from (Gurcha, et al 2014), free for distribution under the Creative Commons Attribution license.

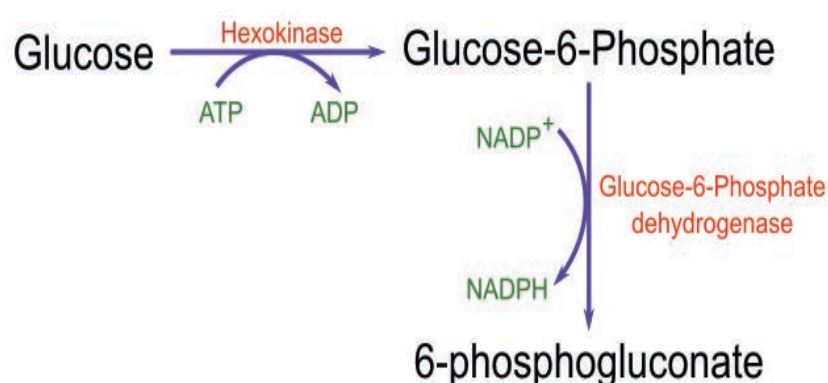


Figure 23. Schematic representation of a tRNA-independent coupled reaction. Free ATP generated from the AspS catalysed reaction feeds a hexokinase, which in turn phosphorylates glucose into glucose-6P. This in turn is oxidised by a glc6P-dehydrogenase to generate 6-phosphogluconate and NADPH, which can be measured fluorimetrically at 450nm. Figure extracted from Wikimedia Commons, no copy right restrictions apply.

A SAR map for the parent compound GSK3448232A (Fig. 20) has been generated based on biological (on-target and whole-cell activity) and physicochemical data. Furthermore, in order to further exploit Mt-AspS as a viable drug target we have identified several chemical entities using a combination of the two mainstream drug discovery approaches. Target-based screening of the GSK TB set of 177 compounds against the tRNA independent coupled reaction in 96-well-format was performed, whereas a whole-cell target-based screening strategy was used to screen the GSK TB box collection of 11,000 chemical entities, allowing the straightforward identification of inhibitors against a given target of interest based on resistance upon target overexpression. However, the main drawback of this assay is the physiological effect of genetic manipulation on the transcriptional regulatory network of alternative signalling pathways, which can potentially up or downregulate alternative targets. Since, it is essential to biochemically validate on-target binding we have miniaturised the tRNA-independent assay to 384-well-format for HTS application. The rationale behind this strategy is to ensure the straightforward identification of Mt-AspS inhibitors by a target-based HTS assay in case whole-cell screening hits fail to be validated against the enzyme due to the reasons stated above.

2.2 Results

2.2.1 *M.tb* AspS protein purification

Soluble amounts of enzymatically active Mt-AspS were obtained when 25 mL of lysis buffer containing 20 mM Tris pH 8, NaCl 500 mM, 10% glycerol and 40 mM imidazole were used to resuspend thawed pellets of C41 *E. coli* that had been chemically induced with IPTG to overexpress the recombinant protein from a pET28b vector. The supernatant was loaded onto a pre-packed Ni²⁺-containing IMAC column and the protein

was eluted with a step-wise imidazole gradient. Relevant fractions containing Mt-AspS (Fig. 24) were pooled, concentrated with an Amicon filtration unit (30 KDa cut-off membrane) and dialysed for 16h in 4 L of 20 mM Tris pH 8, 50 mM NaCl and 10% glycerol to remove imidazole and the high salt concentration that might interfere in follow-up biochemical assays. Similar protein concentrations (250 μ M) were obtained across independent batches at the University of Birmingham, whereas no more than 80 μ M could be obtained in GSK using identical protein purification conditions. However, as described later, the miniaturisation to 20 μ L assay volume compensated for the decrease in protein yield during purification.

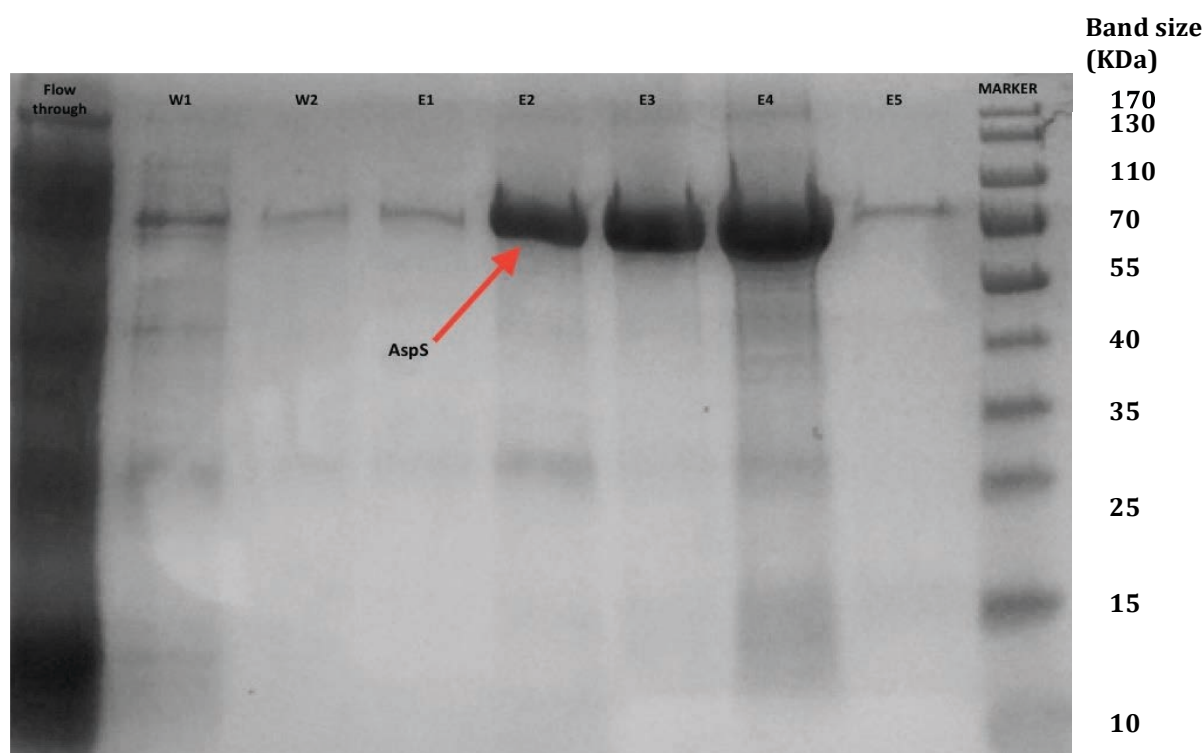


Figure 24. Identification of relevant fractions containing AspS using Bio-Rad pre-cast SDS (10%) Tris-glycine PAGE gels. A step-wise imidazole gradient was used to elute the polyhistidine-tagged AspS protein from a Ni²⁺-containing IMAC column. FT: flow-through (50 mL); W1-2: washing buffer (25 mL); E1-2-3-4-5 (20 mL): elution fractions containing an imidazole gradient (50-75-100-250 and 500 mM imidazole, respectively).

2.2.2 Enzyme activity confirmation by a tRNA-independent biochemical assay

Prior to any screening campaign it is essential to assess enzyme linearity at several protein concentrations to establish assay sensitivity. Desirably, the system should allow detection of enzyme activity from submicromolar amounts of protein with optimal Z' values. If this goal is non-achievable, higher concentrations of enzyme should be employed to increase the signal-to-background ratio, but this is going to limit the maximum measurable compound potency (IC_{50}) to be detected in dose-response assays, which can potentially be problematic to assign accurate IC_{50} values to the most potent compounds. Therefore, an enzyme dose-response concentration curve should be performed between protein batches for the highest possible assay quality and optimal results. The assay was performed at matching K_M values for L-Asp, ADPCP and PPi, excess amounts of the couple enzymes HK and GLC6PDH and varying concentrations of Mt-AspS (Fig. 25), monitoring NADPH fluorescence in a continuous mode using a Pherastar microplate reader. A concentration of 3 μM gave the best results in terms of signal-to-background ratio and Z' values for screening purposes and dose-response studies. Lower concentrations than 1 μM were not represented due to a decrease in assay performance.

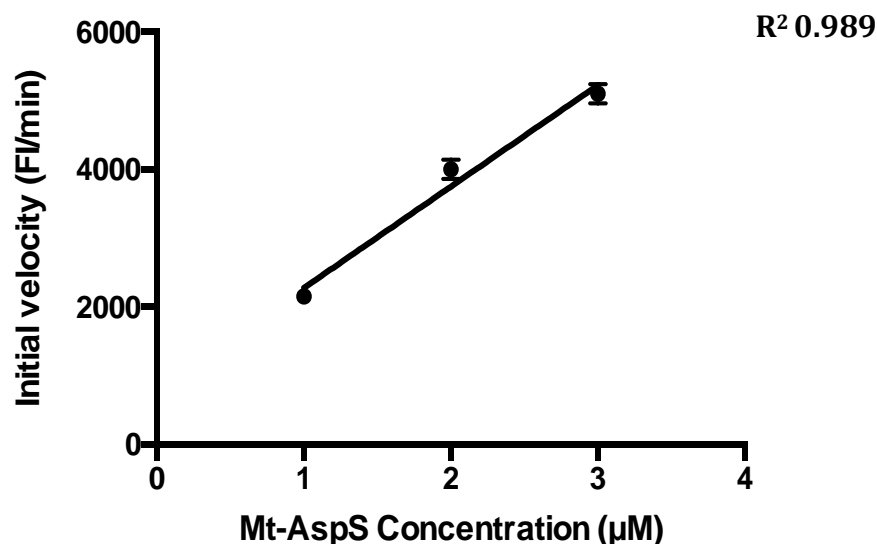


Figure 25. Dose-response *in vitro* Mt-AspS activity at several protein concentrations in order to establish assay quality and sensitivity. Background fluorescence in the absence of enzyme is subtracted to enzyme activity-containing wells and plotted over the total amount of enzyme employed in the assay. A linear regression model was fitted on Excel and R^2 is reported as a measure of goodness of this fit.

2.2.3 Identification of novel *M.tb* AspS inhibitors by a target-based tRNA-independent biochemical assay

Three compounds from the TB set collection of 177 novel chemical entities named CCI14012, GSK9911960A and GSK381407A with batch identification codes PWS/700/1, ST/796668 and ST/476208, respectively (Fig. 26), were validated in dose-response studies after an initial screen at 100 μM was performed in duplicate against Mt-AspS in a tRNA-independent biochemical assay. Optimal assay performance was achieved ($Z' > 0.8$) which was monitored in an inter-plate manner. The initial hits showing inhibitory values higher than 50% were cherry-picked from assay plates for potency determination, giving an overall hit rate of 1.69%. Compounds were received from GSK as 10 mM stocks in 100% DMSO and were dispensed into black-bottom assay plates in a 1:3 dilution fashion

up to a maximum concentration of 300 μM . The assay mixture (200 μL), containing substrate at concentrations matching K_M values was added into each assay well and PPI was used to trigger the reaction in a Pherastar microplate reader. Raw fluorescence kinetic values from a continuously monitored Mt-AspS-catalysed reaction were measured at initial reaction rates (zero order kinetics) and standardised to positive and negative controls using GraphPad Prism 6.0. Enzyme activity percentages were plotted versus the logarithm of the inhibitor concentration and sigmoidal dose-response curves were fitted for IC_{50} determination (Fig. 27).

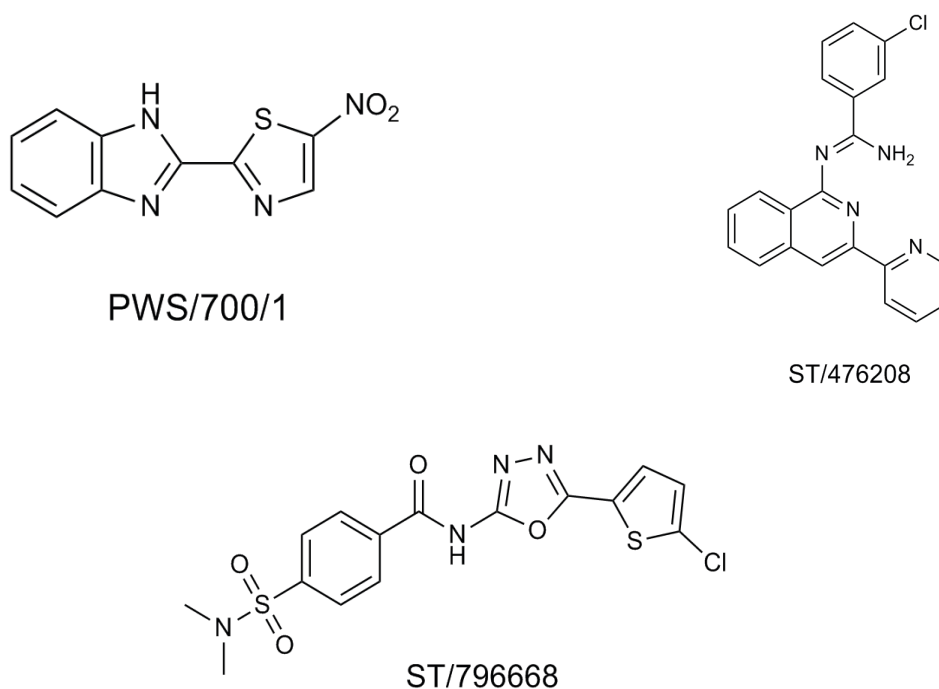


Figure 26. Structure and batch identification codes of the newly identified anti-mycobacterial compounds that target the essential aspartyl-tRNA synthetase Mt-AspS. These hits were identified through a target-based biochemical assay against the GSK TB set collection of 177 compounds (Ballell et al., 2013). Details of the physicochemical and biological data are also shown in the supplementary section together with the rest of AspS validated hits shown in this thesis.

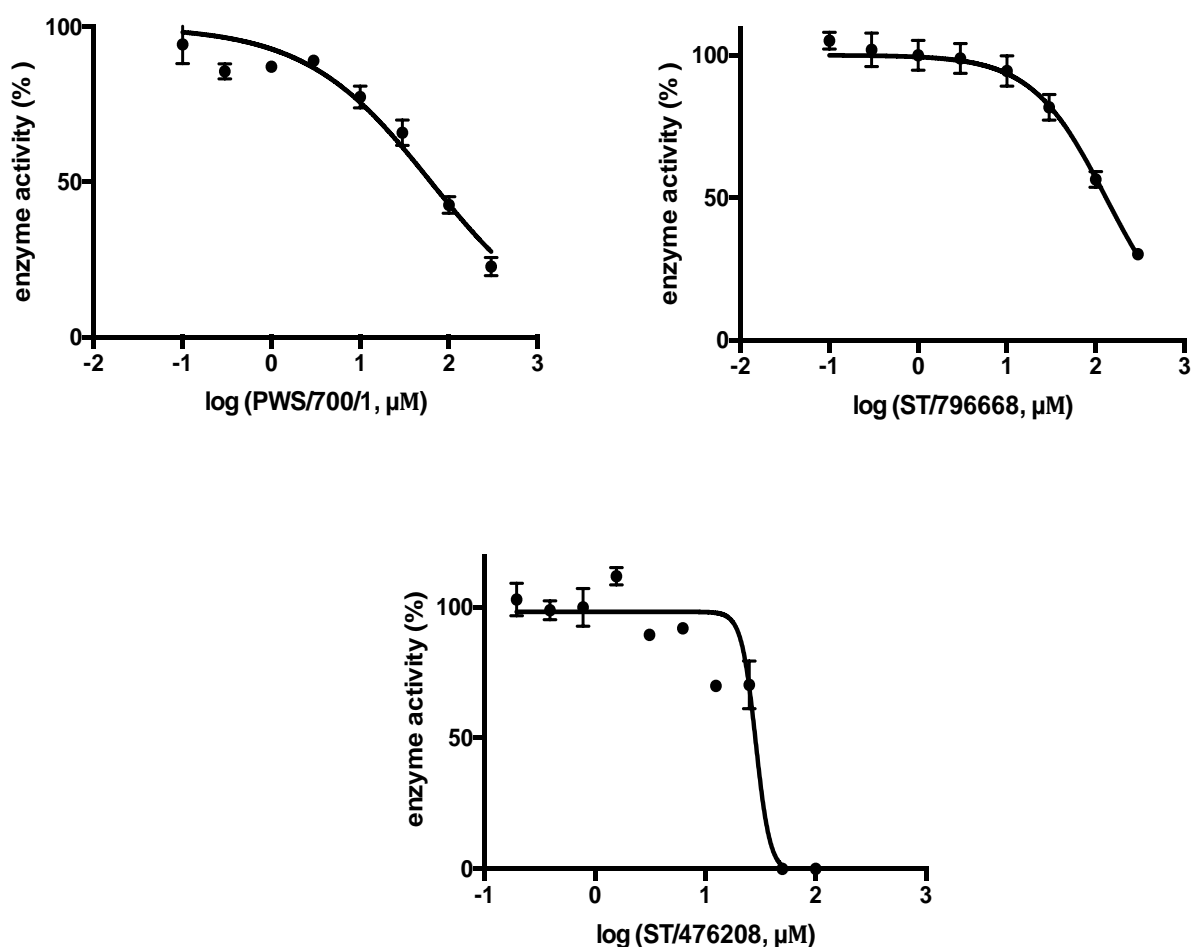


Figure 27. Dose-response *in vitro* activity curves of the effect of several anti-mycobacterial compounds against Mt-AspS in the tRNA-independent aminoacylation reaction. Reaction mixtures were added to increasing compound concentrations and read in the microplate reader Pherastar BMG after the addition of PPI. Slopes corresponding to fluorescence units/minute were obtained on Mars software and plotted versus the logarithm of inhibitor concentration for IC₅₀ determination.

These results indicate a clear dose-dependent inhibition of Mt-AspS activity with apparent IC₅₀ values of 62.44 μ M (PWS/700/1), 130.8 μ M (ST/796668) and 28.66 μ M

(ST/476208). Despite their relatively weak potency these inhibitors represent good starting points for future medicinal chemistry optimisation efforts. The full profiling of these hits is attached in the Supplementary Section.

2.2.4 Counter-screening assay against an HK/GLC6PDH coupled reaction

As mentioned above, the inhibitory activity of these compounds shown in the IC₅₀ plots could be related to compound binding to either HK or GLC6PDH, and not directly from Mt-AspS inhibition. It is therefore essential to find out whether any of these compounds from the 177 hit set are exclusively Mt-AspS inhibitors to de-risk entities with multi-target activities. Each compound from the TB set was tested at 100 μ M against a reaction mixture with HK and GLC6PDH using NADH absorbance kinetics as the method of detection. No assay interference due to off-target activities was detected at this concentration. To confirm on-target activities of these hits, compound PWS/700/1 was tested at 100, 300 and 500 μ M in the HK/GLC6PDH reaction (Fig. 28).

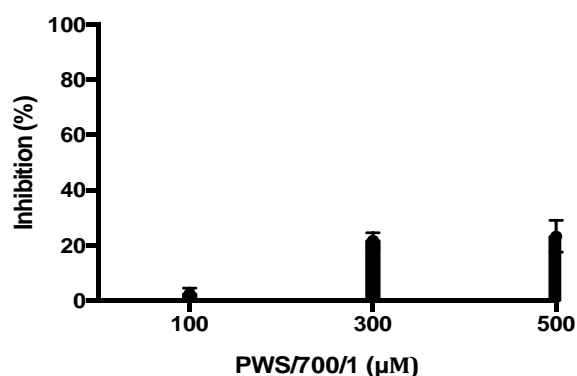


Figure 28. Effect of PWS/700/1 on HK and GLC6PDH activity at 100, 300 and 500 μ M. Glucose was added to reaction mixtures in 96-well-plates and read in a Pherastar BMG in the absorbance mode. Slopes (optical density/min) were standardised to the positive and negative controls for enzyme activity and plotted versus each of the concentrations.

Inhibitory activities can be seen at concentrations above 100 μ M but are most likely due to non-specific binding (aggregation) or interference with the method of detection. It has to be taken into account that in any coupled system the concentration of coupled enzymes is in excess in order to prevent undesired off-target activities.

2.2.5 Mechanistic characterisation of PWS/700/1, ST/476208 and ST/476208, the three screening hits identified from the 177 TB set

2.2.5.1 Mode of action studies

2.2.5.1.1 Substrate competition studies

In order to gain mechanistic insight into compound binding, the activity of Mt-AspS was assessed in a substrate dose-response manner with respect to the aspartyl-adenylate substrate intermediate at several inhibitor concentrations (0, 50 and 100 μ M) to study the effect of the compound on maximum enzyme velocity (V_{max}) and substrate affinity (K_M). Fixed concentrations of L-Asp and PPi were kept at saturation ($10 \times K_M$ values) whilst the concentration of ADPCP was allowed to vary (0-8000 μ M). The reaction was triggered by the addition of 2X substrate mix solution (10 μ L) to a 384 black-bottom polystyrene plate (Corning) containing 2X buffer solution (10 μ L) with 1 μ M Mt-AspS. Plates were then briefly centrifuged and read on an EnVision instrument (Perkin Elmer) using NADPH fluorescence in the kinetic mode for slope determination. The raw data was standardised to controls and plotted versus substrate concentration (Fig. 29). Initial velocities were adjusted to a non-linear Michaelis-Menten regression model for the determination of the kinetic parameters, V_{max} and K_M .

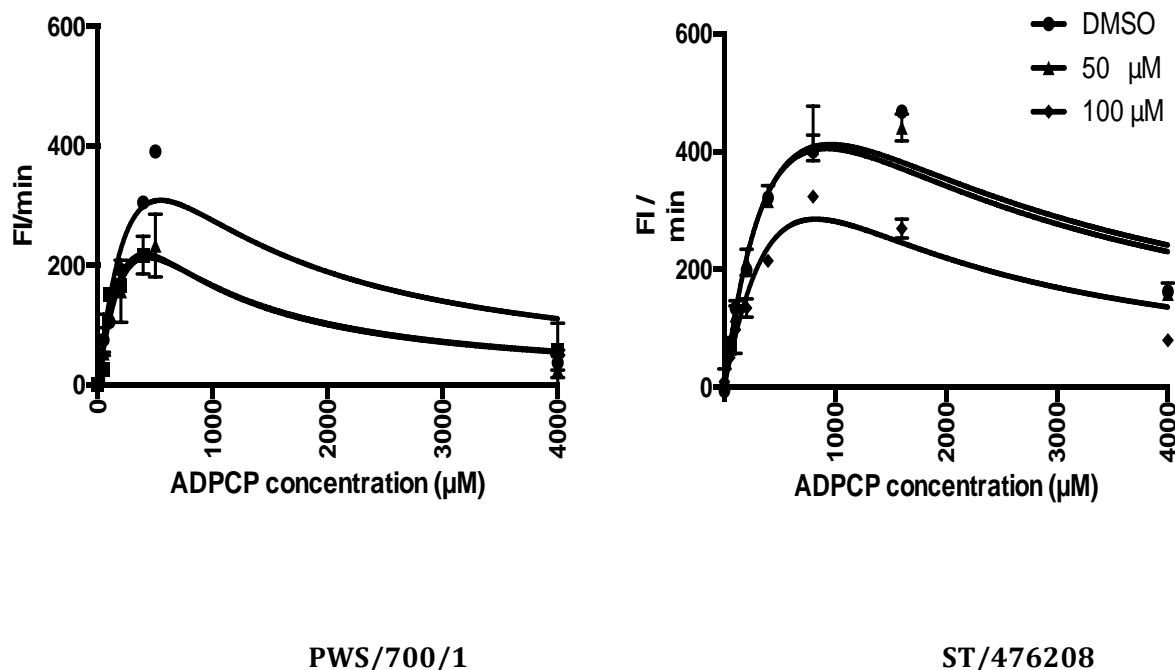


Figure 29. Reversible non-competitive inhibition of PWS/700/1 and ST/476208, two of the Mt-AspS screening hits identified from a biochemical screen. Several ADPCP (0-4000 μM) and inhibitor concentrations (0, 50 and 100 μM) were tested in duplicate alongside a microtiter 384-well-plate and enzyme velocity (raw fluorescence units per minute) plotted against ADPCP for the determination of K_M and V_{max} .

A pronounced decrease in V_{max} for both the two inhibitors tested in the assay was observed (Fig. 29). As expected from the lack of structural similarities between the aspartyladenylate intermediate and the chemical structures of these hits, the entities behave in a non-competitive manner. Note that there is a minor effect on K_M (rightwards shift) for ST/476208, which would explain mixed-type inhibitory activities.

2.2.5.1.2 Time-course dependence

Reversible inhibition in the presence of each entity was assessed over a time period of

one hour in the tRNA-independent assay. Enzyme activity controls in the presence of similar quantities of DMSO were included for data standardisation for each time point, which was assessed in duplicate (Fig. 30). The assay was performed at reported K_M values for the three substrates, 0.5 μ M Mt-AspS and buffer conditions and salt concentrations employed previously. The inhibitor concentration used in the assay was chosen when considering the IC_{50} from previous biochemical assays. Only significant amounts of compound ST/476208 were available for this particular assay.

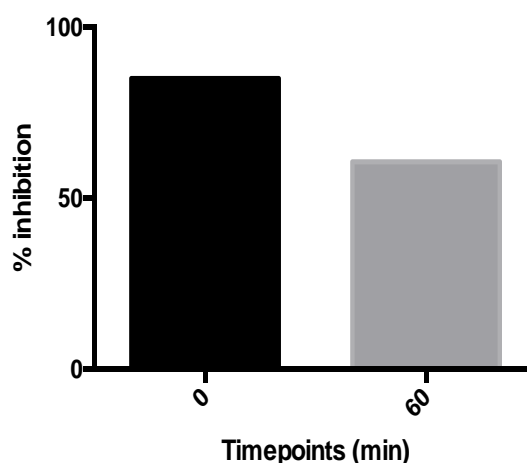


Figure 30. Time-dependence assessment of Mt-AspS inhibition in the presence of ST/476208. A flat-line behaviour can be observed over the period of the assay, suggesting reversible inhibition.

2.2.5.1.3 Enzyme dependence

The presence of non-selective inhibitors can also be determined by increased enzyme concentrations in the assay. Compounds that form colloids have the tendency to aggregate and interfere with enzyme activity in a non-specific manner due to substrate or enzyme sequestration. Due to limitations on compound availability, only ST/476208 was

interrogated for potency in dose-response studies against 0.5 μM and 5 μM Mt-AspS after ensuring that enzyme activity remained linear at high concentrations (Fig. 31).

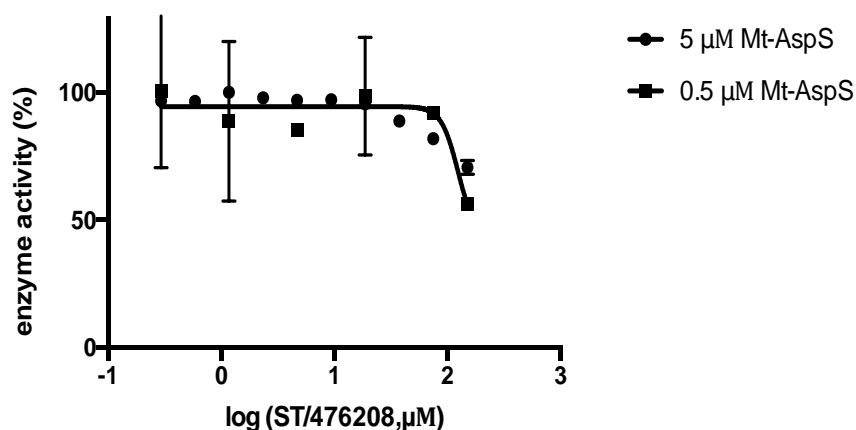


Figure 31. Dose-response *in vitro* assay at 0.5 μM and 5 μM Mt-AspS for compound promiscuity assessment. Note that there is little to no change in compound potency as for what is observed in the assay.

No significant conclusions can be extracted since there is an overall loss of compound potency in comparison to previous dose-response assays. This may happen over time due to the hygroscopic properties of DMSO. Water uptake can cause a decrease in the effective concentration of a given compound stock due to an overall increase in the hydrophilicity of storage conditions or even form small ice crystals during freeze-thaw cycles of the same aliquot (Cheng et al., 2003, Kozikowski et al., 2003).

2.2.5.1.4 DTT dependence

Compound ST/476208 was interrogated for their inhibitory activity in the aminoacylation reaction in the presence and absence of DTT (1 mM) (Fig. 32). Highly electrophilic compounds that react with cysteine residues in a non-specific manner may also react with sulfhydryl groups of reducing agents, rendering the compounds inactive against their intended target. The reaction conditions were kept identical as for substrate and enzyme concentrations previously defined for *in vitro* dose-response assays with screening hits. Slopes were analysed as previously described and normalised data was plotted against the logarithm of inhibitor concentration on GraphPad Prism for IC₅₀ determination.

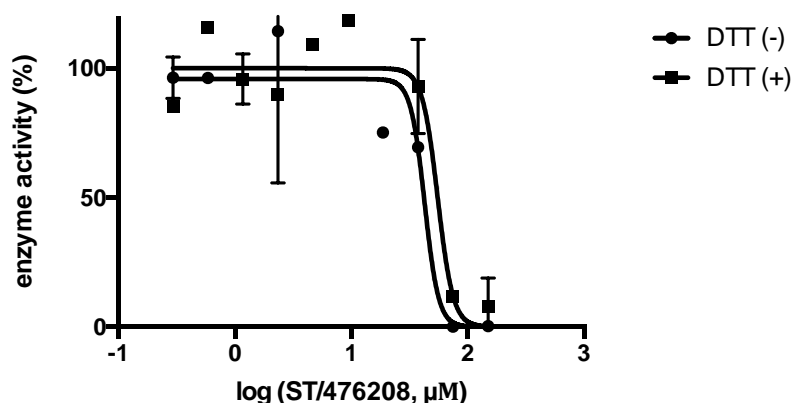


Figure 32. *In vitro* dose-response activity curves of ST/476208 in the presence and absence of 1 mM DTT. The addition of the reducing agent causes little or no effect on compound potency. Note the high variability among inhibitory values at lower compound concentrations and the steepness of the Hill slope curve, suggesting poor solubility and compound aggregation in the assay.

Among the screening hits identified in the target-based biochemical screen only ST/476208 could be tested due to compound availability issues on ST/796668. PWS/700/1, on the other hand, was interrogated in this assay but the compound had lost its potency in the aminoacylation reaction, potentially due to either compound degradation or compound solubility issues at low reaction volumes; a higher tendency to non-specific binding to polystyrene surfaces is observed for hydrophobic compounds when reaction volumes are decreased (increased surface-to-volume ratio). This needs to be considered during the assay miniaturisation phase of screening assays since it may mask compound potency in HTS applications, decreasing hit rates. When scaling assays down for HTS, non-specific binding plates should be considered to minimise the impact of assay miniaturisation on compound solubility.

2.2.6 *In vitro* profiling (SAR) of a series of GSK3448232A analogues

A full biological profiling of a series of analogues of the hit parent compound GSK3448232A was performed during the hit-to-lead optimisation phase (Table 3). The inhibitors were tested at single-shot (100 μ M) and further interrogated for their potency in a dose-response manner against Mt-AspS when inhibition was shown to be higher than 50%. The entities were also interrogated for whole-cell potency using a *M. bovis* BCG strain containing empty pMV261 and a second *M.bovis* BCG strain overexpressing pMV261-Mt-AspS.

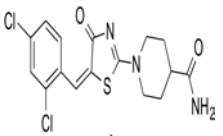
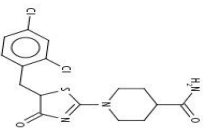
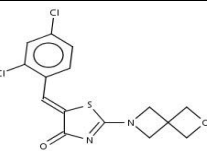
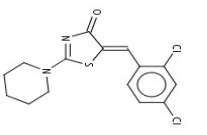
Compound ID	Structure	Mt-AspRS IC50 (μM)	MIC <i>M. bovis</i> WT BCG (μM)	MIC <i>M. bovis</i> BCG pMV261-AspRS (μM)
GSK3448232A		36.97	4	32
GSK3448775A		>300	ND	ND
GSK3485056A		14.58	0.28* ± 0.19	6.33* ± 5.31
GSK3486987A		19.02	0.57* ± 0.23	4.93*

Table 3. Summary of the SAR of the parent compound GSK3448232A. GSK3448775A showed a total drop in activity in the Mt-AspS *in vitro* assay whereas only two entities either conserved or improved whole-cell potency versus the parent compound as indicated by their respective MIC (see graphs below). Some degree of correlation of on-target and whole-cell inhibitory activities is shown by decreased IC50 values against Mt-AspS versus the parent compound. Liquid MIC and IC50 values were calculated as the mean ± SD of two and three biological replicates, respectively. ND: not-determined. Values in asterisk were calculated in liquid media. For extended SAR data check the Supplementary section. Solubility (CLND, ChromLogD) and cytotoxicity values (compound MIC against the liver cell line HepG2) shown in the Supplementary section were kindly provided by GSK.

2.2.6.1 Whole-cell target engagement of GSK3845056A and GSK2486987A

As shown above (Table 3), only two analogues, GSK3845056A and GSK2486987A, have retained their activities against intact bacteria after medicinal chemistry optimization efforts on the parent compound. On-target binding and potency against whole cells of these two entities was studied using an Mt-AspS overexpressor strain that was similarly used for HTS assays. Briefly, raw fluorescence values obtained upon resazurin reduction by viable cells were standardised to cell survival percentages and plotted versus the logarithm of each inhibitor concentration on GraphPad Prism for MIC determination. Resistance upon target overexpression (MIC shift) confirms target engagement in whole-cell assays (Fig. 33), being another piece of evidence that these molecules have managed to retain inhibitory activity against whole cells and the target.

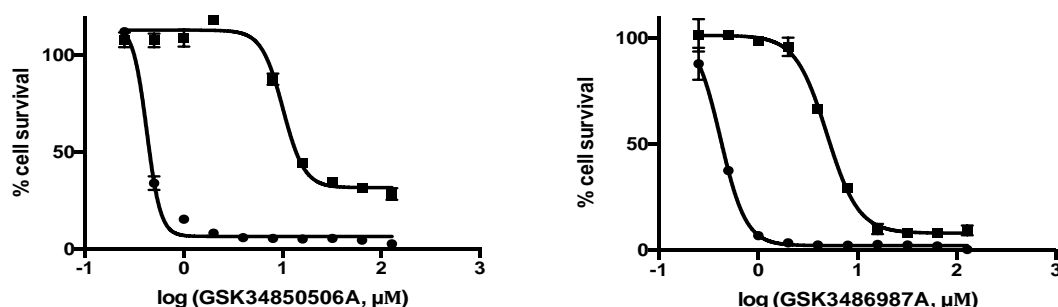


Figure 33. Whole-cell *in vitro* potency assays of two analogues of the parent compound GSK3448232A against a *M. bovis* BCG pMV261-Mt-AspS overexpressor strain (solid squares) and an empty pMV261-containing *M. bovis* BCG strain (solid circles). Raw fluorescence units were standardised to survival percentages values and plotted over the logarithm of a range of inhibitor concentrations (0.125-128 μM). Sigmoidal dose-response curves were fitted on GraphPad Prism to obtain MIC values, here shown as the mean ± SD of two biological replicates (Table 3). Each assay was done in duplicates on two independent days to assess day-to-day reproducibility.

The results highlight the essentiality of the Michael-acceptor group for its inhibitory activity against Mt-AspS. This led us to hypothesise that GSK3448232A and its active analogues could have a covalent mechanism of action. Michael-acceptor groups are α , β -unsaturated carbonyl compounds that have electron-withdrawing properties, making them susceptible to attack by protein nucleophiles, such as the thiol group of cysteine residues. A covalent inhibitor might be deemed useful if its mechanism of action is well defined and not conserved across species (Makarov et al., 2009). The downside of covalent inhibition is that they could react with alternative nucleophiles (off-target properties) with potential detrimental effects to humans. The formation of covalent adducts on other proteins can lead to idiosyncratic drug reactions if the resulting molecule is processed and presented to the adaptive immune system (Warrington, 2012). Therefore, de-risking potential covalent inhibitors requires knowledge on their precise mode of action and affinity of a particular chemical entity. Several counter-screening assays can be informative on the covalent behaviour of a given chemical entity, e.g. activity in the presence and absence of DTT, mass spectrometry analysis of protein-compound adducts, time-dependence, etc.

2.2.6.2 Counter-screening assay against a hexokinase/glucose-6-phosphate dehydrogenase coupled reaction

Each compound was tested against the two-coupled enzymes in order to assess potential off-target effects of this series (Fig. 34). Each compound was tested in duplicate at two concentrations, 100 and 300 μ M and raw absorbance values were normalised to

inhibition percentages with the positive and negative controls for enzyme activity in the presence of DMSO.

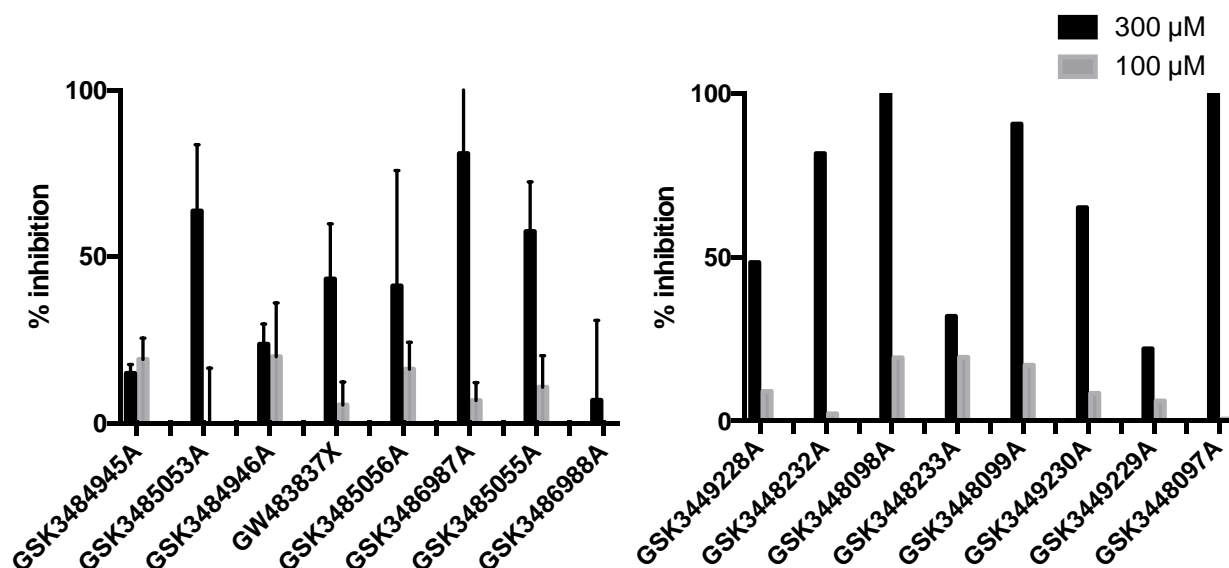


Figure 34. Promiscuous activity of a series of analogues of the parent compound GSK3448232A against the HK/GLC6PDH coupled reaction at two different concentrations (100 and 300 μ M). Glucose was used to trigger the reaction and plates were read in the absorbance mode in a Pherastar plate reader. Raw absorbance units were standardised to the maximum and minimum enzyme activity controls in the presence of DMSO and plotted against each inhibitor concentration.

The apparent increase in compound inhibition from 100 to 300 μ M could potentially be related to an unspecific effect caused by compound aggregation or interference with the method of detection. Some entities were coloured, which would explain interference with absorbance at 450 nm. However, due to the fact that NADH absorbance is measured in continuous kinetic mode and the poor solubility of these analogues in aqueous solutions, such a drop in enzyme activity might be related to an unspecific compound interaction

with HK/GLC6PDH rather than due to interference with the method of detection. The apparent inhibition of the HK/GLC6PDH reaction only occurs at concentrations above the compound IC₅₀ values when Mt-AspS is present, showing that Mt-AspS inhibition is genuine and not a result of assay artefacts. Moreover, in any coupled-reaction based assay the amount of coupled enzyme is well above the target protein concentration, precisely to minimise assay interference due to off-target activities. The apparent inhibitory activities seen in these assays are in fact a result of assay artefact due to the high concentration employed in the assay.

2.2.7 Mechanistic studies of the hit compound against *M.tb* AspS

2.2.7.1 Mass spectrometry analysis of Mt-AspS incubated with the parent compound GSK3448232A

Taking the IC₅₀ data into consideration from previous biochemical assays with parent compound derivatives, we incubated Mt-AspS with the hit compound at a 30:1 compound/protein ratio and submitted our samples for trypsin digestion and mass spectrometry analysis. Among the digested peptides identified covering 63% of the target protein, we could not observe any covalent modification on any of the peptides with residues presumably involved in resistance against the parent compound observed in *M. bovis* BCG spontaneous resistant strains. The full data analysis is attached in the Supplementary Section. However, as in any *in vitro* system, physiological conditions cannot be mimicked completely. The protein protonation pattern might not be identical to that of the bacterial cytosol, possibly changing amino acid reactivity, which could affect compound binding.

2.2.7.2 Structural studies of *M.tb* AspS in complex with GSK3448098A

Several attempts were made to obtain the crystal structure of the Mt-AspS-inhibitor complex with the most soluble compound synthesised by GSK as reflected by chemiluminiscent nitrogen detection (CLND) data (Supplementary Section). However, we could only obtain small diffracting crystals. A weak inhibitor (IC₅₀ in the high micromolar range) requires quite a high compound/protein ratio in order to displace the equilibrium reaction towards the formation of the protein-inhibitor complex. The drawback of such approach is that the crystallisation solution will limit the solubility of the compound under such conditions, which will cause the compound to precipitate out of solution. In the absence of a crystal structure, however, other mechanistic approaches can shed light into the mechanism of action of this set of compounds.

2.2.7.3 Time-course dependence

Enzyme activity in the presence of GSK3449228A, one of our most soluble analogues, was assessed over a time period of two hours in the tRNA-independent assay and enzyme activity controls with DMSO were included for data standardisation for each time point, which was assessed in duplicate (Fig. 35). The assay was performed at reported K_M values for the three substrates using buffer conditions and salt concentrations as in the previous dose-response and mechanistic studies and 0.5 µM Mt-AspS. The inhibitor concentration used was chosen taking into account IC₅₀ inhibitory values from previous biochemical assays at a final protein:compound ratio of 1:30.

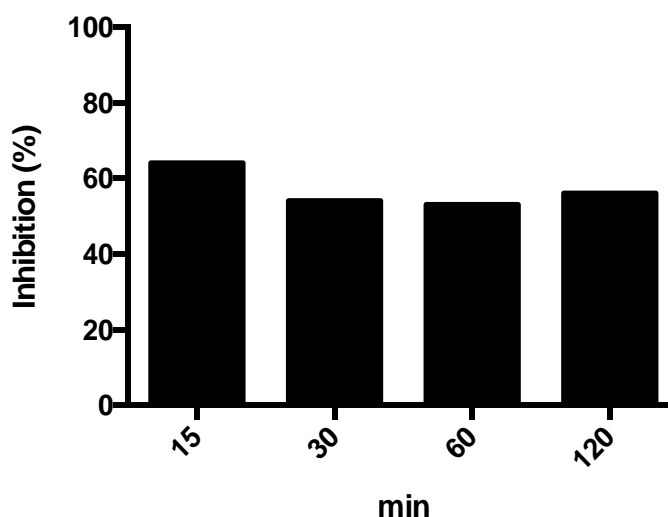


Figure 35. Time-course assessment of GSK3449228A. The compound-enzyme complex was previously incubated at a 30:1 ratio using the same final DMSO concentration as an enzyme activity control at every time-point in the absence of compound.

The flat-line behaviour suggests that the inhibitor reaches an equilibrium state with the enzyme that remains constant throughout the period of the assay, consistent with classical Michaelis-Menten kinetics of rapid, reversible inhibition. If the compound acted in an irreversible or in a slow-tight binding manner the enzyme activity would drop over time due to either the formation of a protein-compound adduct or the gradual increase shown by slow-onset inhibitors.

2.2.7.4 Substrate competition studies

The activity of Mt-AspS was assessed in a substrate dose-response manner at several inhibitor concentrations to study the effect of the compound on V_{max} and K_M with respect to the aspartyl-adenylate intermediate. The concentrations of L-Asp and PPi were kept at saturation ($10 \times K_M$ values) whilst the concentration of ADPCP was allowed to vary. The

reaction was triggered with PPi and read in kinetic mode for slope determination, which was then plotted versus substrate concentration for the determination of V_{max} and K_M (Fig. 39).

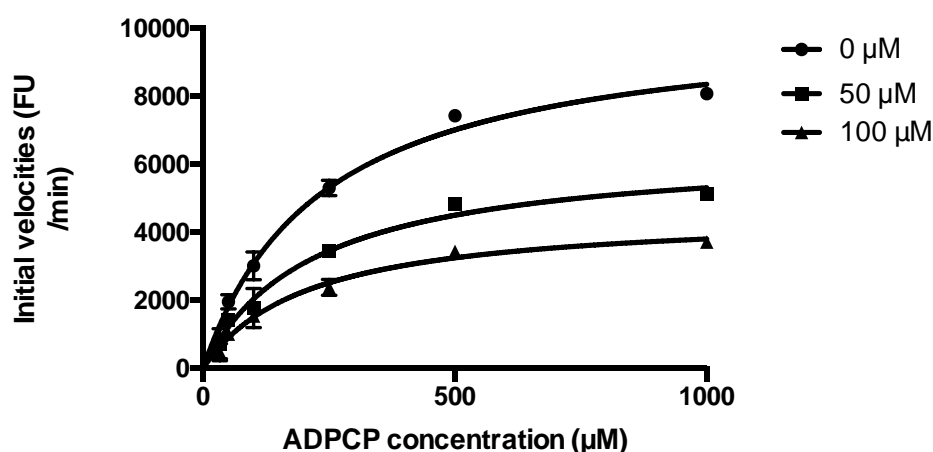


Figure 36. Reversible non-competitive mode of inhibition of GSK3449228A as shown by a decrease in V_{max} . Several substrate and inhibitor concentrations were tested alongside a microtiter 96-well-plate and enzyme velocity (raw fluorescence units per minute) was plotted against each of the inhibitor concentration for the determination of K_M and V_{max} .

A clear reduction in V_{max} values and a slight decrease in apparent K_M was observed as the inhibitor concentration increased from 0 μM (DMSO control) to 100 μM (Fig. 36). This experiment represents one of three independent replicates run on different days to assess reproducibility. Whereas, K_M values change inconsistently across replicates, the pronounced decrease in V_{max} confirms that this series of inhibitors are non-competitive, as expected from the location of the missense mutations identified in whole-genome sequencing studies (binding pocket next to the substrate binding site) and the absence of

structural similarity between this chemical series and the aspartyl-adenylate intermediate.

2.2.8 Purification of recombinant *Homo sapiens* mitochondrial Hs-AspS

Lysis buffer (25 mL) containing 20 mM Tris pH 8, NaCl 500 mM, 10% glycerol and 40 mM imidazole was used to re-suspend thawed pellets of *E. coli* C41 that had been chemically induced with IPTG to overexpress Hs-AspS. Cells were disrupted with 8 sonication cycles (30s on/off) and centrifuged at 15000 rpm for 45 minutes. The supernatant was loaded onto a pre-packed Ni²⁺-containing IMAC column and the protein eluted with a step-wise imidazole gradient. Relevant fractions containing Hs-AspS (Fig. 37) were pooled, concentrated with an Amicon filtration unit (30 KDa cut-off membrane) and dialysed for 16h in 4 L of 20 mM Tris pH 8, 50 mM NaCl and 10% glycerol to remove imidazole and decrease the salt concentration that might interfere with follow-up biochemical assays. Protein concentrations of around 8 mg/mL were obtained across independent batches. The quantities achieved were sufficient to biochemically characterise the enzyme and the inhibitors. As observed in the gel below, the human mitochondrial Hs-AspS was similarly eluted in the same fractions as the mycobacterial counterpart.

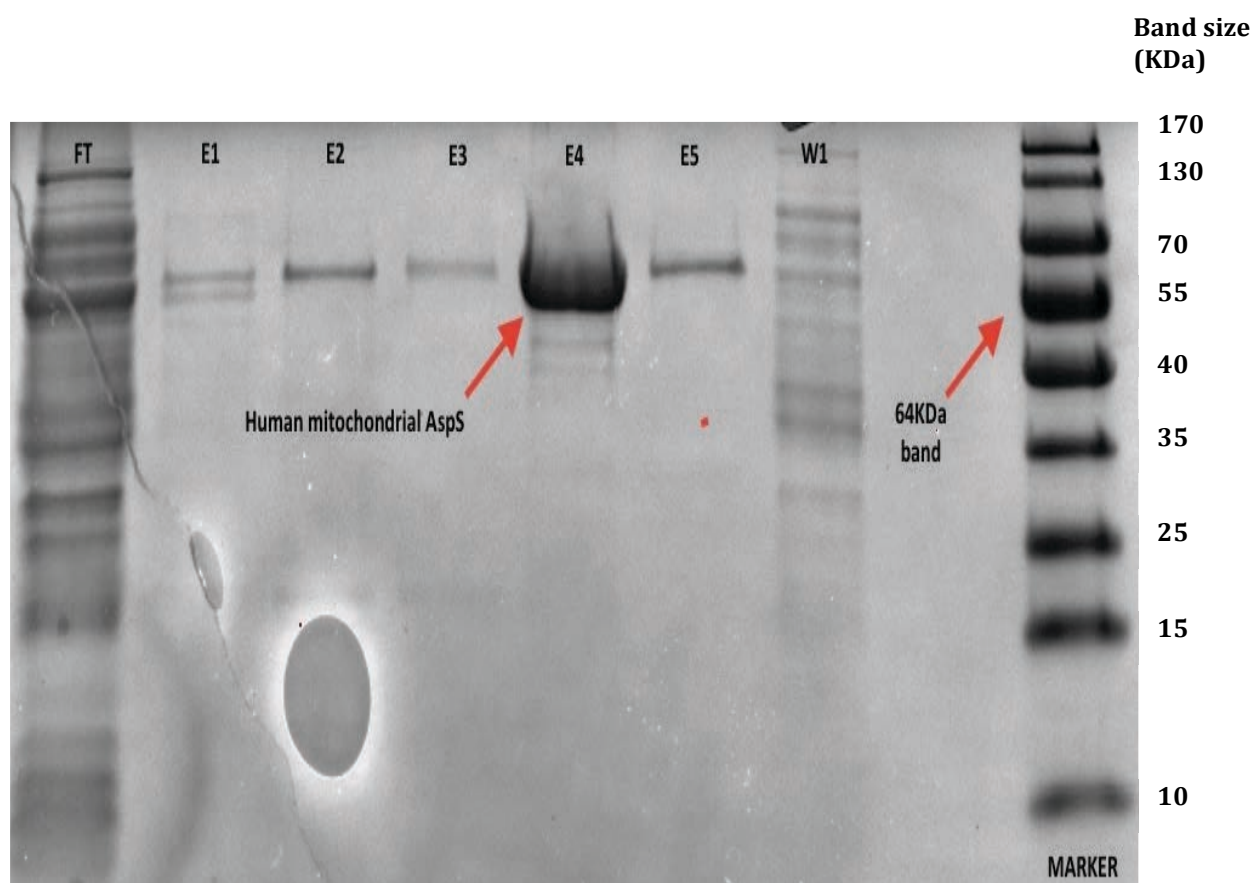


Figure 37. Bio-Rad pre-cast SDS Tris-glycine (10%) PAGE gel showing the relevant fractions containing the human mitochondrial Hs-AspS (67 KDa band) purified by affinity chromatography. A step-wise imidazole gradient was used to elute the polyhistidine-tagged AspS protein from a Ni²⁺-containing IMAC column. From left to right gel lanes: FT: flow-through (50 mL); E1-2-3-4-5 (20 mL), elution fractions containing an imidazole gradient (50-75-100-250 and 500 mM imidazole, respectively); W1: washing buffer (25 mL), Page ruler (Fermentas).

2.2.9 Biochemical characterisation of the human mitochondrial Hs-AspS in the tRNA-independent biochemical assay

2.2.9.1 Assay optimisation

During optimisation of the biochemical assay and prior to compound potency assessment, we tested several pH conditions in order to increase our signal-to-background window and therefore our overall assay quality. Three pH conditions were assessed in 20 mM

HEPES buffer, 500 μ M ADPCP, 3 μ M enzyme and K_M values for L-Asp (143 μ M) and PPi (76 μ M) as previously reported for *M.tb* AspS (Fig. 41) (Gurcha et al., 2014).

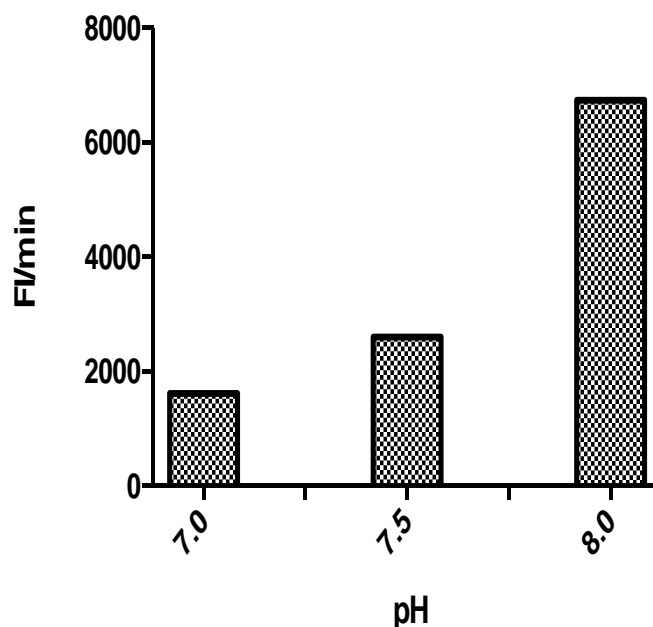


Figure 38. Effect of the pH on the activity of the human mitochondrial AspS. Fluorescence values were acquired as slopes (FI/min, initial velocity) during the substrate-independent initial rate of the aminoacylation reaction.

The data above shows a clear improvement (250%) in enzyme activity at pH 8 compared to the other pH conditions tested in the assay (Fig. 38). As a result, pH 8 was chosen for the determination of enzyme kinetic parameters K_M and V_{max} for the three substrates of the reaction (L-Asp, PPi and ADPCP).

2.2.9.2. Substrate dependence assessment of human mitochondrial Hs-AspS in a tRNA-independent coupled reaction

In order to determine the K_M for each of the three substrates, a wide range of concentrations was interrogated in the tRNA-independent biochemical assay while keeping the other two substrates at fixed, saturating concentrations. Each experiment was performed in duplicate and raw initial slopes ($\mu\text{mol NADPH/s}$) were plotted over substrate concentration on GraphPad Prism for K_M and V_{max} determination (Fig. 39 and Table 4).

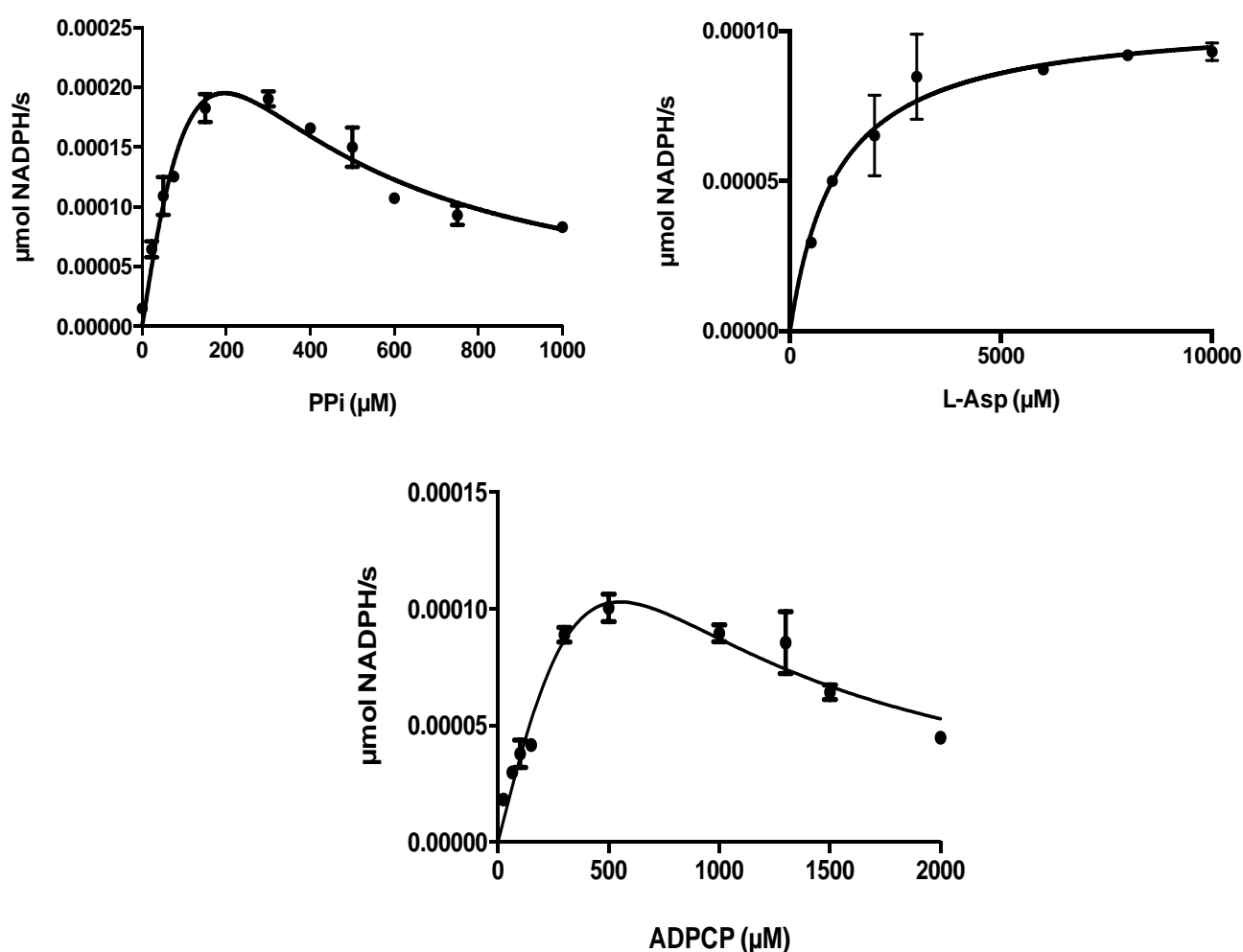


Figure 39. Substrate dependence of human mitochondrial AspS activity. ADPCP, PPI and L-Asp dose-response curves. Each experiment was done in duplicate and raw data corresponding to initial velocities was normalised and fitted to a Michaelis-Menten hyperbolic curve for the determination of the kinetic parameters K_M and V_{max} .

The turnover number (0.33 s^{-1}) was calculated as the division of the maximum enzyme velocity value at saturating L-Asp, $250 \text{ } \mu\text{M}$ PPi and $500 \text{ } \mu\text{M}$ ADPCP ($V_{\text{max}} = 2.1 \times 10^{-4} \text{ } \mu\text{mol/s}$) between the total amounts of enzyme ($6 \times 10^{-4} \text{ } \mu\text{mol}$) employed in a final reaction volume of $200 \text{ } \mu\text{L}$.

It is important to note the high turnover rate of this enzyme, suggesting the presence of product inhibition at high PPi and ADPCP concentrations. ADPCP K_{M} values ($500 \text{ } \mu\text{M}$) were selected for downstream inhibitor testing in order not to bias inhibition towards competitive or uncompetitive inhibitors (Strelow et al., 2004).

Varied substrate	Unvaried substrates	K_{M} (μM) (app)	Correlation coefficient
L-Asp ($250\text{--}8000 \text{ } \mu\text{M}$)	ADPCP (0.5 mM), PPi ($500 \text{ } \mu\text{M}$)	910.7 ± 2.96	0.82
PPi ($25\text{--}1000 \text{ } \mu\text{M}$)	ADPCP (0.5 mM), L-Asp (10 mM)	106.75 ± 8.83	0.87
ADPCP ($25\text{--}2000 \text{ } \mu\text{M}$)	PPi ($500 \text{ } \mu\text{M}$), L-Asp (10 mM)	297.6 ± 53.17	0.959

Table 4. Apparent K_{M} and R^2 values for the three substrates used by the human mitochondrial Hs-AspS enzyme. Values are shown as the mean \pm SD of two replicates.

2.2.10 Compound selectivity assessment against the human mitochondrial aspartyl-tRNA synthetase

Achieving highly selective levels of inhibition of tRNA synthetases is essential in drug discovery programs against these targets due to the highly similar peptide sequences in the ATP binding site of aaRS, rendering many competitive inhibitors non-selective against their intended target (Hurdle et al., 2005). GSK3448232A derivatives and screening hits identified in the target-based biochemical assay were tested against the human mitochondrial Hs-AspS at three increasing concentrations (100, 300 and 500 μM). Each compound was tested in duplicate in black-bottom 96 well plates in the tRNA independent assay at saturating concentrations of L-Asp (10 mM) and PPi (250 μM), and matching K_M values for ADPCP (250 μM) as assessed previously. NADPH fluorescence values during the initial rate of the enzymatic reaction were standardised to the positive and negative controls for enzyme activity in the presence of similar quantities of DMSO. Inhibition values for GSK3448232A analogues were obtained after raw fluorescence values were normalised to the positive (3 μM Hs-AspS) and negative (no enzyme) controls for enzyme activity. The full biological and physicochemical profile of GSK3448232A analogues and screening hits is provided in the Supplementary section.

Compound ID	Percentage inhibition (100µM)	Percentage inhibition (300µM)	Percentage inhibition (500µM)
GSK3449229A	19.27	57.7	57.26
GSK3448232A	72	ND	ND
GSK3448098A	52.17	ND	ND
GSK3449228A	52.02	ND	ND
GSK3448099A	43.608	70.18	94.62
GSK3449230A	45.2	74.72	91.95
GSK3448097A	0	73.8	88.27
GSK3448233A	0	46.97	85.67
GSK3448775A	0	5.52	6.63
GSK3484945A	42.1	72.03	82.48
GSK3484946A	39.22	79.09	87.83
GSK3485053A	68.53	ND	ND
GSK3485054A	ND	ND	ND
GSK3485055A	53.02	ND	ND
GSK3485056A	21.6	73.12	82.91
GSK3486987A	0	84.19	89.04
GSK3486988A	8.43	60.21	ND
GW483837X	55.19	ND	ND
PWS/700/1	63.66	ND	ND
ST/796668	47.25	76.51	ND
ST/476208	47.72	70.84	ND

Table 5. Inhibitory values of parent compound analogues and screening hits against the human mitochondrial AspS at three increasing concentrations (100, 300 and 500 µM).

PPI was used to trigger the reaction and 1% DMSO was included in the enzyme activity controls to check for solvent-related inhibition. Initial rates were obtained with Mars software and used to standardise to the enzyme activity controls.

Almost every analogue synthesised inhibited the human enzyme at concentrations equal to or above 100 µM (Table 5). Note that the absence of the Michael-acceptor renders GSK3448775A also inactive against this enzyme. Despite numerous claims in the literature highlighting the divergence between eukaryotic and prokaryotic aminoacyl tRNA synthetases, achieving high levels of specific inhibition still represents a challenge in drug discovery programs against these enzymes. These results also show that none of the screening hits identified in the tRNA-independent assay (PWS/700/1, ST/796668 and

ST/476208 (Fig.26)), have been able to retain selectivity over the orthologous counterpart. Moreover, among the GSK3448232A analogues synthesised, none is able to retain selectivity against the TB enzyme. The apparent off-target effects of these chemical entities, on the other hand, have been picked up at compound concentrations in the IC₅₀ value range against the TB enzyme, suggesting that the effect against both enzymes is likely to be due off-target effects rather than due to selective inhibition.

2.2.11 Identification of novel antitubercular hits targeting Mt-AspS through a whole-cell target-based high-throughput screening assay

In this study a number of biochemically validated Mt-AspS inhibitors have been identified using a target-based whole-cell screening assay in *Mycobacterium bovis* BCG genetically modified to constitutively express the Mt-AspS open-reading frame. The GSK TB box compound collection of 11,000 compounds (Ballell et al., 2013) was used at three independent concentrations (0.5, 2.5 and 12 μ M) and initial hits were confirmed based on inhibition shift between the two strains (calculated as % inhibition of *M. bovis* BCG pMV261 (empty plasmid) minus % inhibition of *M. bovis* BCG pMV261-AspS [based upon duplicate data]) on ActivityBase (IDBS). Assay quality was monitored in an inter-plate manner with the statistical Z', the gold standard to assess assay quality and reproducibility in HTS assays (Zhang et al., 1999). Plates with Z' values below 0.4 were discarded for further analysis due to poor assay robustness.

Initial hits (250) were cherry-picked for further validation in a dose-response assay at a concentration range of 0.001 up to 100 μ M in a 1:3 dilution fashion to assess whole-cell potency and confirmation of whole-cell target-engagement (MIC₅₀ shift) using the previously reported rhodanine entity as a control compound. Compounds were tested

in duplicate in an inter-plate manner and Sigmoidal dose-response curves were fitted to each data set using TIBCO Spotfire for analysis and data visualisation. This resulted in the identification of 11 compounds with a minimum inhibitory concentration (MIC) shift > 1 (Table 6). The dose-response curves of GSK1560987A and GSK445893A showing whole-cell target engagement against Mt-AspS for are shown below (Fig. 40).

GSK ID	MIC <i>M.bovis</i> pMV261-AspS (μM)	MIC <i>M.bovis</i> empty pMV261 (μM)	Ratio (MIC shift)
GSK3448232A (control)	6.7	0.7	9.1
GSK1531047B	32.8	4.9	6.7
GSK445893A	5.1	0.8	6.4
GSK446688A	1.6	0.5	3.3
GSK2198097C	24.9	10.5	2.4
GSK1990858A	15.3	7.2	2.1
GSK2337840A	18.9	11.7	1.6
GSK362766A	4.7	1.8	2.6
GSK2166789A	50.1	25.4	2.0
GSK942642A	3.0	1.7	1.7

Table 6. Whole-cell target engagement of several GSK whole-cell screening hits. The data shows the ratio between the MIC₅₀ of each inhibitor against a pMV261-Mt-AspS overexpressing *M. bovis* BCG and an empty plasmid containing strain used as a control strain. Values are reported as the mean of two replicates obtained in an inter-plate manner with Z' primes values above 0.4 as assay quality indicator.

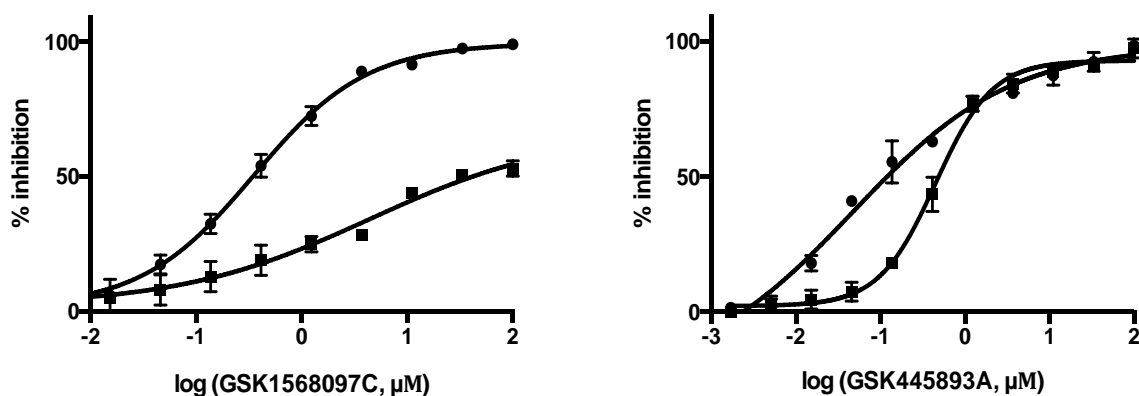


Figure 40. Whole-cell target engagement of GSK1568097C and GSK445893A, two chemical entities against a *M. bovis* BCG pMV261-AspS overexpressor strain (solid squares) and an empty pMV261-containing *M. bovis* BCG strain (solid circles). The shift in compound potency is observed for the pMV261-AspS overexpressor strain in comparison to an empty-plasmid control vector. Notice that AspS hits can be picked up with a MIC shift as small as 3-fold. For structures refer to table containing all hits identified against Mt-AspS in the supplementary section.

2.2.12 Development of a tRNA-based biochemical assay

As aforementioned, biochemical evidence of protein inhibition is needed to further validate on-target inhibitory activities. Since inhibitor potency can be masked due to the absence of the tRNA substrate in the tRNA-independent reaction; uncompetitive inhibitors with regard to the tRNA may fail to appear as validated hits if not present. A classical aminoacylation reaction with Mt-AspS has been developed (Pope et al., 1998a) in a 96-well-format to establish inhibitor potency and guide future hit-to-lead medicinal chemistry programmes. Compared to the tRNA-independent assay, this biochemical assay

mimics physiological conditions in which the presence of tRNA and can directly affect compound binding. Briefly, the process is based on the physical separation of tRNA charged molecules that have been precipitated out of solution under acidic conditions. With this assay we aim therefore to obtain biochemical values close to whole-cell inhibition data as an extra evidence of target validation.

The assay conditions were initially adjusted in order to obtain an initial rate. The assay mixture was sampled at each time-point and precipitable radioactivity was quantified by scintillation counting. Background counts corresponding to free radiolabelled L-Asp were subtracted to each data point, converted to mass units (μmol) and plotted over the time course of the assay (Fig. 41). For substrate dose-response studies, corresponding K_M values, shown in Table 4 as the mean \pm the SD of two duplicates were obtained when hyperbolic Michaelis-Menten curves were fitted to data obtained from tRNA and ATP dose-response studies, whereas L-Asp K_M values were obtained as the IC₅₀ of a Sigmoidal dose-response curve minus the total concentration of radiolabelled L-Asp employed in an isotopic dilution assay. Raw cpm values were converted to initial velocities (μmol aspartyl-tRNA/s) and plotted over each substrate concentration for K_M determination (Fig. 45).

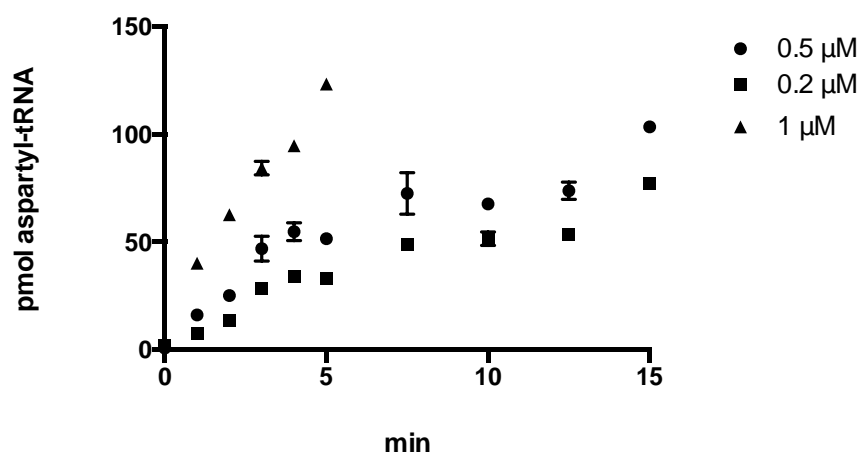


Figure 41. Time-course of the aminoacylation activity monitored using the standard TCA precipitation method at several Mt-AspRS concentrations. Initial cpm values were converted to amount of product (μmol aspartyl-tRNA) and plotted over the time-course of the assay (15min) GraphPad Prism 7.0 for the determination of initial reaction rates.. 0.2 (triangles), 0.5 (circles) and 1 μM (inverted triangles).

The linear rate of enzyme activity remained constant throughout the period of the assay (15 minutes), indicating zero order kinetics (maximum enzyme velocity independent of substrate concentration). The turnover number ($K_{\text{cat}} = 5.14 \times 10^{-3} \text{ s}^{-1}$) was calculated as the division of the maximum enzyme velocity value (0.411 pmol/s) between the total amounts of enzyme (80 pmol) employed at 1 μM Mt-AspS in a final reaction volume of 80 μL .

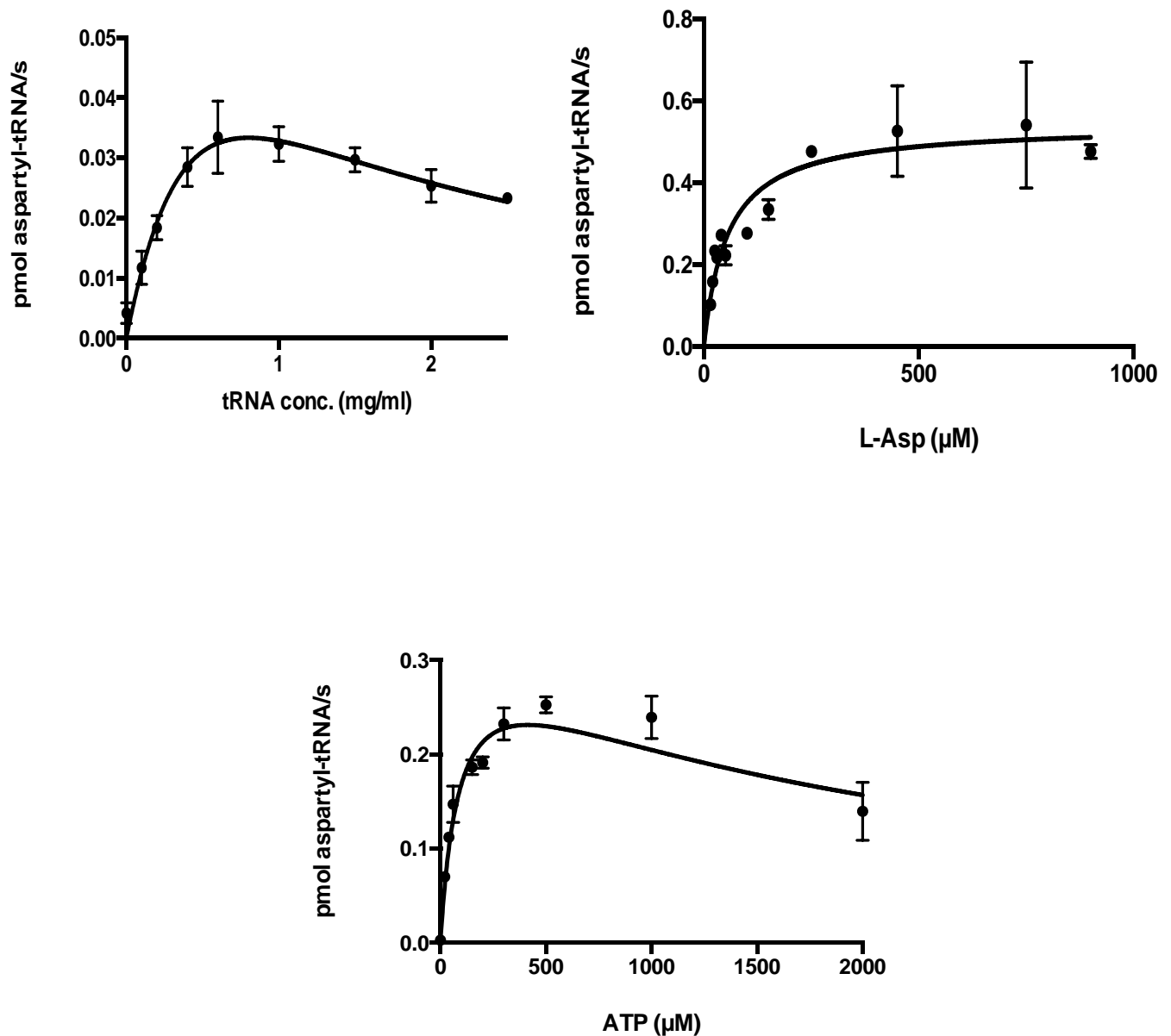


Figure 42. Substrate dependence of Mt-AspS activity in a tRNA-based assay. A sigmoidal dose-response curve was initially fitted to an isotopic dilution of a starter radiolabelled L-Asp concentration of 15μM. Raw cpm values were further converted to μmol aspartyl-tRNA/s and fitted to standard Michaelis-Menten substrate dose-response curves for K_M determination. K_M affinity constants for ATP and tRNA were similarly determined on GraphPad Prism. Each experiment was done keeping two out of three substrates at saturating concentration and K_M values are reported as the mean \pm the standard deviation of two duplicates.

Varied substrate	Unvaried substrates	K_M (μ M) (app)	Correlation coefficient
L-Asp	ATP (500 μ M), tRNA (1mg/mL)	15 ± 9.6	0.98
tRNA	ATP (500 μ M), L-Asp (900 μ M)	0.42 ± 0.22	0.90
ATP	tRNA (1mg/mL), L-Asp (900 μ M)	208.85 ± 8.41	0.89

Table 7. Summary of the reported apparent K_M values for Mt-AspS determined under Michaelis-Menten conditions. Data is expressed as the mean \pm standard deviation of two independent replicates and the correlation coefficient is provided as a measure of goodness of fit for each of the curves.

As seen in figure 45, the diminished enzyme activity observed at high ATP and tRNA concentrations suggests product inhibition, potentially due to the high turnover rate of this enzyme.

2.2.13 Biochemical validation of screening hits in a tRNA-based biochemical assay

Two active novel chemical families identified in the whole-cell target-based HTS assay using the *M. bovis* BCG over-expressing Mt-AspS were validated when interrogated for potency against the isolated enzyme in the aminoacylation reaction (Fig. 44). *In vitro* biochemical dose-response validation assays were performed at 0.2 μ M Mt-AspS and matching apparent K_M values of L-Asp and tRNA while keeping ATP at a saturating concentration (Fig. 43). Compound stocks were made as 10 mM solutions in DMSO and dispensed into 96-well-polystetyrene plates in a 1:3 dilution manner up to a final

concentration of 100 μM . In the maximum (100% activity) and minimum (0% activity) controls similar DMSO concentrations were added to check the absence of solvent-related inhibition. The highest concentration of DMSO and CHAPS used in the assay were 1% and 0.5%, respectively, and precipitable radioactivity was transferred onto GF/C filter plates for scintillation counting. Raw data was standardised to the positive and negative enzyme activity controls and plotted against the logarithm of the inhibitor concentration on Graph Pad Prism for IC₅₀ determination, shown in table 8 as the mean of two replicates.

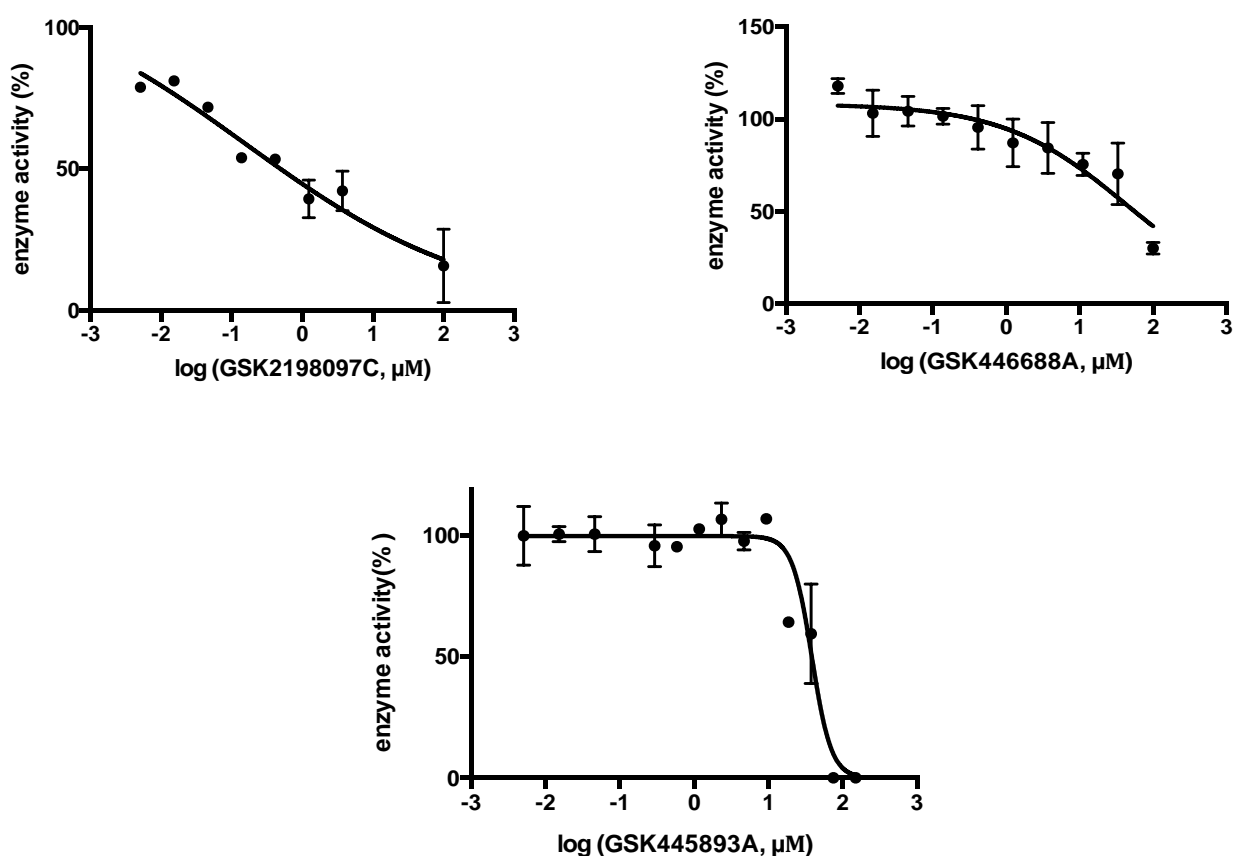
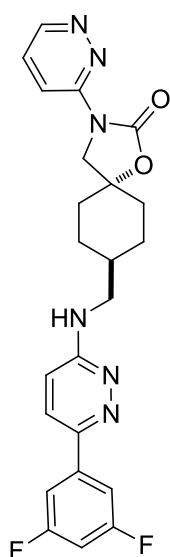


Figure 43. Dose-response *in vitro* activity curves of the effect of several screening hits in the aminoacylation reaction. Reaction mixtures were added to increasing compound concentrations and precipitable radioactivity quantified by scintillation counting in a Microbeta Trilux 1450.

GSK ID	IC50 (μM)
GSK446688A	42.20
GSK445893A	38.62
GSK2198097C	1

Table 8. IC50 values of the three screening hits validated against AspS in the aminoacylation reaction.

GSK2198097C



GSK445893A

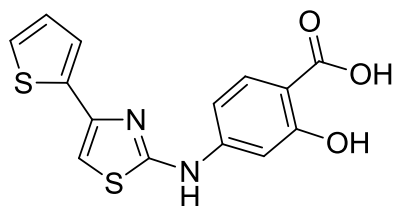


Figure 44. Structure and GSK identification codes of the newly identified anti-mycobacterial chemical families that target the essential aspartyl-tRNA synthetase Mt-AspS. The structure of GSK446688A is not shown since its chemical family is represented by GSK445893A.

Despite the relatively weak potency displayed by these hits, they may represent potential future preclinical entities if submicromolar potency is achievable by medicinal chemistry iterative efforts, paving the way towards the advancement of these hits as antitubercular agents with Mt-AspS as their target.

2.2.14 Mechanistic studies of validated hits against Mt-AspS

2.2.14.1 Substrate competition studies

Mechanistic studies against Mt-AspS with validated hits were performed in a substrate dose-response manner with respect to the aspartyl-adenylate substrate intermediate at several inhibitor concentrations to study the effect of each compound on V_{max} and K_M . These studies were developed in a miniaturised tRNA-independent assay due to the impossibility to miniaturise the ATP-based assay into the SPA bead format. Fixed concentrations of L-Asp and PPi were kept at saturation ($10 \times K_M$ values), whilst the concentration of ADPCP was allowed to vary (0-4000 μ M). The reaction was triggered with the addition of 2X substrate mix solution (10 μ L) to a 384 black-bottom polystyrene plate (Corning) containing 2X buffer solution (10 μ L) with 1 μ M Mt-AspS. Plates were then briefly centrifuged and read on an EnVision instrument (Perkin Elmer) using NADPH fluorescence in the kinetic mode for slope determination. Initial velocities were plotted versus substrate concentration and adjusted to a non-linear Michaelis-Menten regression model for the determination of the kinetic parameters V_{max} and K_M (Fig. 45).

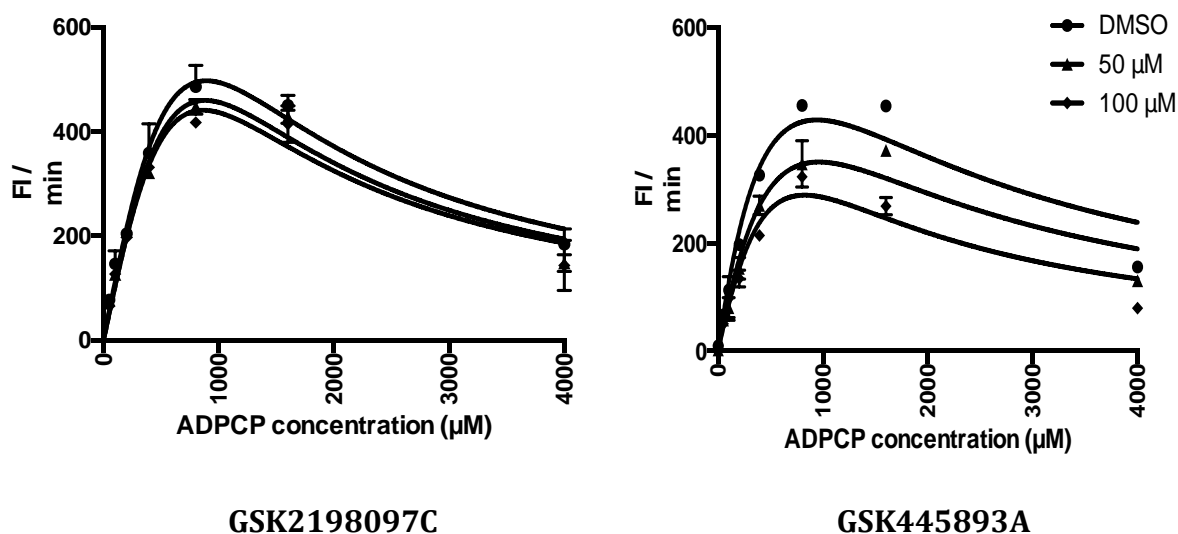


Figure 45. Reversible and non-competitive mode of inhibition of two chemical entities targeting Mt-AspRS. Several substrate and inhibitor concentrations were tested in duplicates alongside a microtiter 384-well-plate and enzyme velocity (raw fluorescence units per minute) was plotted against each of the inhibitor concentration for the determination of K_M and V_{max} .

The data above shows a pronounced decrease in V_{max} for both the two inhibitors tested in the assay. As described above, none of the inhibitors shared structural features with the aspartyl-adenylate intermediate, hence the non-competitive binding manner. Note that there is also minor effect on K_M (rightwards shift) for GSK445893A, suggesting mixed-type inhibition.

2.2.14.2 Time-course dependence

The inhibitors GSK445893A and GSK2198097C were also assessed for their reversible inhibition over a time period of one hour in the tRNA-independent assay. Enzyme activity

controls in the presence of similar quantities of DMSO were included for data standardisation for each time point, which was assessed in duplicate (Fig. 46). The assay was performed at reported K_M values for the three substrates and buffer conditions and salt concentrations as in previous screening, dose-response and mechanistic studies, whereas the inhibitor concentration employed in the assay was chosen considering IC₅₀ inhibitory values from previous biochemical assays.

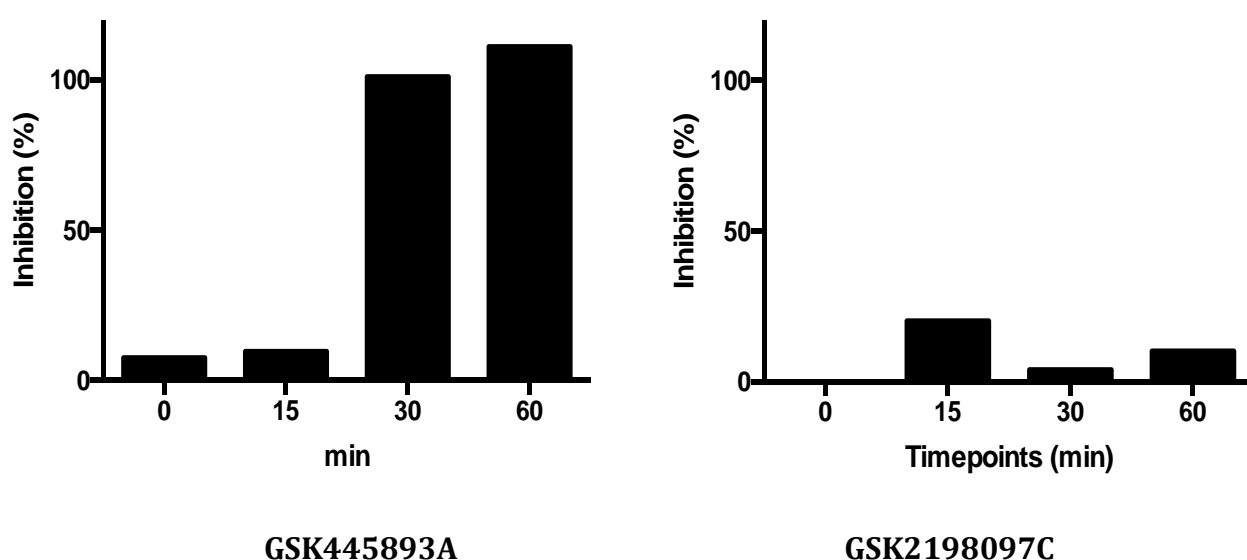


Figure 46. Time-dependence assessment of GSK445893A and GSK2198097C inhibition.

Slow-binding kinetics of GSK445893A. Complete inhibition is observed after a 20 minute incubation period, suggesting a potential covalent modification of the enzyme. Reversible binding kinetics of GSK2198097C as evidenced by a flat-line behaviour of Mt-AspS inhibition over the period of the assay. Note that at the chosen IC₅₀ concentration the potency of GSK2198097C has dropped compared to previous dose-response assays, suggesting compound instability in standard storage conditions.

2.2.14.3 DTT dependence

GSK445893A was interrogated for its activity in the aminoacylation reaction in the presence and absence of DTT (1mM) as previously described for target-based screening hits (Fig. 47). The compound GSK2198097C was not tested due to the loss in potency observed in previous assays and no extra quantities were available for re-ordering from GSK. As described, highly electrophilic compounds that react with cysteine residues on proteins in an unspecific manner may also react with sulfhydryl groups of reducing agents, rendering the compounds inactive against their intended target. The reaction conditions were kept identical as for substrate and enzyme concentrations previously defined for *in vitro* dose-response assays with screening hits. Slopes were analysed as previously described and normalised data was plotted against the logarithm of inhibitor concentration on GraphPad Prism for IC₅₀ determination.

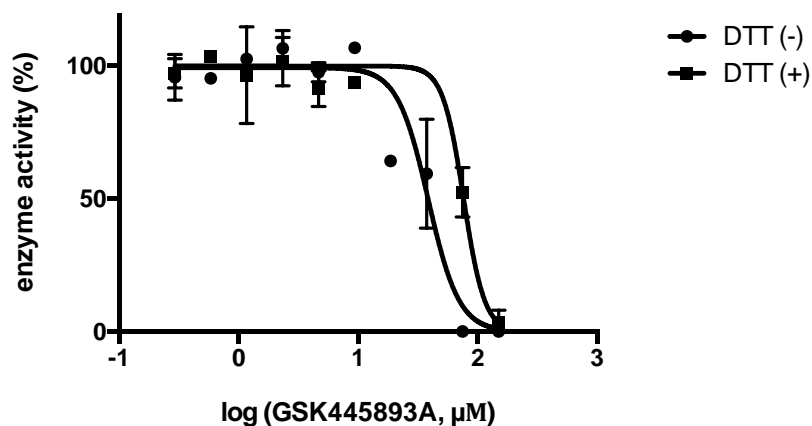


Figure 47. *In vitro* dose-response activity curves of GSK445893A in the presence and absence of 1 mM DTT. The addition of the reducing agent causes a slight shift in compound potency (from 38.69 to 76.5 μM), suggesting the formation of covalent adducts with thiol groups on DTT.

2.2.15 Medium-throughput target-based screening assay of a series of analogues of whole-cell validated hits against Mt-AspS

Two novel chemical entities, analogues of the inhibitor GSK1560987A previously identified in the whole-cell target-based Mt-AspS overexpressor assay, were identified when a small library of analogues of the three whole-cell screening hits (GSK1560987A, GSK2198097C and GSK445893A) were interrogated for their potency at concentrations ranging from 0.05 up to 100 μ M in a miniaturised tRNA independent assay of 20 μ L optimised for HTS purposes (Figs. 48 and 49). Assay stability was previously assessed over the entire period of the HTS and assay quality was monitored in an inter-plate manner ($Z' > 0.4$). Surprisingly, the parent compound GSK1560987A failed to show potency in biochemical validation assays against Mt-AspS, suggesting poor solubility in aqueous solution or compound instability in assay buffer. However, two apparently more soluble analogues of GSK1560987A were confirmed as Mt-AspS inhibitors and structures, biological and physicochemical properties are shown in the Supplementary Section.

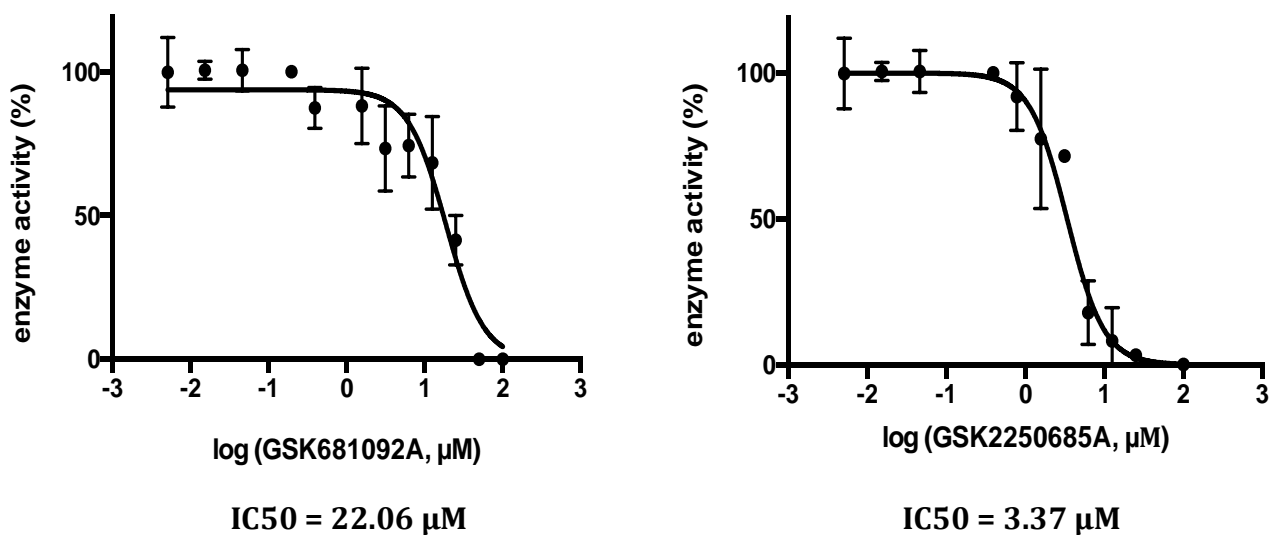


Figure 48. *In vitro* potency of newly identified antitubercular analogues of GSK1568097A targeting Mt-AspS. Dose-response curves of the effect of compounds GSK681092A and GSK2250685A against Mt-AspS in the tRNA-independent amino acylation reaction. Raw fluorescence values corresponding to initial rates of the enzymatic reaction were normalised to the positive and negative control for enzyme activity (plus and minus enzyme, respectively) and plotted versus the logarithm of inhibitor concentration on GraphPad Prism 6.0 for IC₅₀ determination.

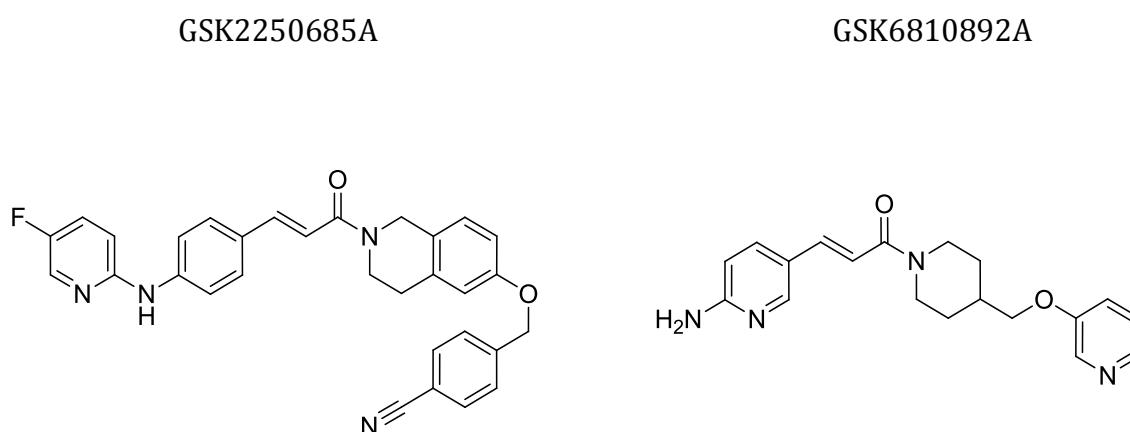


Figure 49. Structures of several antitubercular analogues of GSK1568097A targeting Mt-AspS. These chemical entities were identified in a target-based screening of structural analogues of several whole-cell screening hits in a tRNA-independent aminoacylation reaction.

2.3 Discussion

A combination of whole-cell and target-based screening strategies has led to the discovery of a total of 6 chemical families with activity against the M.tb AspRS enzyme. However, despite an improvement in the biological and physicochemical properties of these molecules could be improved during hit-to-lead optimisation it should be noted that severe structural alerts (nitro and nitrile groups, Michael acceptors and rhodanine scaffolds) might hamper the potential of these molecules as leads.

These structural features have extensively been reported in the literature (Baell and Holloway, 2010, Dahlin et al., 2015, Erlanson, 2015) and care should be taken during the decision-making process in early stages of drug discovery to avoid an unnecessary waste of time and resources in the advancement of a chemical series. However, in some particular cases the presence of a potential liability does not necessarily translate into a dead-end drug discovery project. A structural moiety may help dock the molecule in the right orientation within the binding pocket and therefore establish either covalent, hydrogen bonds or Van der Waal interactions with key residues of a given target. For instance, the most promising clinical candidate for TB treatment, PBTZ043, harbours a nitro group that forms a covalent bond with a cysteine residue (Batt et al., 2012). The nitro group is regarded as a highly reactive nucleophile and compounds harbouring such groups should be handled carefully, but by no means should the project be abandoned unless guided by de-risking experiments (inhibitory activities in the presence/absence of reducing agents, glutathione trapping assays, etc.). Other considerations include the activity against the isolated target enzyme versus whole cell activity and lipophilicity indicators (low CLND and high logP values) as potential cytotoxicity predictions. The advancement of a chemical series with potential structural alerts needs to be dealt in a

case-by-case scenario and with a wide range of biological and physicochemical data used in the decision-making process.

Focusing on the identified screening hits that display a range of micromolar potency against Mt-AspS, the GSK3448232A rhodanine-based compound displayed reactivity with the trapping agent glutathione in an experiment performed by GSK using liver microsome fractions. This entity harbours a Michael acceptor and a rhodanine. The former being an α - β -unsaturated carbonyl group that can readily react with biologically relevant nucleophiles on protein targets, while the latter has also displayed promiscuous reactivity with biological molecules. The extensive SAR performed on this molecule explains that the reduction of the double bond renders the resulting compound inactive against Mt-AspS, suggesting that the Michael-acceptor on the molecule interacts with cysteines in a covalent manner. However, mass spectrometry experiments and a flat-line behaviour in time-course assays indicated a non-covalent mechanism of action, consistent with classical Michaelis-Menten inhibition of enzyme activity. As described above, it is likely that the presence of the rigidity provided by the double bond fixes the molecule in a particular orientation in the binding pocket and its removal would prevent the compound from attaching correctly. Such a mechanism can perfectly co-exist with a covalent one depending on the target in question. It is perfectly possible that this molecule presents a reversible, non-covalent mechanism against Mt-AspS but also establishes covalent bonds with alternate biological molecules or as the trapping assay suggests, being metabolically activated by microsomes and irreversibly binding glutathione. A protein- ligand crystal would have shed clarity on the mechanism of action. However, poor solubility and weak affinities observed in biochemical assays hampered our efforts to implement a structure-guided hit-to-lead programme. The SAR performed on this parent compound however, shows an improvement in some of the biological and physicochemical properties of the

compound series. Some entities displayed an improved potency versus the parent compound in enzyme and whole cell-based assays, confirming that our activity-guided medicinal chemistry efforts have led to the development of more potent compounds, despite the absence of insight at the compound-protein molecular interface. We have also made significant improvements in solubility, although experimentally, GSK3448098A precipitated despite having one of the highest CLND values of the analogues synthesised. There are some discrepancies that need to be highlighted on the parent compound and some other screening hits that we have identified as Mt-AspS inhibitors. GSK445893A and the parent compound analogues displayed a lack of correlation between on-target and whole-cell activities. Altogether, with the presence of structural alerts this is another piece of evidence of off-target effects due to the promiscuous activity of these entities and should therefore be validated in secondary assays to confirm the absence of potential liabilities. GSK445893A represents a promising starting point due to the absence of highly reactive groups. Its low potency could be further improved by medicinal chemistry, but attention should be paid to the low MIC value observed in whole-cell assays, indicating that Mt-AspS might not be the primary target. It also seems to display a slow-onset inhibition/covalent as shown by an increased activity over an hour incubation period. However, it cannot be concluded that this slow inhibition is related to the formation of covalent adducts, because slow-onset inhibitors also display time-dependent activity. Further mass spectrometry studies will help elucidate the interaction of this screening hit with Mt-AspS. The rest of the screening hits seem to display a classical, reversible, time-independent mechanism as evidenced by their flat-line behaviour in time-course assays. In terms of overall on-target potency, GSK2198097C and GSK2250685A have displayed the strongest inhibition in biochemical assays against Mt-AspS. It is worth mentioning that GSK2198097C has lost potency from its initial biochemical validation studies, despite

storage conditions being kept according to industry standards (-20°C). It is possible that the inhibitor either degrades over several freeze-thaw cycles or that water uptake decreases the effective DMSO concentration, causing the compound to precipitate out of solution. Further studies will be required to investigate the reasons for the instability of this entity in DMSO storage conditions.

On the other hand, substrate competition studies have shown that some of our compounds display a non-competitive/mixed-type inhibitory mechanism with respect to the ATP analogue ADPCP. This allosteric-type behaviour is expected from the absence of structural similarities with ATP and it is worth highlighting that these are the first-in-class aaRS inhibitors to display such a mechanism. As described above, drug discovery strategies against aaRS have traditionally exploited residues on the substrate-binding site to develop ATP mimetic inhibitors. Our results show that a non-competitive mode of action would overcome traditional limitations of ATP-competitive inhibitors by helping retain selectivity versus human aaRS counterparts. Due to timing, neither GSK2250685A nor GSK681092A could be further investigated as to their mechanism of Mt-AspS inhibition, but a similar non-competitive/mixed type mechanism is expected due to the reasons described above. However, the lack of selectivity of some of our inhibitors (PWS/700/1, ST/796668 and ST/476208) seems to explain that other allosteric binding sites besides the ATP-binding site may also be conserved across species. It is worth mentioning that 40% sequence identity is shared between Mt-AspS and the human mitochondrial Hs-AspS. It is therefore possible that binding sites may be conserved. Further selectivity studies with the human mitochondrial AspS needs to be performed with GSK445893A, GSK2198097C and the analogues GSK2250685A and GSK681092A in the future.

All in all, it remains to be seen whether medicinal chemistry can further improve the activity against Mt-AspS. Despite raising concerns as to the potential of these compounds as leads, their presence does not necessarily be a reason for abandonment if selectivity can be retained and no liabilities are observed in secondary assays. Each molecule should be dealt with in a case-by-case manner and every option should be contemplated before making a final decision.

CHAPTER III

IDENTIFICATION OF NEW TARGETS AND RESISTANCE MECHANISMS IN *M.tb*

3.1 Introduction

The discovery of new targets remains a huge task in drug discovery programmes against bacterial infections. In order to obtain effective control of TB burden, the availability of new druggable biology is of great importance due to the potential to uncover novel areas of the chemical space that can be further exploited in drug discovery programmes. Moreover, a deeper understanding of the mechanism of action of a chemical entity can further pose a significant advancement in drug discovery projects, not only due to the availability of new targets, but also due to the presence of compound-activating proteins and efflux pumps that play an important role in their resistance mechanism, which can also be targeted. A retrospective analysis of the mechanism of action of two front-line TB drugs, isoniazid and ethionamide, highlights the need to precisely pinpoint the mode of action of novel chemical entities to further exploit opportunities in TB drug discovery. Isoniazid, the front-line anti-TB drug, is biochemically activated by a catalase-peroxidase, KatG, an enzyme that also plays a role in protection against the oxidative burst within macrophages (Timmins and Deretic, 2006, Manca et al., 1999). Upon activation and adduct formation with NADH by KatG, the complex targets the enoyl reductase InhA, the target protein, in a slow-tight binding manner (Rawat et al., 2003, Timmins and Deretic, 2006, Lei et al., 2000, Zhang et al., 1992). The role of these proteins, in particular KatG, in the rise of multidrug-resistant *M.tb* is highlighted by the presence of missense mutations in the open reading frames of KatG and InhA in resistant isolates from TB patients (Pym et al., 2002, Niehaus et al., 2015, Baulard et al., 2000). In a similar manner the second-line TB drug, ethionamide, is activated by a monooxygenase, EthA, prior to targeting InhA (DeBarber et al., 2000, Vannelli et al., 2002). The gene encoding the ethionamide activator was surprisingly found next to an open reading frame in the *M.tb* genome that conferred resistance to ethionamide upon overexpression, therefore playing a role in its regulation

(Baulard et al., 2000). Currently, several groups are focusing on the identification of EthR binders that can trigger an upregulation of EthA leading to a higher turnover of ethionamide and enhanced anti-TB activity (Nikiforov et al., 2017, Wohlkonig et al., 2017). This approach can potentially lead to smaller doses of ethionamide in TB treatment regimens, decreasing potential ethionamide-related cytotoxic effects and by-passing ethionamide resistance (Blondiaux and Moune, 2017). It is therefore important to discover potential compound activators and its related regulators in order to uncover new chemical entities that may be co-administered with TB drugs to decrease cytotoxicity, enhance drug efficacy and overcome antibiotic resistance.

3.2 Results

3.2.1 Generation of *M. bovis* BCG resistant isolates against GSK756354A and confirmation of their resistance phenotype.

M. bovis BCG resistant colonies were isolated at a frequency of 3×10^8 at 5x MIC of GSK756354A after a two-week incubation period at 37°C. Isolated, potential resistant colonies were used to inoculate 5 mL of antibiotic-free 7H9 media for further studies. When potentially resistant cultures reached log-phase of growth, 10^4 bacterial cells were added into black 96-well-plates containing increasing concentrations of GSK756354A. Resazurin reduction (fluorimetric REMA) was chosen as the method of detection of viable cells. Raw fluorescence values from resazurin (blue) reduction to resorufin (pink) by viable cells were standardised to the positive and negative control for cell growth for the determination of cell survival percentages for each compound concentration. DMSO was included in both controls at the final assay concentration to check for solvent-related cell growth inhibition and Sigmoidal dose-response curves for each strain interrogated in the

assay were fitted on Graph Pad Prism 7.0 for MIC determination (Fig. 50). Experiments were run in duplicate on independent days to assess day-to-day reproducibility. Consistent Z' values above 0.8 were obtained across experiments indicating excellent assay robustness.

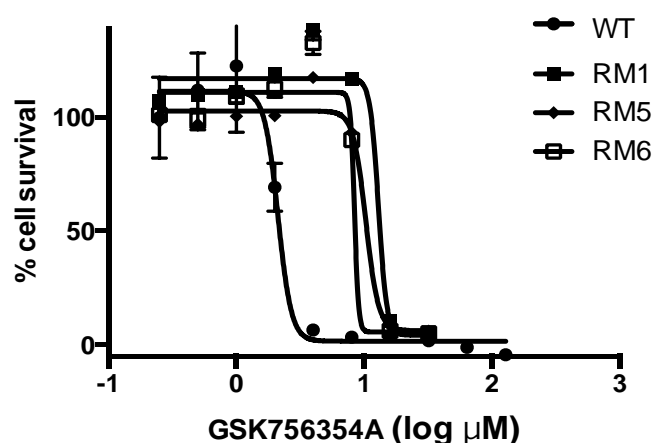


Figure 50. Whole-cell *in vitro* potency assessment of GSK756354A against several *M. bovis* BCG strains. Note the MIC₅₀ shift between the wild-type (WT) and resistant strains (RM) confirming the resistance phenotype of the isolated colonies.

A higher than 4-fold MIC shift between the WT and resistant mutants (RM) indicates a clear genetic-based resistance mechanism that could uncover a novel mechanism of action (Table 9). In order to gain more confidence on the resistant phenotype of these strains to this hit compound we also interrogated them for cross-resistance against several GSK756354A analogues before proceeding to whole-genome sequencing studies

3.2.2 Cross-resistance of GSK756354A-resistant strains to GSK756354A analogues

Medicinal chemistry optimisation during the hit-to-lead phase in drug discovery is essential in order to develop more potent and soluble compounds that can be readily administered in animal models of TB infection. Given that we are still lacking information about the mechanism of action of this new chemical entity our chemistry has focused on improving solubility whilst retaining potency in whole-cell assays against *M.tb* and *M. bovis* BCG. So far, four analogues of this compound have been synthesised and we have assessed their potency in whole-cell assays against wild-type (WT) and spontaneous resistant isolates (RM) of *M. bovis* BCG strains generated against the parent compound GSK756354A to assess cross-resistance (Fig. 51)

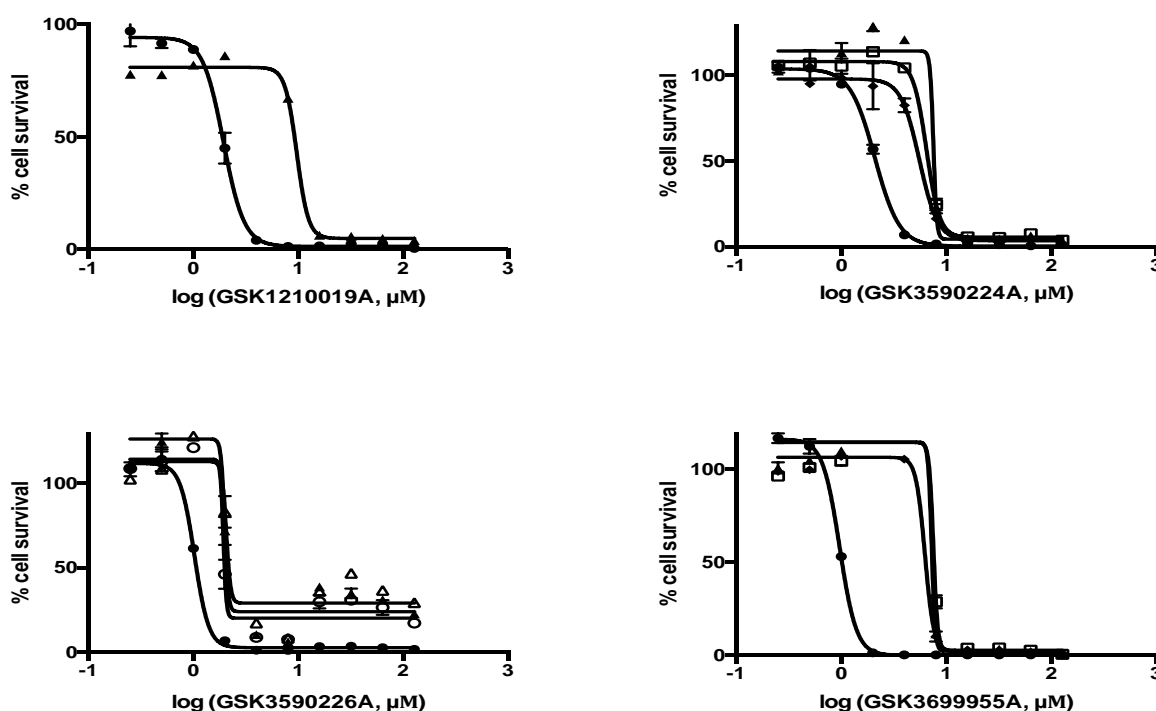


Figure 51. Whole-cell *in vitro* dose-response activity curves of GSK756354A analogues against several *M. bovis* BCG strains. A significant MIC fold (>4) can be observed between the WT (solid circles) and RM strains (RM1, solid triangles; RM5, solid diamonds; RM6, empty squares), highlighting cross-resistance to these chemical entities.

The presence of cross-resistance to these compounds suggests that medicinal chemistry optimisation efforts on GSK756354A have managed to retain whole-cell activity against *M. bovis* BCG, and that its mechanism of action remains unchanged (Fig. 51). As shown in Table 9, these entities also display acceptable whole-cell activities against *M.tb* H37Rv (MIC values in the low μM potency range), whereas significant improvements in solubility have also been accomplished (CLND value of $35\mu\text{M}$ for GSK3590224A against $8\mu\text{M}$ for the parent compound).

GSK ID	CLND (μM)	MIC ₉₀ <i>M.tb</i> H37Rv (μM)	MIC ₉₀ <i>M.bovis</i> WT BCG (μM)	MIC ₉₀ <i>M.bovis</i> BCG RM1 (μM)	MIC ₉₀ <i>M.bovis</i> BCG RM5 (μM)	MIC ₉₀ <i>M.bovis</i> BCG RM6 (μM)
GSK756354A	8	8	2.89	16.18	14.82	9.33
GSK1210019A	1	10	3.26	13.48	N/A	N/A
GSK3590224A	35	10	3.83	8.45	9.35	10.07
GSK3590226A	3	5	1.54	3.99	3.99	7.99
GSK3639955A	1	1.87	1.62	8.12	7.99	8.51

Table 9. Structure-activity relationship map of several GSK756354A analogues. Note the improvement in solubility for GSK3590226A and the increased potency of GSK3639955A against *M.tb* ($1.87\mu\text{M}$ vs $8\mu\text{M}$). N/A: non-available. CLND values were provided by GSK.

3.2.3 Whole-genome sequencing studies of spontaneous resistant isolates against GSK756354A

In order to gain more insight into the genetic basis of the resistant phenotype to this hit compound we extracted the genomic DNA from liquid cultures grown at log-phase which was then subjected to whole-genome sequencing studies to identify SNPs in potential

targets. Three resistant strains were sequenced, and missense, potentially resistance-conferring mutations identified in several open reading frames. First, V689A-MmpL3 (the trehalose monomycolate transporter); second, T67A in GlpK (a glycerol kinase); third, D83A in *Mb3185c*, a probable dioxygenase which seems to be involved in the metabolism of aromatic compounds and C86M-dipZ, a frame-shifting mutation in a protein presumably involved in the biogenesis of the cytochrome BC1-AA supercomplex of the electron transport chain (Goldstone et al., 2005). No further assays were done with GlpK due to the well-known lack of essentiality of this gene when alternative carbon sources are used in *M.tb* cultures. With regard to the frame-shifting mutation observed in dipZ, despite the initial interest in this gene due to the mutation in the cysteine residue, no follow-up studies were performed since such mutation would render an essential protein inactive. The most attractive gene was a dioxygenase encoded by *Mb3185c* that appears to be involved in the metabolism of aromatic compounds. Moreover, the involvement of oxygenases in compound activation is well characterised in *M.tb*, so a potential resistance mechanism could be unveiled.

3.2.4 Mechanism of action studies: effect of *Mb3185* overexpression on resistance/sensitivity against GSK756354A

3.2.4.1 *Mb3185* cloning

A standard PCR amplification protocol from *M. bovis* BCG genomic DNA was performed using *Bam*HI and *Hind*III restriction sites in the forward and reverse primer, respectively. Initial reactions were performed in assay volume (20 µL) using a gradient annealing temperature PCR protocol at 65±10°C. We then selected the optimal annealing

temperature based on band intensity and replicated the amplification conditions to get sufficient amounts of PCR product for further experiments (Fig. 52). Gel bands containing the desired amplified DNA fragment were excised out of the gel and the resulting DNA was purified using the DNA gel extraction kit from Qiagen.

Band size (bp)

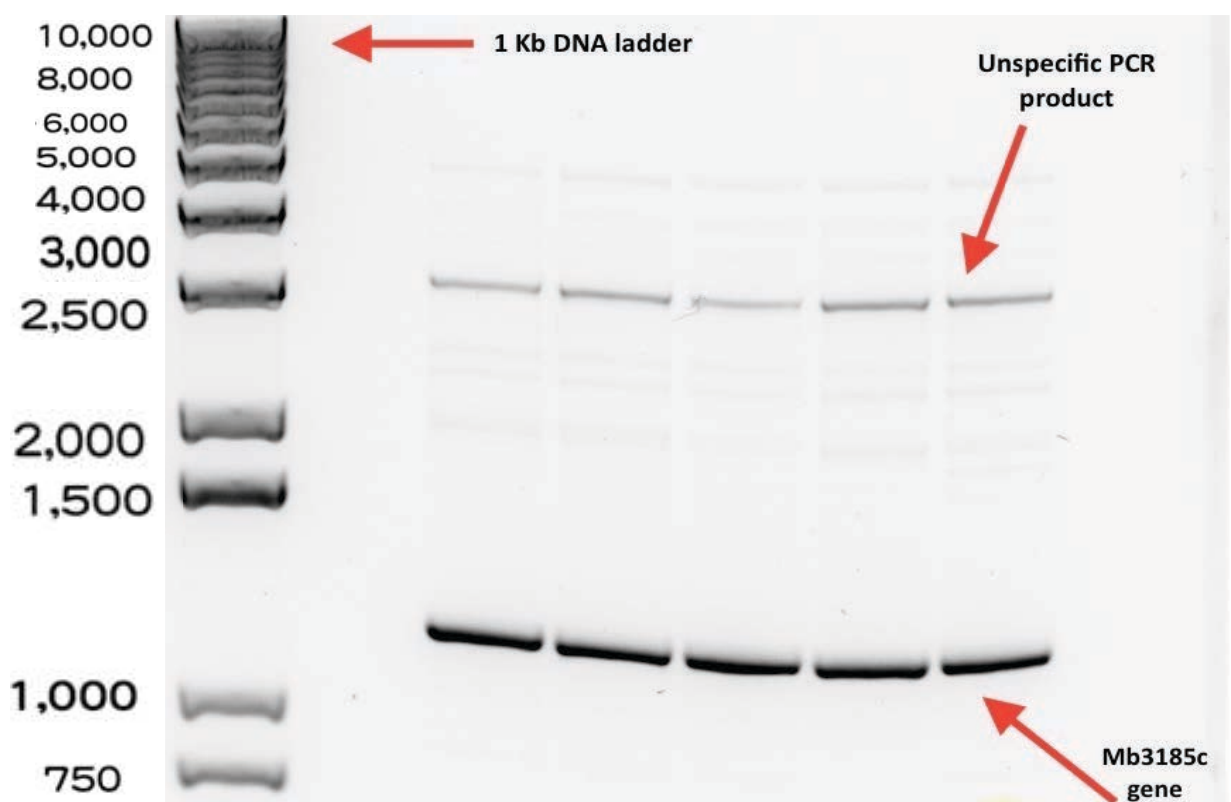


Figure 52. Agarose gel (1%) showing the amplified *Mb3185c* gene product at 1.150 Kb. The optimal annealing temperature (65°C) was determined after an initial, gradual amplification at 65±10°C was performed to determine the optimal amplification conditions.

3.2.4.2 Enzymatic digestion with BamH1/HindIII

The purified gene product was then double digested using 10U of *BamH1* and *HindIII* in 3.1 restriction buffer for subcloning purposes. After initial experiments using *Cutsmart* buffer showed star activity of these restriction enzymes, the gene and plasmid were efficiently cut in 3.1 restriction buffer as shown in Fig 53.

Band size (bp)

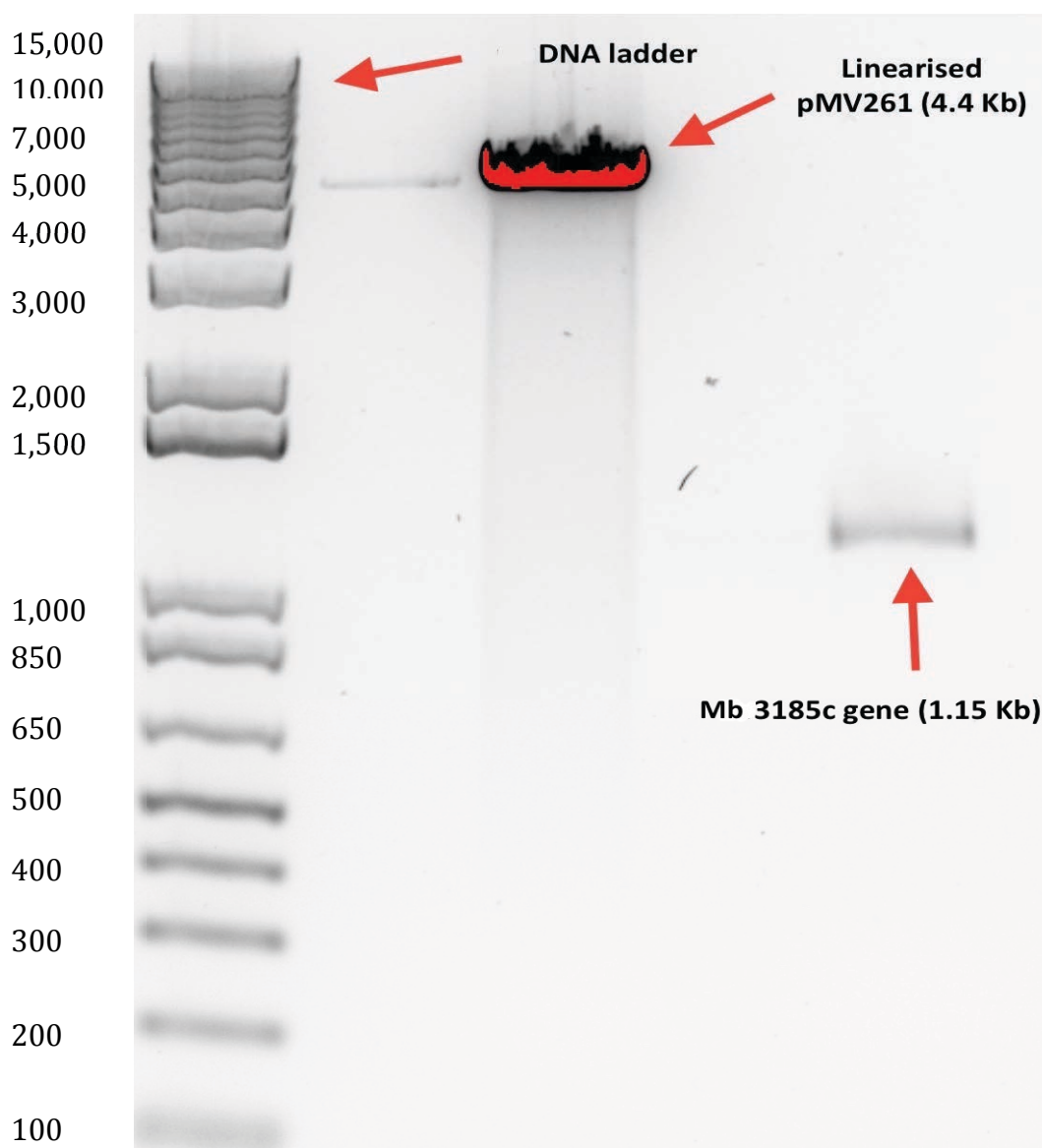


Figure 53. Agarose (1%) gel showing the digested products of the *BamH1* and *HindIII* reaction.

The digested products were then excised out of the gel, purified and pooled into a mixture of T4 ligase buffer for the generation of a recombinant pMV261-*Mb3185c* construct for constitutive expression in *M. bovis* BCG. The overnight ligation reaction was then used to transform chemically competent *E. coli* DH5 α cells for plasmid propagation and further construct restriction and gene sequencing analysis.

3.2.4.3 Restriction analysis of recombinant *E. coli* DH5 α colonies

Several transformant colonies were individually picked and grown overnight in 5 mL LB broth at 37 °C for plasmid extraction. Purified, recombinant plasmid was quantified in Nanodrop and verified by restriction analysis using *Bam*H1/*Hind*III for correct gene insertion (Fig. 54).

Band size (Bp)

15,000
10,000
7,000
5,000
4,000
3,000
2,000
1,500

1,000
850
650
500
400
300
200
100

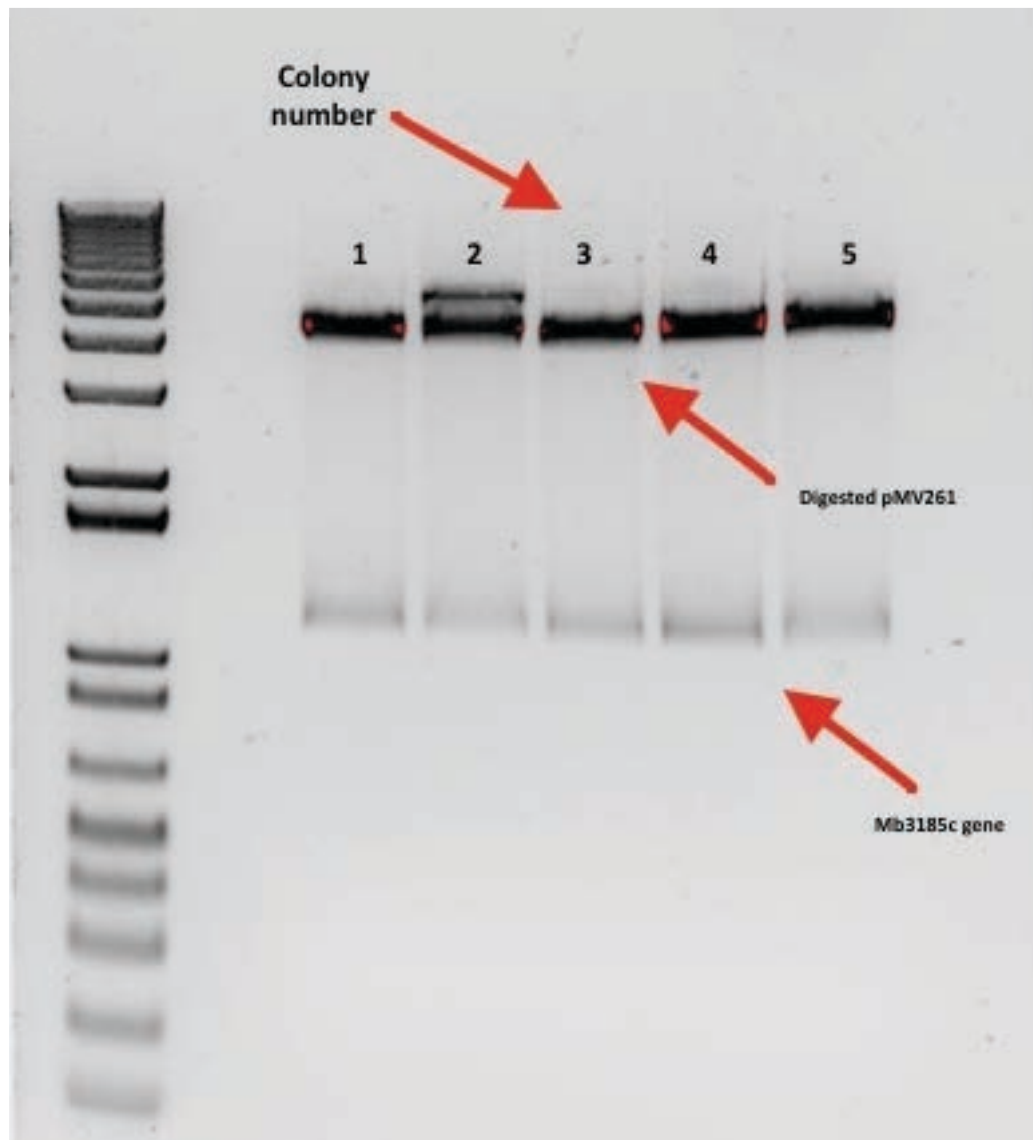


Figure 54. Restriction analysis of recombinant *E. coli* DH5α colonies transformed with pMV261-Mb3185c. Agarose gel (1%) showing the expected band size of the insert (1.15 Kb) and the digested linearized vector backbone (4.4 Kb band size) of plasmid sequences from five cherry-picked DH5α transformant colonies, confirming the correct ligation of the insert into the plasmid.

3.2.5 Overexpression studies with pMV261-Mb3185c

In order to assess the potential role of *Mb3185c* on resistance or sensitivity, recombinant pMV261- *Mb3185c* was subsequently used to transform electrocompetent *M. bovis* BCG

cells to study the effects of *Mb3185c* overexpression on *M. bovis* BCG susceptibility against GSK756354A (Fig. 55). After a 2 week incubation period at 37 °C on solid 7H10 agar plates containing kanamycin at 25 µg/mL, sufficiently grown recombinant colonies were observed and subsequently grown in liquid 7H9 media for further studies. When *M. bovis* BCG overexpressing recombinant pMV261- *Mb3185c* reached mid-log phase (OD 0.8) 10⁴ cells were added into white Greiner 96-well-plates containing increases doses of GSK756354A (0.005-100 µM) in a 1:3 dilution fashion for MIC determination of GSK756354A. Raw luminescent units were obtained after the addition of Bac-titer Glo and data was standardised to the positive and negative control for cell growth in the presence of 1% DMSO (cells and 7H9 media, respectively). Cell growth percentages were plotted against the logarithm of inhibitor concentration on GraphPad Prism for MIC determination.

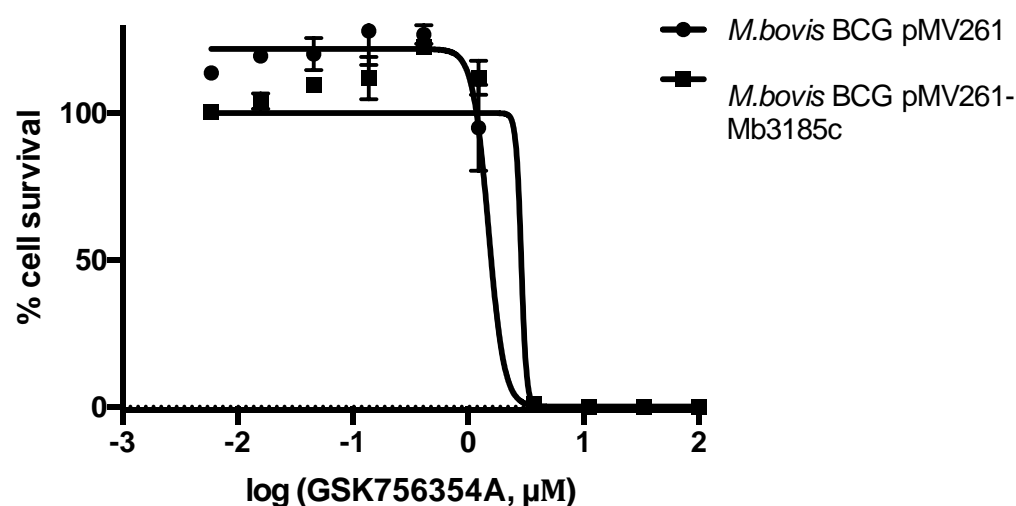


Figure 55. Dose-response *in vitro* activity curves of the effect of GSK756354A on *M. bovis* BCG pMV261- *Mb3185c* (solid squares) and *M. bovis* BCG pMV261 strains (solid circles). A small shift can be observed between the two strains, suggesting a possible role of *Mb3185c* in resistance against GSK756354A.

3.3 Discussion

The discovery and development of novel chemical entities for the treatment of TB is subject not only to the identification of new areas of chemical space but also target identification. Unraveling new aspects of TB biology is of utmost importance to gain insight into pathogenesis, but can also open up exciting possibilities for TB drug discovery. As described above, several groups have focused on the identification of small molecules aborting resistance compounds (SMART) that target transcriptional regulators of compound-activating proteins in *M.tb* (Blondiaux and Moune, 2017), which can potentially decrease ethionamide doses in combinatorial treatment (Nikiforov et al., 2017). We do not have enough scientific evidence to conclude that *Mb3185c* deactivates the GSK756354A chemical series but the small shift observed in *Mb3185c* overexpression studies in *M. bovis* BCG suggests a possible role in resistance. Mass spectrometry studies may help to confirm the activity of the *Mb3185c* expressed protein on GSK756354A, such as the addition of a hydroxo group onto its structure.

In terms of the other SNPs identified in whole-genome sequencing studies of *M. bovis* BCG spontaneous resistant isolates against GSK756354A, we decided not to follow them up because of time limitations. MmpL3 in particular, several mutations have been reported against multiple inhibitors and none of them have been validated biochemically, hence the unlikelihood of being the target of these entities. It is worth mentioning the high lipophilic properties of these inhibitors as the main cause of the appearance of mutations in membrane proteins in spontaneous resistant isolates (Goldman, 2013). To further support this claim, it is worth noting that the pronounced steepness of *in vitro* whole-cell dose-response curves of GSK756354A suggests non-specific inhibition due to compound aggregation (Sittampalam GS, 2004), likely due to non-specific binding to bacterial

membranes due to the lipophilic properties of these hits. We have also observed compound precipitation at high concentrations in solid agar, further supporting this hypothesis. There have been a number of lipophilic compounds discovered in HTS phenotypic approaches against *M.tb* and they should be handled with care as high logP values are regarded as potential cytotoxicity indicators in drug discovery programmes (Waring, 2010). It is possible that mutations in MmpL3 contribute to phenotypic resistance against these inhibitors, but more likely due to a pathway-related effect rather than due to a direct disruption of protein-target interaction. As described above, drug resistance due to target overexpression may not be target-related but rather due to an effect on pathway-related proteins (Kalscheuer et al., 2010).

In terms of the other SNPs identified, the glycerol kinase GlpK, is unlikely to be a good drug target in TB. Glycerol, despite being the main carbon source employed in TB cultures thanks to its speed and convenience, its usage is absent during host infection (Guengerich, 2006, Pethe et al., 2010). An easy experiment to find out whether GlpK was the target of the GSK756354A series would have been to interrogate the inhibitors for its potency against *M. bovis* BCG grown in cholesterol-enriched media. However, the non-essentiality of this protein renders GlpK as a non-attractive target for TB drug discovery, hence our lack of interest in follow-up studies.

The last non-synonymous mutation detected in whole-genome sequencing studies that we could have further explored was C86M-dipZ, a protein involved in cytochrome C biogenesis. A cysteine residue change to methionine possibly indicates a covalent mechanism of action (Makarov et al., 2009). However, a frame-shifting mutation would have been not tolerated in an essential protein, rendering DipZ as a non-essential target in *M.tb*.

If we focus on SAR studies on GSK756354A there has been a significant improvement in solubility (CLND of 35 μ M for the analogue GSK3590224A versus 8 μ M for the parent compound GSK756354A) while retaining similar potencies in whole-cell *M.tb* and *M. bovis* BCG assays. At this stage it is too early to assess the suitability of these entities as antitubercular lead molecules, especially without conclusive knowledge about their mechanism of action. However, further medicinal chemistry optimisation efforts should aim at improving the physicochemical properties of these entities to ensure optimal PK properties. Target identification, despite being helpful in early optimisation studies, may not be essential if these compounds are potent against susceptible and drug-resistant *M.tb* strains and show a good PK/PD profile. During the golden age of antibiotic discovery there was an urgent need for antitubercular drugs. For instance, isoniazid and rifampicin were approved without knowledge on their precise mode of action but safety and efficacy were demonstrated.

CHAPTER IV

CONCLUSIONS

Conclusions

I would firstly like to start by writing a few words about the piece of work that my thesis represents. Despite having identified hits that target Mt-AspS where I have worked intensively to characterise the mode of action of hits from the GSK compound collection, our results highlight the need to diversify the current drug discovery pipeline as soon as possible. From a PhD student perspective, this thesis has enabled me to discover the most valuable feature that any scientist should have - curiosity. Not only it has been a learning experience in how to think about how a given assay needs to be performed e.g. controls, robustness, reproducibility, etc., but also and more importantly, the ability to question everything around you- critical thinking. However, from an industrial scenario, only one project may be too much of a bet for success. Pharmaceutical companies around the world, including GSK, have a diversified portfolio knowing that only one out of thirty drug discovery projects will eventually lead to a new drug launching on the market.

It is for these reasons why it is not surprising that we have only been able to advance our hits until the hit confirmation and profiling phase (GSK681092A, GSK2250685A, GSK2198097C, GSK445893A, GSK991960A, GSK381407A and CCI14012) and to the hit-to-lead phase for GSK3448232A, the rhodanine hit compound. However, the only candidate showing biochemical target engagement is GSK2250685A, a series shown to possess low-micromolar range activities against the enzyme and similar potencies in whole-cell assays. However, the presence of highly reactive functional groups within the molecule hampers its advancement towards *in vivo* experiments. All the other hits, however, despite displaying some degree of potency in the aminoacylation reaction (as evidenced by IC₅₀ in the high micromolar range), fail to show similar inhibitory activities when interrogated in whole-cell assays. This is likely a result of off-target effects rather

than specific inhibition of enzyme activity. Moreover, these hits have been detected due to the high compound concentrations employed in the target-based screening assay of the TB set collection and hit confirmation studies after the whole-cell target-based screening assays of the TB box. An MIC shift may not therefore be of sufficient evidence of target engagement and should only be treated as an option to biochemical target validation, when proteins and substrates are not easy to obtain. Pharmacological evidence of target inhibition following biochemical validation assays is essential to any drug discovery programme following the target-to-drug approach, so-called target engagement.

However, despite the benefits that target identification represents, this may not always be necessary for a successful drug discovery programme. Many antitubercular drugs, such as isoniazid and rifampicin were discovered many decades ago before the advent of *omics* technologies. If the drug-to-target strategy guides drug discovery programmes, there are two requirements a given clinical candidate must have - safety and efficacy. If these two are met, no target identification programme is needed and therefore the target identification bottleneck disappears. Moreover, the recent advancement of β -lactam inhibitors as potential candidates for TB clearly exemplifies that no in-depth target validation is needed as long as safety and efficacy are demonstrated. It would however be of great interest for the scientific community to gain insight into the mode of action of these entities in non-replicating conditions, but no transpeptidase target have been validated to date as the target of this class of repurposed antibiotics. That being said, however, knowledge of the precise mode of action of a preclinical candidate can greatly facilitate drug discovery programmes by enhancing compound binding affinities. Knowledge of the protein-compound complex structure can aid medicinal chemists in developing stronger compound-target interactions through increased number of hydrogen bonds, van der Waals forces, etc.

Despite my limited expertise in the field, I think that the ideal strategy to identify promising screening hits would be to start by a HTS whole-cell target-based assay (where the protein of interest is either overexpressed or under-expressed) and have a robust and sensitive biochemical assay for further validation. Despite the main drawbacks of this approach, as mentioned above, the low costs and the ability to virtually screen against any given target make whole-cell assays the most appropriate approach for the initial identification of active hits in HTS screening campaigns. However, I would like to strengthen the fact of the need for an optimal biochemical assay for target validation. A minimum amount of protein employed in the assay would limit the observed potency of validated hits (e.g. compounds with IC₅₀ in the nanomolar range will not be detected if the effective enzyme concentration is in micromolar quantities). An optimal assay configuration is therefore essential to obtain maximum sensitivities and validate/compare the tightest inhibitors, which are often the most specific ones.

If we focus on what conclusions can be extracted for each project, we have now built a SAR for the hit compound against Mt-AspS that has been inconclusive in terms of the mechanism of inhibition at an atomic level. In the absence of a crystal structure of the protein-compound complex our medicinal chemistry efforts have been based on *in vitro* biochemical (IC₅₀) and compound solubility data in aqueous solutions, therefore preventing us from streamlining chemical synthesis from the knowledge of compound-target interactions. Among the rhodanine analogues synthesised so far, the most potent inhibitor shows an IC₅₀ value of 15 μ M, and when considering the enzyme concentration used in the biochemical assay (3 μ M), we can conclude that this series of inhibitors are suboptimal in terms of binding affinity. Usually potent inhibitors are the most specific ones, with IC₅₀ or K_d in the nanomolar range and with similar whole-cell growth

inhibitory activities (MIC). In our case, we don't observe a correlation between IC₅₀ and MIC values, the former being 10 orders of magnitude higher than the latter, which suggests:

Multiple-target inhibition. The result of the whole-cell growth activities is the sum of inhibition against multiple targets. We have generated spontaneous resistant mutants against the most potent analogue and cloned out the Mt-AspS gene into the pMV261 vector. When sequenced, we identified another mutation next to the enzyme active site in close proximity to the SNPs previously identified from whole-genome sequencing studies, showing that Mt-AspS is involved in resistance despite not being fully inhibited in biochemical assays.

Incorrect assay configuration. Our biochemical assay consists of a tRNA independent PP_i exchange assay. In the absence of tRNA, inhibitory values need to be handled carefully, especially if as our experiments suggest this series of hits act in a non-competitive manner. To test this hypothesis, we have designed and optimised a classical radioactive tRNA aminoacylation assay that uses a pool of commercial tRNA from *E. coli* in order to mimic physiological conditions. However, the activities of several screening hits against Mt-AspS in the tRNA-independent assay (e.g. GSK6810892A, GSK2250685A) are also in the micromolar potency range, therefore discarding this hypothesis as responsible for the lack of correlating activities.

Pathway-related effects. Resistance conferred by mutations in spontaneous resistant mutants and by gene overexpression would be pathway-related, but not coming straight from the hit binding to Mt-AspS. Its overexpression or mutated aminoacids may have an impact up or down the pathway. For instance, mutations may make the enzyme more catalytically efficient, depleting substrate and accumulating product. *M.tb* may sense this

alteration in the pathway and respond by regulating expression of other proteins, which can in turn be responsible for the observed resistance. Other groups have shown how gene expression can be regulated after external disturbances (Kalscheuer et al., 2010).

Focusing on the full compound profiling that we ran for the hit compound, the drop in activity as a result of the removal of the double bond in GSK3448775A, it can't be explained. If the hit behaved in an irreversible manner then we would have observed a decrease in enzyme activity over the time-course of the assay. However, enzyme activity remains flat, suggesting a reversible mechanism of inhibition. A covalent reversible mechanism could explain this behaviour. We have also incubated the enzyme with the inhibitor and subjected it to mass spectrometry, and no covalent modification was found for peptides containing the T570 amino acid, the mutated residue identified by WGS (supplementary section) If the compound was covalent, the drop in activity as a consequence of the removal of the double bond will be easily explained by the absence of a Michael acceptor, a highly reactive electrophile that would covalently bind nucleophiles, such as sulfhydryl groups, in target cysteines. But since the compound seems to act in a reversible manner, we can discard this functional group behaving like a Michael acceptor. Moreover, spontaneous resistant isolates do not harbour mutations in cysteines as shown by whole-genome sequencing studies. For now, we can only speculate as to how the compound binds the enzyme in the absence of a crystal structure of the protein-inhibitor complex.

In order to get away from this Michael-acceptor containing compound we have identified several active hits that inhibit Mt-AspS in a dose-dependent fashion. Almost every hit identified from our screening efforts displayed potencies against Mt-AspS in the high micromolar range, suggesting they are far from ideal. Moreover, only a few hits displayed

acceptable potencies in whole-cell assays (GSK445893A and GSK446688A). However, two of the hits identified, GSK2250685A and GSK681092A, harbour potencies in the low micromolar range with similar activities against whole-cell bacteria. It remains to be seen whether GSK would like to advance these hits any further given the presence of structural alerts within the molecules. However, it is undeniable the fact that these compounds represent, by far, the most potent antitubercular compounds identified to date that inhibit Mt-AspS. Despite the presence of highly reactive functional groups, they will represent potent starting chemical entities for future hit-to-lead programmes against this enzyme if these groups can be removed while preserving similar levels of activity.

On the other hand, selective inhibition against Mt-AspS has not been achieved for three out of five validated families against Mt-AspS. This suggests that the target may not be as conserved as initially described and that selective inhibition is challenging in drug discovery programmes against tRNA synthetases. However, it may all not be bad news. Specific inhibition can be achieved (Fang et al., 2015), but in order for this to be attainable, a full in-depth knowledge of the enzyme active site is needed e.g. specific residues involved in enzyme activity towards the inhibitor, thereby leading SAR efforts. All in all, one of the main conclusions that can be extracted from my thesis is that the irrational approach that high throughput screening of random libraries may not be the most suitable approach for the identification of specific protein inhibitors. The HTS is not to blame. Automation only allows performing experiments faster. The chemical diversity of the compound libraries is in my opinion what drives the outcome of any given screening campaign. It is also true that some targets are more druggable than others and this feature is the main driver of the selection of target proteins for drug discovery programmes, even with challenging proteins. In fact, today's drug pipelines have a diversified portfolio of strategies ranging from target-based focused approaches and

phenotypic assays against random libraries. Again, the greater the pipeline diversity the more chances of success, and projects need to be handled in a case-by-case scenario. Due to the peculiar characteristics of the cell wall of *M.tb* direct drug discovery efforts are directed towards the screening of random compound collections given the wide physicochemical spectra of available TB drugs. If a target-specific programme is being considered, a more rational-based structure-guided strategy should be pursued to increase the chances to identify potent and selective inhibitors.

In terms of the identification of novel modes of action for this new series of chemical entities (compound GSK756354A), the small shift conferred by the overexpression of *Mb3185c* in *M. bovis* BCG suggests a possible role in resistance. However, and as it similarly happens with target validation studies, biochemical evidence of compound inactivation is needed to further validate this hypothesis. The role of oxygenases in resistance mechanisms has been thoroughly assessed in the literature in the past (Baulard et al., 2000) and it would be of no surprise to discover a similar role for *Mb3185c*. The exact role of this protein in *M.tb* is unknown, but since it seems to play a role in metabolism and respiration the possibility of a possible role in compound detoxification is possible. However, it is also true that the consistent polymorphism observed in this open-reading frame across resistant isolates may have a resistance-related effect but on related pathways given the plasticity of signalling pathways and their role in drug resistance. In this regard, a lot of controversy has centred the role of the mycolate transporter *MmpL3* in drug resistance. Almost 15 structurally unrelated scaffolds have displayed resistance-related mutations in this open reading frame in spontaneous resistant mutants. It is still not very clear the role of this protein in drug resistance and virtually every scientist in the TB community has admitted that, without any biochemical evidence of compound-protein interaction, it is very unlikely that this

transporter is the target of any of these series of hits. Overexpression experiments with this transporter have rendered the strain either more susceptible or resistant to different scaffolds, with no strong evidence in favour to neither resistance nor susceptibility. Moreover, some of the entities are active against organisms that do not synthesize mycolic acids, such as SQ109 (Makobongo et al., 2013). It is for this reason that the presence of polymorphisms in spontaneous resistant mutants gives an indication of a possible resistance mechanism, but it may not be conclusive in terms of the mechanism of action of a given chemical entity. As mentioned above, mutations in drug efflux pumps or activator proteins might play a role in drug resistance that are not target-related. Whole-genome sequencing studies of *in vitro*-generated resistant mutants are then a very straightforward experiment that can provide valuable insight mode of action studies, but it certainly should be treated as part of a systematic experimental approach to target identification. Consequently, there is no ideal strategy to address questions regarding target identification in drug discovery and experiments should be considered in a case-by-case scenario. The overwhelming complexity of drug tolerance is especially noticeable in the presence of drug-tolerant *M.tb* sub-populations within drug-susceptible cultures. This tolerance is not a result of a genetic-based mechanism but rather due to the inherent plasticity of signalling pathways in response to external stress conditions. It is therefore naïve to think that this organism can be eradicated with single-drug based therapies. A combination of similarly effective drugs is necessary not only to overcome the emergence of drug-resistant strains but also to attack the intrinsic non-genetic phenotypic heterogeneity of *M.tb* populations.

The final eradication of TB requires a coordinated response between pharmaceutical companies, public agencies, foundations and academic labs. My thesis demonstrates that in order to diversify the current chemical space of pre-clinical chemical hits and therefore

accelerate drug discovery, more funding is needed. However, having new drugs, not only in the anti-tubercular pipeline but also against other infectious diseases, will only be the first step towards the complete eradication of bacterial infections. It will be of no use to anyone if new drugs are available but TB patients cannot access them. In this regard, and due to the fact that TB is associated to poverty in low-income countries, Governments need to take a more active role against TB. It is unacceptable that most of the funding in TB research comes either from the Bill & Melinda Gates foundation or the National Institute of Health in the United States. Moreover, the funding landscape towards diseases with little to no revenue is expected to decline in the next decades with an ageing population and a constantly-changing world does not guarantee an uninterrupted funding flow towards academic institutions and not-for-profit organisations. It is for these reasons that countries with high TB burdens, such as India or China need to escalate their research efforts. Despite a steady decline in TB incidence and mortality during the past decade, new infrastructure and improved healthcare access to people in these areas, in conjunction with available drugs and effective vaccines will certainly put an end to the epidemic. A global response will only dictate the final outcome of this disease and other drug resistant bacterial infections of the 21st century.

CHAPTER V

MATERIALS AND METHODS

5. Chapter V. Materials and Method

5.1 General chemical and media preparation

All Chemicals and Solvents were from Sigma-Aldrich, Bio-Rad or Fisher Chemicals, unless otherwise stated. Restriction enzymes were from Thermo Scientific.

5.1.1 Luria-Bertani (LB) Broth

37 g of LB Broth (Merck Millipore) in 1 L Water (H₂O), autoclaved at 121 °C for 15 min.

5.1.2 Luria-Bertani (LB) Agar

37 g of LB Broth (Merck Millipore), 15 g Bacto Agar (BD, Difco) in 1 L H₂O, autoclaved at 121 °C for 15 min. Incubated at 55 °C, then poured into petri dishes (25 mL/plate).

5.2 Transformation Buffers

5.2.1 Transformation Buffer 1 (TFB1)

85 mM Calcium Chloride (CaCl₂, 15 % glycerol (v/v).

5.3 Lysis Buffer

20 mM Tris-Cl pH 8, 500 mM NaCl, 40 mM Imidazole.

5.4 Dialysis Buffer

Mt-AspS 'Storage' Buffer – 20mM Tris-Cl pH 8, 50 mM NaCl, 1 μM EDTA, 10 % glycerol (v/v), made up to 4 L.

5.5 Mt-AspS coupled Reaction Buffer

20 mM HEPES pH 7.6, 4 mM MgCl₂, 50 mM KCl, 1.5% CHAPS.

5.6 tRNA-based Mt-AspS Reaction Buffer

20 mM HEPES pH 7.6, 4 mM MgCl₂, 50 mM KCl, 0.5% CHAPS.

5.7 HK/GLC6PDH Reaction Buffer

20 mM HEPES pH 7.6, 4 mM MgCl₂, 50 mM KCl, 1 mM DTT, 1.5% CHAPS.

5.8 Human mitochondrial AspS Reaction Buffer

20mM HEPES pH 8, 4 mM MgCl₂, 50 mM KCl, 1.5 % CHAPS.

5.9 Bacterial Strains and Conditions

E. coli Top 10 cells were used for propagation of plasmid DNA. These cells were routinely grown in LB broth, or LB agar at 37 °C. *E. coli* C41 (DE3) cells were used for the overproduction of recombinant protein in LB Broth at 37 °C.

5.10 Preparation of competent cells

5.10.1 *E. coli* chemically competent cells

An overnight *E. coli* culture was diluted 1:100 in 50 mL of LB broth and incubated at 37°C until mid-log phase was reached. Cells were then pelleted by centrifugation at 3,300 × *g* for 15 min and the supernatant discarded. From this point, pelleted cells were kept on ice and were then re-suspended in 10 mL of ice-cold calcium chloride. The suspension was then incubated on ice for 20 min, before centrifugation at 3,300 × *g* for 15 min at 4 °C. The supernatant was discarded, and the cells were re-suspended in 2.5 mL of ice-cold calcium chloride containing 15% glycerol and immediately aliquoted in microcentrifuge tubes for storage at -80°C until needed.

5.10.2 *M. bovis BCG* electrocompetent cells

M. bovis BCG cells were grown at 37 °C to OD₆₀₀ = 0.4-0.5 and pelleted by centrifugation at 3,300 × *g* for 15 min at 4 °C. The supernatant was discarded and the pellet was re-suspended in 0.5 volume of ice-cold 10 % glycerol (v/v). The suspension was then incubated on ice for 10 min. Cells were pelleted by centrifugation at 3,300 × *g* for 15 min

at 4 °C, before being resuspended in 0.3 volume of ice-cold 10 % glycerol (v/v). The suspension was incubated on ice for 10 min. Successive rounds of centrifugation, resuspension and incubation continued 3 times, reducing the volume of 10 % glycerol in each round (0.15 volume, 0.1 volume and 0.04 volume, successively). Once the cells had been incubated in 0.04 volume 10 % glycerol (v/v), cells were aliquoted into microcentrifuge tubes. Each aliquot was then stored at -80 °C until further usage.

5.11 Transformation of bacterial cells

5.11.1 Transformation of *E. coli* cells by heat shock method

Chemically competent *E. coli* cells (100 µL) were added on top of 1 µL plasmid DNA and incubated on ice for 15 min. The cell suspension was then subjected to 'heat shock', incubation at 42 °C for 1 min. Cells were then returned to ice for a further 2 min, before 250 µL LB broth was added and the suspension incubated at 37 °C for 1 h. The suspension was then plated onto LB agar plates (supplemented with correct antibiotic) and incubated overnight at 37 °C.

5.11.2 Transformation of *M. bovis* BCG cells by electroporation

Electrocompetent *M. bovis* BCG cells and plasmid DNA were incubated on ice until thawed. Plasmid DNA (5 µL or 1 µg) was then inserted into a 1 mm electroporation cuvette (Cell Projects) and incubated on ice for 20 min. Then 200 µL of *M. bovis* BCG cells were added to the cuvette and incubated on ice for 30 min. The cuvette was then inserted into an electroporator 2510 (Eppendorf) and pulsed at 1,800V before incubation on ice for 15 min. Cells were rescued by the addition of 1 mL antibiotic-free 7H9 broth and incubation at 37 °C overnight to allow the expression of antibiotic resistance genes. The next day the cells were pelleted and plated out on 7H9 agar plates containing 25 µg/mL kanamycin for selection of transformants.

5.12 DNA work

5.12.1 Polymerase Chain Reaction (PCR) amplification of *Mb3185c*

Amplification reactions were performed in 20 μ L reactions, consisting of 0.5 μ M forward primer (5'-GATCGATCGGATCCATGTTATCAACTGA-3'), 0.5 μ M reverse primer (5'-GATCGATCAAGCTTCTAGCTGGCACCTGG-3'), 250 ng genomic DNA (*M. tb*), 200 μ M dNTP mix, 1.5 mM MgCl₂, 3 % dimethyl sulfoxide (DMSO), 1 U/(50 μ L reaction) Phusion DNA polymerase (New England Biolabs), 1 \times Phusion 5 \times GC buffer (New England Biolabs) and made up to 20 μ L with nuclease free H₂O. Each reaction was then subjected to cycling conditions (Table 5.1) for gene amplification, inside a Mastercycler Gradient thermocycler (Eppendorf).

5.12.2 Agarose gel DNA electrophoresis

DNA samples were added to Loading Dye (5 % glycerol (v/v), 0.04 % Bromophenol Blue), and loaded onto TAE (40 mM Tris-acetate, 1 mM EDTA, pH 8.0) 1 % agarose gel, containing 5 % Midori Green dye (v/v) (Nippon Genetics) alongside 1 Kb DNA ladder (New England Biolabs). Gel was run in 1 \times TAE buffer at 120 V, 400 mA for 40 min. The bands were then visualised using a Gel Doc XR (Bio-Rad) with Image Lab software.

5.12.3 DNA extraction from agarose gel

DNA was extracted from agarose gel with the use of QIAquick gel extraction kit (Qiagen). The DNA band was excised from the agarose gel using a scalpel, but by minimising the amount of excess agarose in the slice. The agarose slice was then weighed and 3 volumes of Buffer QG were added to every 1 volume of agarose (3 μ L: 1 mg). The agarose was then incubated at 50 $^{\circ}$ C for 10 min, until the agarose dissolved. The pH of the solution was then checked, by assuring the mixture was yellow in color (indicator shows pH \leq 7.5). One gel

volume of isopropanol was added to the solution and mixed, before being transferred to a QIAquick spin column. The column was centrifuged at $18,000 \times g$ for 1 min, and the flow through discarded. This was repeated until the entire sample volume was passed through the spin column. The spin column was then washed with 500 μL of Buffer QG and centrifuged at $18,000 \times g$ for 1 min. The flow through was discarded before 750 μL of Buffer PE (Qiagen) was added to the spin column and centrifuged at $18,000 \times g$ for 1 min. The flow through was discarded and the spin column was again centrifuged at $18,000 \times g$ for 1 min, to extract any residual flow through, which was then also discarded. The spin column was then inserted into a microcentrifuge tube, with 30 μL of Elution Buffer (EB) being added to the column for 2 min. The tube was then centrifuged at $18,000 \times g$ for 1 min and the DNA in the flow through was retained and stored at -20°C .

5.12.4 PCR clean up

DNA that contained enzymes and buffers from the PCR reaction was cleaned up with the PCR clean up kit from Qiagen. The DNA sample was mixed with 500 μL of Buffer QG and transferred to a QIAquick spin column. The column was then centrifuged at $18,000 \times g$ for 1 min and the flow through discarded. The spin column was then washed with 750 μL of Buffer PE (Qiagen) by centrifugation at $18,000 \times g$ for 1 min. The flow through was discarded and the spin column was again centrifuged at $18,000 \times g$ for 1 min, to extract any residual flow through, which was then also discarded. The spin column was then inserted into a microcentrifuge tube, with 30 μL of EB buffer being added to the column for 2 min. The tube was then centrifuged at $18,000 \times g$ for 1 min and the cleaned DNA in the flow through was retained and stored at -20°C .

5.12.5 Genomic DNA extraction

Genomic DNA was extracted from 25 mL of bacterial culture grown in 7H9 media, centrifuged at $3,300 \times g$ for 15 min. Pelleted cells were resuspended in 450 μL of 50 mM Tris-HCl pH 8, 10 mM EDTA and 100 $\mu\text{g}/\text{mL}$ RNase A and 50 μL of 10 mg/mL lysozyme, incubated at 37 °C overnight. 10 % SDS (100 μL) was added to the suspension, alongside 50 μL of 10 mg/mL proteinase K. The suspension was gently mixed and incubated at 55°C for 4 h. 5 M NaCl (200 μL) was added to the suspension and incubated at 65 °C for 15 min. Once the suspension was cooled, chloroform (500 μL) was added, gently mixed for 5 min, and then centrifuged at $18,000 \times g$ for 5 min. The aqueous layer was taken, ice-cold isopropanol (350 μL) added, gently mixed by inversion to allow for DNA precipitation and centrifuged at $18,000 \times g$ for 10 min at 4 °C. The supernatant was removed, ice-cold 70 % ethanol (1 mL) was added and the tube inverted gently. The sample was centrifuged at $18,000 \times g$ for 5 min at 4 °C. The supernatant was removed and the DNA pellet was dried at room temperature for 20 min. The DNA was finally resuspended in 30 μL of nuclease-free H_2O and stored at -20°C until further usage.

5.12.6 Plasmid DNA extraction

Plasmid DNA was extracted from 5 mL of bacterial culture using a QIAprep spin miniprep kit (Qiagen). Cells were pelleted by centrifugation at $3,300 \times g$ for 15 min and the supernatant discarded. Pellets were re-suspended in 250 μL of Buffer P1 containing RNase A (Qiagen) and transferred into microcentrifuge tubes. After this, 250 μL of Buffer P2 (Qiagen) was added and mixed by tube inversion, before the addition of 350 μL of Buffer N3 (Qiagen), which was also mixed by tube inversion. Mixtures were then centrifuged at $18,000 \times g$ for 10 min and the supernatant was extracted and transferred into a Miniprep spin column (Qiagen). The spin column was centrifuged at $18,000 \times g$ for

1 min and the flow through discarded. The spin column was then washed with 500 μ L of Buffer PB (Qiagen) by centrifugation at $18,000 \times g$ for 1 min and the flow through discarded. A final wash step of 750 μ L Buffer PE (Qiagen) was then added to the spin column, and was centrifuged at $18,000 \times g$ for 1 min, with the flow through being discarded. The spin column was again centrifuged at $18,000 \times g$ for 1 min, to extract any residual flow through, which was then discarded. The spin column was then inserted into a microcentrifuge tube, and 30 μ L of EB buffer were added onto the column and left stand for 2 min. The tube was then centrifuged at $18,000 \times g$ for 1 min and the plasmid DNA in the flow through was retained and stored at -20°C .

5.13 Mt-AspS recombinant protein purification

The construct pET28b-Mt-AspS with the C-Terminal His₆tag was transformed into *E. coli* C41 competent cells for protein expression. An overnight starter culture was prepared by inoculating a single colony from a freshly transformed plate into LB broth containing 25 $\mu\text{g}/\text{mL}$ kanamycin. A 1% inoculum of the starter culture was used to inoculate 1 L of LB broth containing 25 $\mu\text{g}/\text{mL}$ kanamycin and grown at 37°C until an OD of 0.6. Protein expression was then induced by the addition of 1 mM IPTG and cultured overnight at 16°C . The harvested cells were resuspended in lysis buffer containing 20 mM Tris-HCl pH 8.0, 500 mM NaCl, 10% glycerol, 40 mM imidazole, 1mg/mL lysozyme and protease inhibitor tablet and disrupted by sonication with eight cycles of 30 s pulses and 30 s intervals. The crude lysate was clarified by centrifugation at 15,000 rpm for 45 min. The supernatant was loaded onto a pre-packed Ni²⁺ Sepharose HisTrap column (GE healthcare), which was previously equilibrated with buffer A (lysis buffer without lysozyme and protease inhibitor). The column was then washed with buffer A and eluted with a stepwise gradient of imidazole (50, 75, 100, 250 and 500 mM) in buffer A. The

purified fractions were analysed by SDS-PAGE and relevant fractions containing Mt-AspS were pooled and dialysed against buffer B (20 mM Tris-HCl pH 8.0, 50 mM NaCl, 10% glycerol, 1 mM DT and 100 μ M EDTA) and concentrated with an Amicon ultrafiltration unit containing a 10 KDa cut off membrane. Protein concentration was measured using the Pierce BCA protein reagent kit with BSA as a standard. A 1:50 mixture of reagents A and B (2 mL) were added into 2 mL microcentrifuge tubes containing several known BSA concentrations and absorbance values were obtained at 562 nm in a spectrophotometer. Mt-AspS stock concentrations were calculated from interpolated values from a standard BSA calibration curve multiplied by the dilution factor of the sample used for final quantification.

5.14 SDS-PAGE

Protein fractions were mixed with SDS loading dye (2 % SDS, 125 mM Tris pH 6.8, 715 mM β -mercaptoethanol, 20 % glycerol made up to 1 mL with H₂O) and incubated at 100 °C for 10 min. Boiled samples, alongside PageRuler (Thermo Scientific) protein marker, were then ran on a mini-PROTEAN TGX precast (Bio-Rad) gels at 200 V, 50 mA for 30 min. Gels were then incubated in Instant Blue stain (Expedeon) at room temperature with shaking for 1 h.

5.15 Mt-AspS-based screening of the GSK TB set compound library

The GSK hit set of 177 novel chemical entities was evaluated at a single 100 μ M cut-off concentration in a 96-well black-bottom microplate-adapted ATP release assay. The reaction mixture consisted of 20 mM HEPES pH 7.6, 4 mM MgCl₂, 50 mM KCl, 1 mM DTT, 2 mM ADPCP, 10 mM D-glucose, 0.5 mM NADP⁺, 10 mM L- Asp, 3 μ g of yeast hexokinase and *L. mesenteroides* glucose-6- phosphate dehydrogenase mixture and 3 μ M of Mt-AspS. This enzyme concentration was within the linear range of the V_i vs E curve, although quite

high to increase the assay signal over background ratio. The amount of coupled enzymes used was high enough to limit non-specific interactions that could affect the outcome of the assay. Compound dilutions were previously made in 100% DMSO and 2 μ L were added into its corresponding well and filled up manually to 200 μ L with assay mix. The reaction was triggered with 500 μ M inorganic pyrophosphate and read in the fluorescence mode at a 450 nm emission wavelength in a BMG Pherastar plate reader. The concentration of the tested compounds was set at 100 μ M since a poor hit rate at lower concentrations could be expected by the high Mt-AspS concentration employed in the assay. Cherry-picked compounds showing inhibition above 50% were further interrogated in a dose-response manner in a 0.1 – 300 μ M concentration range for IC₅₀ determination. Background fluorescence was reported in the absence of enzyme for each of the concentrations tested to calculate the standard error (3 replicates per concentration) and positive and negative controls containing DMSO at the same concentration of the tested wells were included to check for absence of solvent-related inhibition, assay quality determination and data standardisation. The raw data was fitted to a dose-response inhibition curve using non-linear regression on GraphPad Prism and the IC₅₀ reported as the inhibitor concentration reducing enzyme activity by 50%.

5.16 HK/GLC6PDH-based TB set screening

All the GSK hits were tested against the hexokinase (HK)/glucose 6 phosphate dehydrogenase (GLC6PDH) coupled reaction (without Mt-AspS) in order to remove promiscuous compounds. Compounds were tested at 100 μ M by adding 2 μ L of a 10 mM stock in 100% DMSO in a reaction mixture consisting of 20 mM HEPES pH 7.6, 4 mM MgCl₂, 1 mM DTT, 0.1 mM ATP, 50 mM KCl, 0.5 mM NADP⁺, 120 ng of yeast hexokinase and *L. mesenteroides* glucose-6-phosphate dehydrogenase mixture in a total volume of 200

μL. The reaction was initiated with the addition of 10 mM glucose and read in the absorbance mode at 340 nm in a clear-bottom black Greiner plate in the BMG Pherastar plate reader. Background absorbance was as well reported in the absence of enzyme for standard error calculation and both positive and negative controls were included to assess assay quality in the presence of DMSO.

5.17 Whole-cell compound potency determination (MIC)

5.17.1 Solid MIC determination

Bacterial cells (10^6) growing at log-phase (0.8 OD) were spotted onto solid plates containing 2-fold increasing concentrations from 1 μM up to 32 μM of inhibitor, sealed with parafilm, covered with aluminium foil and incubated for 2 weeks at 37°C in a static incubator. Presence or absence of growth was reported as an indicator of compound activity. For whole-cell potency assessment against overexpressor strains, gene overexpression was confirmed with the MIC shift for the parent compound as an internal control.

5.17.2 Liquid MIC determination

In order to determine more accurate MIC values for those entities that showed inhibition in the solid MIC assay, these compounds were dispensed in a dose-response manner (0.25-128 μM) with the HP D300 dispenser into Greiner clear bottom-96-well plates. Cells (10^4) were plated out from cultures grown at log-phase (0.8 OD) into each assay well and filled up to 200 μL with 7H9 media. Plates were then covered with aluminium foil and incubated at 37°C and 5% CO₂. After 7 days, 25 μL of a 0.8% resazurin solution (250 mg resazurin tablet in 30mL PBS, filter-sterilised) were added into each assay well (0.02% final resazurin concentration), covered with aluminium foil and incubated for a further 48 h at 37°C and 5% CO₂.

5.18 Compound profiling studies

5.18.1 Time-course dependence

The Mt-AspS protein stock was diluted to 1 μM in the presence of assay buffer (10 μL) (20 mM HEPES pH 7.5, 4 mM MgCl_2 , 50 mM KCl, 2 mM ADPCP, 10 mM D-glucose, 0.5 mM NADP^+ , 10 mM L-Asp, 3 μg of yeast hexokinase and *L. mesenteroides* glucose-6-phosphate dehydrogenase mixture. The reaction was then triggered with the addition of 10 μL of a 2X substrate mix solution to a 384-black-bottom polystyrene plate (Corning). The final GSK3449228A concentration was chosen considering IC_{50} values from previous biochemical assays. Similar DMSO concentrations to the test compound were added into the control wells of 384-black bottom plates. Similar amounts of enzyme were incubated with DMSO at the same concentration of the assay wells as an enzyme activity control for each time point.

5.18.2 Substrate competition studies

The inhibitory activities of new compounds targeting Mt-AspS was assessed at several β - γ -methyladenosine triphosphate (0, 25, 33, 50, 100, 250, 500 and 1000 μM) and inhibitor concentrations (DMSO, 50 and 100 μM) while keeping fixed concentrations of L-Asp and PPI at saturating values ($10 \times K_M$). The reaction was triggered with the addition of 10 μL of a 2X substrate mix solution to a 384 black-bottom polystyrene plate (Corning) containing 10 μL of a 2X buffer solution with 0.5 μM Mt-AspS in 20 mM HEPES pH 7.6, 4 mM MgCl_2 and 50 mM KCl. Plates were then briefly centrifuged and read on EnVision (Perkin Elmer) using NADPH fluorescence in the kinetic mode as the method of detection. Slopes corresponding to initial reaction rates were plotted versus against substrate concentration for each inhibitor concentration and data points were fitted to standard

hyperbolic Michaelis Menten curves on GraphPad Prism 7.0 for K_M and V_{max} determination.

5.18.3 DTT dependence

Compound potency (IC₅₀) was interrogated in the presence and absence of 1mM DTT to identify potential promiscuous compounds. The reaction conditions were kept as previously described and initial reaction velocities were normalised and plotted against the logarithm of inhibitor concentration. Sigmoidal dose-response curves were plotted on GraphPad Prism for IC₅₀ determination.

5.19 Biochemical characterisation of human mitochondrial Hs-AspS & assay development for selectivity assessment

5.19.1 Recombinant protein purification

The human mitochondrial Hs-AspS-containing pDEST14 vector carrying ampicillin resistance was a gift from Dr. Marie Sissler from the University of Strasbourg and was used to transform 100 μ L of chemically competent C41 *E. coli* cells. A single colony was picked to inoculate a starter culture volume of 100 mL containing 100 μ g/mL ampicillin. Large culture volumes (4 L) were inoculated with 1% of the starter culture, grown at 37°C for two hours and when protein expression was induced with 1 mM IPTG, cultures were incubated at 16°C overnight. Harvested cells were resuspended in lysis buffer containing 20 mM Tris-HCl pH 8.0, 500 mM NaCl, 10% glycerol, 40 mM imidazole, 1 mg/mL lysozyme and protease inhibitor tablet and disrupted by sonication with eight cycles of 30 s pulses and 30 s intervals. The crude lysate was clarified by centrifugation at 15,000 rpm for 45 min. The supernatant was loaded into a pre-packed Ni²⁺ Sepharose HisTrap column (GE healthcare), which was previously equilibrated with buffer A (lysis buffer without

lysozyme and protease inhibitor). The column was washed with buffer A and eluted with a stepwise gradient of imidazole (50, 75, 100, 250 and 500 mM) in buffer A. The purified fractions were analysed by SDS-PAGE and relevant fractions containing Hs-AspS were pooled and dialysed against buffer B (20 mM Tris-HCl pH 8.0, 50 mM NaCl, 10% glycerol, 1 mM DTT and 100 μ M EDTA) and concentrated with an Amicon ultrafiltration unit containing a 10 KDa cut off membrane. Protein concentration was measured with the BCA protein reagent kit using BSA as a standard.

5.19.2 Substrate dependence of human mitochondrial AspS

The substrate dependence of Hs-AspS was assessed using a range of β - γ -methyladenosine triphosphate (ADPCP), L-Asp and PPi concentrations in the tRNA-independent assay. Reactions were performed in HEPES pH 8, 4mM MgCl₂, 50 mM KCl and 3 μ M of human AspS in a final assay volume of 200 μ L, using NADPH fluorescence as the method of detection. For kinetic studies, two out of the three substrates were kept at fixed saturating concentrations while a concentration range of the third substrate was used to study initial enzyme reaction rates for K_M determination. For the calculation of K_{cat} the maximum enzyme velocity (zero order kinetics) was divided by the total amounts of AspS employed in the assay at a final volume of 200 μ L

5.19.3 Compound selectivity assessment

In order to assess inhibitory activity against the Hs-AspS, a reaction mixture (200 μ L) consisting of 20 mM HEPES MgCl₂, 50 mM KCl, 0.5 mM NADP⁺, 3 μ M Hs-AspS 120 ng of yeast hexokinase and *L. mesenteroides* glucose-6-phosphate dehydrogenase was employed to study the effect of each compound on the aminoacylation reaction. The substrate concentrations were fixed at saturation for PPi and L-Asp (250 μ M and 10 mM, respectively) and at matching K_M values for ADPCP (250 μ M). Among the entities tested,

we included those identified from the target-based Mt-AspS screening and the current series of analogues of the parent compound hit-to-lead optimisation programme. Each inhibitor was tested in duplicate at three independent concentrations and DMSO was included in the positive (maximum enzyme activity) and negative control (minimum enzyme activity) at the same concentration of the tested compounds to check for solvent interference with assay signal. Initial reaction rates were standardised to the positive and negative control values to determine inhibitory percentages of each inhibitor.

5.20 Whole-cell target-based high throughput screening assay

The GSK TB box collection (11,000 chemical entities) was screened for Mt-AspS inhibitors based on resistance upon Mt-AspS overexpression. We selected three different concentrations (0.5, 2.5 and 12.5 μM) based on compound potency in order not to miss any potential hits. 10^4 cells (25 μL) of a log-phase culture of a genetically engineered *M. bovis* BCG strain overexpressing AspS from a replicative pMV261 plasmid was added into each assay well of a 384-well-plate (Greiner) with white opaque walls with a Multidrop™ Combi dispenser (Thermo Scientific), increasing automation and shortening assay developing times. To control evaporation, plates were individually sealed with parafilm, covered with aluminium foil, stacked in groups of 5 with dummy plates both at the bottom and the top, and stored in plastic boxes inside a 37°C and 5% CO₂ incubator with humidity control. At day 7, 25 μL of reconstituted Bac-titer GLO reagent (Promega), which extracts physiological ATP upon cell lysis, were added into each assay well. A recombinant then luciferase produces light upon an ATP-dependent oxyluciferin reaction. Plates were briefly shaken prior to luminescence reading in a Spectra Max M5 (Molecular Devices). Raw luminescence values were standardised to cell survival percentages using the positive and negative control for cell growth and the effect of a given inhibitor

calculated as: % inhibition= $100 * ((\text{data} - \text{control 1}) / (\text{control 2} - \text{control 1}))$, where control 1 = maximum activity (DMSO only; uninhibited growth in column 6), and control 2 = bacterial growth completely inhibited (by treatment with 10 μM rifampicin in column 18). Assay performance statistics (signal to background ratio and Z') were calculated using templates in ActivityBase XE (ID Bussines Solutions Ltd, Surrey, UK). Dose-response confirmation studies were performed at a concentration range of 0.04 up to 50 μM and raw luminescence values were standardised to the maximum and minimum percentage of inhibition as stated for single-shot experiments. Dose-response curves were obtained on Tibco Spotfire and whole-cell target engagement confirmed by the MIC shift, reported here as the ratio between the mean of the MIC values for each strain.

5.21 tRNA-based biochemical assay

5.21.1 Filtration assay

5.21.1.1 Substrate dependence of Mt-AspS in a tRNA-based assay

The aminoacylation reaction was performed in a final assay mixture of 80 μL consisting of 20 mM HEPES buffer pH 7.7, 4 mM MgCl_2 , 50 mM KCl and a range of substrate and enzyme concentrations in order to determine the initial rate and the kinetic constants of the aminoacylation reaction. The values obtained in these experiments were therefore obtained under steady-state conditions following classical Michaelis-Menten guidelines for enzyme kinetic studies. For the determination of the initial rate of the aminoacylation reaction, several enzyme concentrations (0.2, 0.5 and 1 μM) were incubated at 37°C in the presence of 1 mg/mL tRNA from *E. coli* 600 MRE, 15 μM L-Asp (200 mCi/mmol, Perkin Elmer) and 4 mM ATP. The reaction was quenched at several time points over a period of fifteen minutes with 50 μL of 10% TCA and a white precipitate was observed; at an acidic

pH, the phosphate backbone of nucleic acids becomes protonated, precipitating out of solution due to the inability to form hydrogen bonds with water. When the time-course was complete, the plates were incubated at 4°C during 30 min to allow for tRNA precipitation. The aminoacylated product was then transferred onto GF/C 96-well filter plates (Packard), extensively washed in an excess volume of 10% TCA, once with 95% ethanol and then dried under a heat lamp prior to scintillation counting in a Microbeta Trilux 1450 model, basically in accordance with the method previously described for classical studies of aminoacyl-tRNA synthetases (Pope et al., 1998b). The enzyme concentration (0.2 μ M) was chosen to assess Mt-AspS substrate dependence based on linearity of product formation. For K_M determination, varying substrate concentrations were assayed keeping the others at a fixed saturating concentration. For L-Asp kinetic studies, a starter concentration of radiolabelled L-Asp of 15 μ M was serially diluted with non-radioactive L-Asp up to a final concentration of 900 μ M where saturation was observed. The obtained data points were fitted to a Sigmoidal dose-response curve on Graph Pad Prism 7.0, and its IC50 value corresponds to the K_M plus the concentration of radiolabelled L-Asp used in the assay. For presentation purposes, initial cpm values were converted to μ mol aspartyl-tRNA/s. For K_{cat} determination, maximum enzyme velocity (zero order kinetics) was divided by the total amounts of Mt-AspS employed in the assay at a final volume of 80 μ L.

5.21.1.2 Biochemical validation of screening hits in a tRNA-based assay

Whole-cell screening hits were interrogated for their potency against Mt-AspS in the aminoacylation reaction. The IC50 dose response assays for each were done at 0.2 μ M Mt-AspS and matching apparent K_M values of L-Asp and tRNA while keeping ATP at saturating concentrations in order to filter out probable ATP-competitive inhibitors.

Compound stocks were made as 10mM solutions in 100% DMSO and dispensed into 96-well-polystyrene plates in a 1:3 dilution manner up to a final concentration of 100 μ M. In the maximum (100% activity) and minimum (0% activity) controls similar DMSO concentrations were added to check the absence of solvent-related inhibition. The highest concentration of DMSO and CHAPS used in the assay were 1% and 0.5%, respectively, and precipitable radioactivity was transferred onto GF/C filter plates for scintillation counting.

5.21.2 Scintillation Proximity Assay (SPA)

The availability of the SPA technology allows the development of a homogenous assay based on the excitation of a scintillator and light emission when a radiolabelled molecule is in close proximity. Several beads have been reported to bind nucleic acids, therefore allowing the direct measurement of tRNA aminoacylation without the physical separation needed in the TCA filtration assay. In order to optimise the assay for HTS applications (optimal Z' and S/B ratios) several bead types have been tested in a dose-response manner (YOx, YSi) (Perkin Elmer).

5.22 Medium-throughput screening assay of a series of analogues in a tRNA-independent biochemical assay

A number of structurally related analogues to the Mt-AspS screening hits GSK2198097C, GSK445893A and GSK1568097C from the GSK TB box collection were evaluated in a dose-response manner (0.05-100 μ M) in a 384-well black-bottom microplate-adapted ATP release assay optimised for HTS purposes. The reaction mixture consisted of 20 mM HEPES pH 7.6, 4 mM MgCl₂, 50 mM KCl, 1 mM DTT, 2 mM ADPCP, 10 mM D-glucose, 0.5 mM NADP⁺, 10 mM L- Asp, 3 μ g of yeast hexokinase and *L. mesenteroides* glucose-6-

phosphate dehydrogenase mixture and 0.5 μ M of Mt-AspRS in a final assay volume of 20 μ L. The amount of coupled enzymes used was high enough to minimise assay interference. Stock compounds were dispensed with the Echo 555 (Labcyte) into black bottom 384-well- plates (Corning) and were stored at -80°C until needed. Enzymes and substrates were kept separately in 2 working solutions prepared at 2X the final assay concentrations. Reactions were triggered with the addition of substrate solution into plates pre-plated with enzyme and no-enzyme control wells. The assay was performed at room temperature and fluorescence values were continuously monitored in EnVision (Perkin Elmer) during the period of the assay (4 minutes). Similar amounts of DMSO (1%) were added into control wells to check for absence of solvent-related inhibition. The raw data was normalised to the positive and negative controls for enzyme activity in Excel and was further processed in Excel and GraphPad Prism 6.0 for IC₅₀ determination.

5.23 Generation of spontaneous resistant isolates against GSK756354A

M. bovis BCG WT of a log-phase culture (10^8) were plated out on 7H11 agar plates containing 5x, 10x and 20x MIC of GSK756354A to induce the generation of spontaneous resistant mutants. Plates were sealed with parafilm and incubated for 6 weeks at 37°C until colonies were observed.

5.23.1 Confirmation of the resistant phenotype

Resistant colonies were individually picked and grown in antibiotic-free 7H9 media for downstream experiments. Cells (10^6) were spotted from log-phase grown cultures onto 7H11 plates containing 5x MIC of GSK756354A. A control plate was used to check cell growth in the absence of compound and *M. bovis* WT BCG used as a susceptible control strain.

5.23.2 Genome extraction from resistant strains

Genomic DNA extraction was performed as stated previously. For whole-genome sequencing applications care was taken to avoid adding any chelating agent in the resuspension buffer since it will inhibit the amplification-based reactions that such application requires. Genomic DNA was extracted from 25 mL of bacterial culture grown in 7H9 media, centrifuged at $3,300 \times g$ for 15 min. Pelleted cells were resuspended in 450 μ L of 50 mM Tris-HCl pH 8, 10 mM EDTA and 100 μ g/mL RNase A and 50 μ L of 10 mg/mL lysozyme, incubated at 37 °C overnight. 10 % SDS (100 μ L) was added to the suspension, alongside 50 μ L of 10 mg/mL proteinase K. The suspension was gently mixed and incubated at 55°C for 4 h. 5 M NaCl (200 μ L) was added to the suspension and incubated at 65 °C for 15 min. Once the suspension was cooled, chloroform (500 μ L) was added, gently mixed for 5 min, and then centrifuged at $18,000 \times g$ for 5 min. The aqueous layer was taken, ice-cold isopropanol (350 μ L) added, gently mixed by inversion to allow for DNA precipitation and centrifuged at $18,000 \times g$ for 10 min at 4 °C. The supernatant was removed, ice-cold 70 % ethanol (1 mL) was added and the tube inverted gently. The sample was centrifuged at $18,000 \times g$ for 5 min at 4 °C. The supernatant was removed and the DNA pellet was dried at room temperature for 20 min. The DNA was finally resuspended in 30 μ L of nuclease-free H₂O and stored at -20°C until further usage.

5.23.3 Genomic DNA whole-genome sequencing of *M. bovis* BCG resistant isolates

Genomic DNA was sequenced using a HiSeq Illumina 2500 platform using 2 x 250bp paired-end reads (Microbesng.uk, 2017). Three beads were washed with extraction buffer containing lysozyme and RNase A, incubated for 25 min at 37°C. Proteinase K and RNaseA were added and incubated for 5 min at 65°C. Genomic DNA was purified using an equal volume of SPRI beads and resuspended in EB buffer.

DNA was quantified in triplicates with the Quantit dsDNA HS assay in an Eppendorf AF2200 plate reader. Genomic DNA libraries were prepared using Nextera XT Library Prep Kit (Illumina, San Diego, USA) following the manufacturer's protocol with the following modifications: two nanograms of DNA instead of one were used as input, and PCR elongation time was increased to 1 min from 30 seconds. DNA quantification and library preparation were carried out on a Hamilton Microlab STAR automated liquid handling system. Pooled libraries were quantified using the Kapa Biosystems Library Quantification Kit for Illumina on a Roche light cycler 96 qPCR machine. Libraries were sequenced on the Illumina HiSeq using a 250 bp paired end protocol. Reads were adapter trimmed using Trimmomatic 0.30 with a sliding window quality cutoff of Q15 (Bolger et al., 2014). *De novo* assembly was performed on samples using SPAdes version 3.7 (Bankevich et al., 2012), and contigs were annotated using Prokka 1.11 (Seemann, 2014). Variant calling was then performed by to identify single nucleotide polymorphisms (SNPs) in the genome of resistant strains compared to WT *Mycobacterium bovis* BCG reference sequence.

CHAPTER VI

REFERENCES

References

- ABRAHAM, K. A., COX, J. A., SPIVEY, V. L., LOMAN, N. J., PALLAN, M. J., CONSTANTINIDOU, C., FERNANDEZ, R., ALEMPARTE, C., REMUINAN, M. J., BARROS, D., BALLELL, L. & BESRA, G. S. 2012. Identification of novel imidazo[1,2-a]pyridine inhibitors targeting M. tuberculosis QcrB. *PLoS One*, 7, e52951.
- AINSA, J. A., BLOKPOEL, M. C., OTAL, I., YOUNG, D. B., DE SMET, K. A. & MARTIN, C. 1998. Molecular cloning and characterization of Tap, a putative multidrug efflux pump present in Mycobacterium fortuitum and Mycobacterium tuberculosis. *J Bacteriol*, 180, 5836-43.
- AL-ZAMEL, F. A. 2009. Detection and diagnosis of Mycobacterium tuberculosis. *Expert Rev Anti Infect Ther*, 7, 1099-108.
- AMINOV, R. I. 2010. A brief history of the antibiotic era: lessons learned and challenges for the future. *Front Microbiol*, 1, 134.
- ANDERSSON, D. I. & HUGHES, D. 2014. Microbiological effects of sublethal levels of antibiotics. *Nat Rev Microbiol*, 12, 465-78.
- ANDRIES, K., VERHASSELT, P., GUILLEMONT, J., GOHLMANN, H. W., NEEFS, J. M., WINKLER, H., VAN GESTEL, J., TIMMERMAN, P., ZHU, M., LEE, E., WILLIAMS, P., DE CHAFFOY, D., HUITRIC, E., HOFFNER, S., CAMBAU, E., TRUFFOT-PERNOT, C., LOUNIS, N. & JARLIER, V. 2005. A diarylquinoline drug active on the ATP synthase of Mycobacterium tuberculosis. *Science*, 307, 223-7.
- ARASTU-KAPUR, S., PONDER, E. L., FONOVIĆ, U. P., YEOH, S., YUAN, F., FONOVIĆ, M., GRAINGER, M., PHILLIPS, C. I., POWERS, J. C. & BOGYO, M. 2008. Identification of proteases that regulate erythrocyte rupture by the malaria parasite Plasmodium falciparum. *Nat Chem Biol*, 4, 203-13.

- BAELL, J. B. & HOLLOWAY, G. A. 2010. New substructure filters for removal of pan assay interference compounds (PAINS) from screening libraries and for their exclusion in bioassays. *J Med Chem*, 53, 2719-40.
- BALLELL, L., BATES, R. H., YOUNG, R. J., ALVAREZ-GOMEZ, D., ALVAREZ-RUIZ, E., BARROSO, V., BLANCO, D., CRESPO, B., ESCRIBANO, J., GONZALEZ, R., LOZANO, S., HUSS, S., SANTOS-VILLAREJO, A., MARTIN-PLAZA, J. J., MENDOZA, A., REBOLLO-LOPEZ, M. J., REMUINAN-BLANCO, M., LAVANDERA, J. L., PEREZ-HERRAN, E., GAMO-BENITO, F. J., GARCIA-BUSTOS, J. F., BARROS, D., CASTRO, J. P. & CAMMACK, N. 2013. Fueling open-source drug discovery: 177 small-molecule leads against tuberculosis. *ChemMedChem*, 8, 313-21.
- BANKEVICH, A., NURK, S., ANTIPOV, D., GUREVICH, A. A., DVORKIN, M., KULIKOV, A. S., LESIN, V. M., NIKOLENKO, S. I., PHAM, S., PRJIBELSKI, A. D., PYSHKIN, A. V., SIROTKIN, A. V., VYAHHI, N., TESLER, G., ALEKSEYEV, M. A. & PEVZNER, P. A. 2012. SPAdes: a new genome assembly algorithm and its applications to single-cell sequencing. *J Comput Biol*, 19, 455-77.
- BATT, S. M., JABEEN, T., BHOWRUTH, V., QUILL, L., LUND, P. A., EGGELING, L., ALDERWICK, L. J., FUTTERER, K. & BESRA, G. S. 2012. Structural basis of inhibition of Mycobacterium tuberculosis DprE1 by benzothiazinone inhibitors. *Proc Natl Acad Sci U S A*, 109, 11354-9.
- BAULARD, A. R., BETTS, J. C., ENGOHANG-NDONG, J., QUAN, S., MCADAM, R. A., BRENNAN, P. J., LOCHT, C. & BESRA, G. S. 2000. Activation of the pro-drug ethionamide is regulated in mycobacteria. *J Biol Chem*, 275, 28326-31.
- BECKER, H. D. & KERN, D. 1998. Thermus thermophilus: a link in evolution of the tRNA-dependent amino acid amidation pathways. *Proc Natl Acad Sci U S A*, 95, 12832-7.
- BELANGER, A. E., BESRA, G. S., FORD, M. E., MIKUSOVA, K., BELISLE, J. T., BRENNAN, P. J. & INAMINE, J. M. 1996. The embAB genes of Mycobacterium avium encode an arabinosyl

- transferase involved in cell wall arabinan biosynthesis that is the target for the antimycobacterial drug ethambutol. *Proc Natl Acad Sci U S A*, 93, 11919-24.
- BEYOGLU, D. & IDLE, J. R. 2013. Metabolomics and its potential in drug development. *Biochem Pharmacol*, 85, 12-20.
- BHATT, A., FUJIWARA, N., BHATT, K., GURCHA, S. S., KREMER, L., CHEN, B., CHAN, J., PORCELLI, S. A., KOBAYASHI, K., BESRA, G. S. & JACOBS, W. R., JR. 2007. Deletion of kasB in *Mycobacterium tuberculosis* causes loss of acid-fastness and subclinical latent tuberculosis in immunocompetent mice. *Proc Natl Acad Sci U S A*, 104, 5157-62.
- BIRKENSTOCK, T., LIEBEKE, M., WINSTEL, V., KRISMER, B., GEKELER, C., NIEMIEC, M. J., BISSWANGER, H., LALK, M. & PESCHEL, A. 2012. Exometabolome analysis identifies pyruvate dehydrogenase as a target for the antibiotic triphenylbismuthdichloride in multiresistant bacterial pathogens. *J Biol Chem*, 287, 2887-95.
- BLONDIAUX, N. & MOUNE, M. 2017. Reversion of antibiotic resistance in *Mycobacterium tuberculosis* by spiroisoxazoline SMART-420. 355, 1206-1211.
- BOLGER, A. M., LOHSE, M. & USADEL, B. 2014. Trimmomatic: a flexible trimmer for Illumina sequence data. *Bioinformatics*, 30, 2114-20.
- BOLLA, J. R., SU, C. C., DO, S. V., RADHAKRISHNAN, A., KUMAR, N., LONG, F., CHOU, T. H., DELMAR, J. A., LEI, H. T., RAJASHANKAR, K. R., SHAFER, W. M. & YU, E. W. 2014. Crystal structure of the *Neisseria gonorrhoeae* MtrD inner membrane multidrug efflux pump. *PLoS One*, 9, e97903.
- BOSHOFF, H. I., MYERS, T. G., COPP, B. R., MCNEIL, M. R., WILSON, M. A. & BARRY, C. E., 3RD 2004. The transcriptional responses of *Mycobacterium tuberculosis* to inhibitors of metabolism: novel insights into drug mechanisms of action. *J Biol Chem*, 279, 40174-84.

- BOSHOF, H. I., REED, M. B., BARRY, C. E., 3RD & MIZRAHI, V. 2003. DnaE2 polymerase contributes to in vivo survival and the emergence of drug resistance in *Mycobacterium tuberculosis*. *Cell*, 113, 183-93.
- CADE, C. E., DLOUHY, A. C., MEDZIHRADESKY, K. F., SALAS-CASTILLO, S. P. & GHILADI, R. A. 2010. Isoniazid-resistance conferring mutations in *Mycobacterium tuberculosis* KatG: catalase, peroxidase, and INH-NADH adduct formation activities. *Protein Sci*, 19, 458-74.
- CHAMBERS, H. F. 1997. Methicillin resistance in staphylococci: molecular and biochemical basis and clinical implications. *Clin Microbiol Rev*, 10, 781-91.
- CHANDRASEKARA, N. S., BERUBE, B. J., SHETYE, G., CHETTIAR, S., O'MALLEY, T., MANNING, A., FLINT, L., AWASTHI, D., IOERGER, T. R., SACCHETTINI, J. C., MASQUELIN, T., HIPSKIND, P. A., ODINGO, J. & PARISH, T. 2017. Improved phenoxyalkylbenzimidazoles with activity against *Mycobacterium tuberculosis* appear to target QcrB. *ACS Infect Dis*.
- CHENG, X., HOCHLOWSKI, J., TANG, H., HEPP, D., BECKNER, C., KANTOR, S. & SCHMITT, R. 2003. Studies on repository compound stability in DMSO under various conditions. *J Biomol Screen*, 8, 292-304.
- CHIANG, I. H., SUO, J., BAI, K. J., LIN, T. P., LUH, K. T., YU, C. J. & YANG, P. C. 1997. Serodiagnosis of tuberculosis. A study comparing three specific mycobacterial antigens. *Am J Respir Crit Care Med*, 156, 906-11.
- CHOPRA, I., HESSE, L. & O'NEILL, A. J. 2002. Exploiting current understanding of antibiotic action for discovery of new drugs. *J Appl Microbiol*, 92 Suppl, 4s-15s.
- CHRISTOPHE, T., JACKSON, M., JEON, H. K., FENISTEIN, D., CONTRERAS-DOMINGUEZ, M., KIM, J., GENOVESIO, A., CARRALOT, J. P., EWANN, F., KIM, E. H., LEE, S. Y., KANG, S., SEO, M. J., PARK, E. J., SKOVIEROVA, H., PHAM, H., RICCARDI, G., NAM, J. Y., MARSOLLIER, L., KEMPF, M., JOLY-GUILLOU, M. L., OH, T., SHIN, W. K., NO, Z., NEHRBASS, U., BROSCHE, R., COLE, S. T. & BRODIN, P. 2009. High content screening identifies decaprenyl-

phosphoribose 2' epimerase as a target for intracellular antimycobacterial inhibitors.

PLoS Pathog, 5, e1000645.

- COLE, S. T., BROSCHE, R., PARKHILL, J., GARNIER, T., CHURCHER, C., HARRIS, D., GORDON, S. V., EIGLMEIER, K., GAS, S., BARRY, C. E., 3RD, TEKAIA, F., BADCOCK, K., BASHAM, D., BROWN, D., CHILLINGWORTH, T., CONNOR, R., DAVIES, R., DEVLIN, K., FELTWELL, T., GENTLES, S., HAMLIN, N., HOLROYD, S., HORNSBY, T., JAGELS, K., KROGH, A., MCLEAN, J., MOULE, S., MURPHY, L., OLIVER, K., OSBORNE, J., QUAIL, M. A., RAJANDREAM, M. A., ROGERS, J., RUTTER, S., SEEGER, K., SKELTON, J., SQUARES, R., SQUARES, S., SULSTON, J. E., TAYLOR, K., WHITEHEAD, S. & BARRELL, B. G. 1998. Deciphering the biology of *Mycobacterium tuberculosis* from the complete genome sequence. *Nature*, 393, 537-44.
- CORBETT, E. L., WATT, C. J., WALKER, N., MAHER, D., WILLIAMS, B. G., RAVIGLIONE, M. C. & DYE, C. 2003. The growing burden of tuberculosis: global trends and interactions with the HIV epidemic. *Arch Intern Med*, 163, 1009-21.
- CREEK, D. J. & BARRETT, M. P. 2014. Determination of antiprotozoal drug mechanisms by metabolomics approaches. *Parasitology*, 141, 83-92.
- DAHLIN, J. L., NISSINK, J. W., STRASSER, J. M., FRANCIS, S., HIGGINS, L., ZHOU, H., ZHANG, Z. & WALTERS, M. A. 2015. PAINS in the assay: chemical mechanisms of assay interference and promiscuous enzymatic inhibition observed during a sulfhydryl-scavenging HTS. *J Med Chem*, 58, 2091-113.
- DANIEL, T. M., DE MURILLO, G. L., SAWYER, J. A., GRIFFIN, A. M., PINTO, E., DEBANNE, S. M., ESPINOSA, P. & CESPEDES, E. 1986. Field evaluation of enzyme-linked immunosorbent assay for the serodiagnosis of tuberculosis. *Am Rev Respir Dis*, 134, 662-5.
- DAVIES, J. & DAVIES, D. 2010. Origins and evolution of antibiotic resistance. *Microbiol Mol Biol Rev*, 74, 417-33.

- DAVIS, M. I., HUNT, J. P., HERRGARD, S., CICERI, P., WODICKA, L. M., PALLARES, G., HOCKER, M., TREIBER, D. K. & ZARRINKAR, P. P. 2011. Comprehensive analysis of kinase inhibitor selectivity. *Nat Biotechnol*, 29, 1046-51.
- DEBARBER, A. E., MDLULI, K., BOSMAN, M., BEKKER, L. G. & BARRY, C. E., 3RD 2000. Ethionamide activation and sensitivity in multidrug-resistant *Mycobacterium tuberculosis*. *Proc Natl Acad Sci U S A*, 97, 9677-82.
- DEMAIN, A. L. & ELANDER, R. P. 1999. The beta-lactam antibiotics: past, present, and future. *Antonie Van Leeuwenhoek*, 75, 5-19.
- DERETIC, V., SINGH, S., MASTER, S., HARRIS, J., ROBERTS, E., KYEI, G., DAVIS, A., DE HARO, S., NAYLOR, J., LEE, H. H. & VERGNE, I. 2006. *Mycobacterium tuberculosis* inhibition of phagolysosome biogenesis and autophagy as a host defence mechanism. *Cell Microbiol*, 8, 719-27.
- DINCER, I., ERGIN, A. & KOCAGOZ, T. 2004. The vitro efficacy of beta-lactam and beta-lactamase inhibitors against multidrug resistant clinical strains of *Mycobacterium tuberculosis*. *Int J Antimicrob Agents*, 23, 408-11.
- DORMAN, S. E. 2010. New diagnostic tests for tuberculosis: bench, bedside, and beyond. *Clin Infect Dis*, 50 Suppl 3, S173-7.
- DYE, C., SCHEELE, S., DOLIN, P., PATHANIA, V. & RAVIGLIONE, M. C. 1999. Consensus statement. Global burden of tuberculosis: estimated incidence, prevalence, and mortality by country. WHO Global Surveillance and Monitoring Project. *JAMA*, 282, 677-86.
- ERLANSON, D. A. 2015. Learning from PAINful lessons. *J Med Chem*, 58, 2088-90.
- FALAGAS, M. E. & KARAGEORGOPOULOS, D. E. 2009. Extended-spectrum beta-lactamase-producing organisms. *J Hosp Infect*, 73, 345-54.
- FANG, P., HAN, H., WANG, J., CHEN, K., CHEN, X. & GUO, M. 2015. Structural Basis for Specific Inhibition of tRNA Synthetase by an ATP Competitive Inhibitor. *Chem Biol*, 22, 734-44.

- FONTANA, A., DE LAURETO, P. P., SPOLAORE, B., FRARE, E., PICOTTI, P. & ZAMBONIN, M. 2004. Probing protein structure by limited proteolysis. *Acta Biochim Pol*, 51, 299-321.
- FRANCKLYN, C. S., FIRST, E. A., PERONA, J. J. & HOU, Y. M. 2008. Methods for kinetic and thermodynamic analysis of aminoacyl-tRNA synthetases. *Methods*, 44, 100-18.
- GALHARDO, R. S., HASTINGS, P. J. & ROSENBERG, S. M. 2007. Mutation as a stress response and the regulation of evolvability. *Crit Rev Biochem Mol Biol*, 42, 399-435.
- GOLDMAN, R. C. 2013. Why are membrane targets discovered by phenotypic screens and genome sequencing in *Mycobacterium tuberculosis*? *Tuberculosis (Edinb)*, 93, 569-88.
- GOLDSTONE, D., BAKER, E. N. & METCALF, P. 2005. Crystallization and preliminary diffraction studies of the C-terminal domain of the DipZ homologue from *Mycobacterium tuberculosis*. *Acta Crystallogr Sect F Struct Biol Cryst Commun*, 61, 243-5.
- GROSSMAN, T. H., SHOEN, C. M., JONES, S. M., JONES, P. L., CYNAMON, M. H. & LOCHER, C. P. 2015. The efflux pump inhibitor timcodar improves the potency of antimycobacterial agents. *Antimicrob Agents Chemother*, 59, 1534-41.
- GRZEGORZEWICZ, A. E., PHAM, H., GUNDI, V. A., SCHERMAN, M. S., NORTH, E. J., HESS, T., JONES, V., GRUPPO, V., BORN, S. E., KORDULAKOVA, J., CHAVADI, S. S., MORISSEAU, C., LENAERTS, A. J., LEE, R. E., MCNEIL, M. R. & JACKSON, M. 2012. Inhibition of mycolic acid transport across the *Mycobacterium tuberculosis* plasma membrane. *Nat Chem Biol*, 8, 334-41.
- GUENGERICH, F. P. 2006. Cytochrome P450s and other enzymes in drug metabolism and toxicity. *AAPS J*, 8, E101-11.
- GURCHA, S. S., USHA, V., COX, J. A., FUTTERER, K., ABRAHAMS, K. A., BHATT, A., ALDERWICK, L. J., REYNOLDS, R. C., LOMAN, N. J., NATARAJ, V., ALEMPARTE, C., BARROS, D., LLOYD, A. J., BALLELL, L., HOBRATH, J. V. & BESRA, G. S. 2014. Biochemical and

- structural characterization of mycobacterial aspartyl-tRNA synthetase AspS, a promising TB drug target. *PLoS One*, 9, e113568.
- HARDING, C. V. & BOOM, W. H. 2010. Regulation of antigen presentation by *Mycobacterium tuberculosis*: a role for Toll-like receptors. *Nat Rev Microbiol*, 8, 296-307.
- HARRIS, P. N., TAMBYAH, P. A. & PATERSON, D. L. 2015. beta-lactam and beta-lactamase inhibitor combinations in the treatment of extended-spectrum beta-lactamase producing Enterobacteriaceae: time for a reappraisal in the era of few antibiotic options? *Lancet Infect Dis*, 15, 475-85.
- HE, G., LUO, W., LI, P., REMMERS, C., NETZER, W. J., HENDRICK, J., BETTAYEB, K., FLAJOLET, M., GORELICK, F., WENNOGLE, L. P. & GREENGARD, P. 2010. Gamma-secretase activating protein is a therapeutic target for Alzheimer's disease. *Nature*, 467, 95-8.
- HU, Q. H., HUANG, Q. & WANG, E. D. 2013. Crucial role of the C-terminal domain of *Mycobacterium tuberculosis* leucyl-tRNA synthetase in aminoacylation and editing. *Nucleic Acids Res*, 41, 1859-72.
- HUEBNER, R. E., SCHEIN, M. F. & BASS, J. B., JR. 1993. The tuberculin skin test. *Clin Infect Dis*, 17, 968-75.
- HUGONNET, J. E. & BLANCHARD, J. S. 2007. Irreversible inhibition of the *Mycobacterium tuberculosis* beta-lactamase by clavulanate. *Biochemistry*, 46, 11998-2004.
- HUGONNET, J. E., TREMBLAY, L. W., BOSHOFF, H. I., BARRY, C. E., 3RD & BLANCHARD, J. S. 2009. Meropenem-clavulanate is effective against extensively drug-resistant *Mycobacterium tuberculosis*. *Science*, 323, 1215-8.
- HURDLE, J. G., O'NEILL, A. J. & CHOPRA, I. 2005. Prospects for aminoacyl-tRNA synthetase inhibitors as new antimicrobial agents. *Antimicrob Agents Chemother*, 49, 4821-33.
- I.HALL, C. 2011. Chemical genetic screen identifies *Toxoplasma* DJ-1 as a regulator of parasite secretion, attachment and invasion. *PNAS*.

- IBBA, M. & SOLL, D. 2000. Aminoacyl-tRNA synthesis. *Annu Rev Biochem*, 69, 617-50.
- IOERGER, T. R., O'MALLEY, T., LIAO, R., GUINN, K. M., HICKEY, M. J., MOHAIDEEN, N., MURPHY, K. C., BOSHOFF, H. I., MIZRAHI, V., RUBIN, E. J., SASSETTI, C. M., BARRY, C. E., 3RD, SHERMAN, D. R., PARISH, T. & SACCHETTINI, J. C. 2013. Identification of new drug targets and resistance mechanisms in *Mycobacterium tuberculosis*. *PLoS One*, 8, e75245.
- JAGIELSKI, T., BAKULA, Z., ROESKE, K., KAMINSKI, M., NAPIORKOWSKA, A., AUGUSTYNOWICZ-KOPEC, E., ZWOLSKA, Z. & BIELECKI, J. 2015. Mutation profiling for detection of isoniazid resistance in *Mycobacterium tuberculosis* clinical isolates. *J Antimicrob Chemother*, 70, 3214-21.
- JAMES, J. N., HASAN, Z. U., IOERGER, T. R., BROWN, A. C., PERSONNE, Y., CARROLL, P., IKEH, M., TILSTON-LUNEL, N. L., PALAVECINO, C., SACCHETTINI, J. C. & PARISH, T. 2012. Deletion of SenX3-RegX3, a key two-component regulatory system of *Mycobacterium smegmatis*, results in growth defects under phosphate-limiting conditions. *Microbiology*, 158, 2724-31.
- KALSCHEUER, R., SYSON, K., VEERARAGHAVAN, U., WEINRICK, B., BIERMANN, K. E., LIU, Z., SACCHETTINI, J. C., BESRA, G., BORNEMANN, S. & JACOBS, W. R., JR. 2010. Self-poisoning of *Mycobacterium tuberculosis* by targeting GlgE in an alpha-glucan pathway. *Nat Chem Biol*, 6, 376-84.
- KARAKOUSIS, P. C., WILLIAMS, E. P. & BISHAI, W. R. 2008. Altered expression of isoniazid-regulated genes in drug-treated dormant *Mycobacterium tuberculosis*. *J Antimicrob Chemother*, 61, 323-31.
- KING, F. J., SELINGER, D. W., MAPA, F. A., JANES, J., WU, H., SMITH, T. R., WANG, Q.-Y., NIYOMRATTANAKITAND, P., SIPES, D. G. & BRINKER, A. 2009. Pathway Reporter Assays Reveal Small Molecule Mechanisms of Action. *Journal of the Association for Laboratory Automation*, 14, 374-382.

- KONG, K. F., SCHNEPER, L. & MATHEE, K. 2010. Beta-lactam antibiotics: from antibiosis to resistance and bacteriology. *Apmis*, 118, 1-36.
- KOUL, A., DENDOUGA, N., VERGAUWEN, K., MOLENBERGHS, B., VRANCKX, L., WILLEBRORDS, R., RISTIC, Z., LILL, H., DORANGE, I., GUILLEMONT, J., BALD, D. & ANDRIES, K. 2007. Diarylquinolines target subunit c of mycobacterial ATP synthase. *Nat Chem Biol*, 3, 323-4.
- KOZIKOWSKI, B. A., BURT, T. M., TIREY, D. A., WILLIAMS, L. E., KUZMAK, B. R., STANTON, D. T., MORAND, K. L. & NELSON, S. L. 2003. The effect of room-temperature storage on the stability of compounds in DMSO. *J Biomol Screen*, 8, 205-9.
- LAURSEN, B. S., SORENSEN, H. P., MORTENSEN, K. K. & SPERLING-PETERSEN, H. U. 2005. Initiation of protein synthesis in bacteria. *Microbiol Mol Biol Rev*, 69, 101-23.
- LECHARTIER, B., RYBNIKER, J., ZUMLA, A. & COLE, S. T. 2014. Tuberculosis drug discovery in the post-post-genomic era. *EMBO Mol Med*, 6, 158-68.
- LEE, J. & BOGYO, M. 2013. Target deconvolution techniques in modern phenotypic profiling. *Curr Opin Chem Biol*, 17, 118-26.
- LEI, B., WEI, C. J. & TU, S. C. 2000. Action mechanism of antitubercular isoniazid. Activation by Mycobacterium tuberculosis KatG, isolation, and characterization of inhA inhibitor. *J Biol Chem*, 275, 2520-6.
- LI, K., SCHURIG-BRICCIO, L. A., FENG, X., UPADHYAY, A., PUJARI, V., LECHARTIER, B., FONTES, F. L., YANG, H., RAO, G., ZHU, W., GULATI, A., NO, J. H., CINTRA, G., BOGUE, S., LIU, Y. L., MOLOHON, K., ORLEAN, P., MITCHELL, D. A., FREITAS-JUNIOR, L., REN, F., SUN, H., JIANG, T., LI, Y., GUO, R. T., COLE, S. T., GENNIS, R. B., CRICK, D. C. & OLDFIELD, E. 2014. Multitarget drug discovery for tuberculosis and other infectious diseases. *J Med Chem*, 57, 3126-39.

- LIU, R., LYU, X., BATT, S. M., HSU, M. H., HARBUT, M. B., VILCHEZE, C., CHENG, B., AJAYI, K., YANG, B., YANG, Y., GUO, H., LIN, C., GAN, F. & WANG, C. 2017. Determinants of the Inhibition of DprE1 and CYP2C9 by Antitubercular Thiophenes. *56*, 13011-13015.
- LLOYD, A. J., POTTER, N. J., FISHWICK, C. W., ROPER, D. I. & DOWSON, C. G. 2013. Adenosine tetraphosphoadenosine drives a continuous ATP-release assay for aminoacyl-tRNA synthetases and other adenylate-forming enzymes. *ACS Chem Biol*, *8*, 2157-63.
- LOMENICK, B., OLSEN, R. W. & HUANG, J. 2011. Identification of direct protein targets of small molecules. *ACS Chem Biol*, *6*, 34-46.
- LOO, J. A., DEJOHN, D. E., DU, P., STEVENSON, T. I. & OGORZALEK LOO, R. R. 1999. Application of mass spectrometry for target identification and characterization. *Med Res Rev*, *19*, 307-19.
- LOUW, G. E., WARREN, R. M., GEY VAN PITTIUS, N. C., LEON, R., JIMENEZ, A., HERNANDEZ-PANDO, R., MCEVOY, C. R., GROBBELAAR, M., MURRAY, M., VAN HELDEN, P. D. & VICTOR, T. C. 2011. Rifampicin reduces susceptibility to ofloxacin in rifampicin-resistant *Mycobacterium tuberculosis* through efflux. *Am J Respir Crit Care Med*, *184*, 269-76.
- MACALLAN, D. C. 1999. Malnutrition in tuberculosis. *Diagn Microbiol Infect Dis*, *34*, 153-7.
- MAKAROV, V., MANINA, G., MIKUSOVA, K., MOLLMANN, U., RYABOVA, O., SAINT-JOANIS, B., DHAR, N., PASCA, M. R., BURONI, S., LUCARELLI, A. P., MILANO, A., DE ROSSI, E., BELANOVA, M., BOBOVSKA, A., DIANISKOVA, P., KORDULAKOVA, J., SALA, C., FULLAM, E., SCHNEIDER, P., MCKINNEY, J. D., BRODIN, P., CHRISTOPHE, T., WADDELL, S., BUTCHER, P., ALBRETHSEN, J., ROSENKRANDS, I., BROSCHE, R., NANDI, V., BHARATH, S., GAONKAR, S., SHANDIL, R. K., BALASUBRAMANIAN, V., BALGANESH, T., TYAGI, S., GROSSET, J., RICCARDI, G. & COLE, S. T. 2009. Benzothiazinones kill *Mycobacterium tuberculosis* by blocking arabinan synthesis. *Science*, *324*, 801-4.

- MAKOBONGO, M. O., EINCK, L., PEEK, R. M., JR. & MERRELL, D. S. 2013. In vitro characterization of the anti-bacterial activity of SQ109 against *Helicobacter pylori*. *PLoS One*, 8, e68917.
- MALLOY, A. M. & CAMPOS, J. M. 2011. Extended-spectrum beta-lactamases: a brief clinical update. *Pediatr Infect Dis J*, 30, 1092-3.
- MANCA, C., PAUL, S., BARRY, C. E., 3RD, FREEDMAN, V. H. & KAPLAN, G. 1999. Mycobacterium tuberculosis catalase and peroxidase activities and resistance to oxidative killing in human monocytes in vitro. *Infect Immun*, 67, 74-9.
- MANINA, G., DHAR, N. & MCKINNEY, J. D. 2015. Stress and host immunity amplify Mycobacterium tuberculosis phenotypic heterogeneity and induce nongrowing metabolically active forms. *Cell Host Microbe*, 17, 32-46.
- MANINA, G., PASCA, M. R., BURONI, S., DE ROSSI, E. & RICCARDI, G. 2010. Decaprenylphosphoryl-beta-D-ribose 2'-epimerase from Mycobacterium tuberculosis is a magic drug target. *Curr Med Chem*, 17, 3099-108.
- MEDEIROS, A. A. 1997. Evolution and dissemination of beta-lactamases accelerated by generations of beta-lactam antibiotics. *Clin Infect Dis*, 24 Suppl 1, S19-45.
- MIGLIORI, G. B., LODDENKEMPER, R., BLASI, F. & RAVIGLIONE, M. C. 2007. 125 years after Robert Koch's discovery of the tubercle bacillus: the new XDR-TB threat. Is "science" enough to tackle the epidemic? *Eur Respir J*, 29, 423-7.
- MIKUSOVA, K., HUANG, H., YAGI, T., HOLSTERS, M., VEREECKE, D., D'HAENZE, W., SCHERMAN, M. S., BRENNAN, P. J., MCNEIL, M. R. & CRICK, D. C. 2005. Decaprenylphosphoryl arabinofuranose, the donor of the D-arabinofuranosyl residues of mycobacterial arabinan, is formed via a two-step epimerization of decaprenylphosphoryl ribose. *J Bacteriol*, 187, 8020-5.

- MYKULIAK, V. V., DRAGAN, A. I. & KORNELIYUK, A. I. 2014. Structural states of the flexible catalytic loop of *M. tuberculosis* tyrosyl-tRNA synthetase in different enzyme-substrate complexes. *Eur Biophys J*, 43, 613-22.
- NAKAMA, T., NUREKI, O. & YOKOYAMA, S. 2001. Structural basis for the recognition of isoleucyl-adenylate and an antibiotic, mupirocin, by isoleucyl-tRNA synthetase. *J Biol Chem*, 276, 47387-93.
- NG, V. H., COX, J. S., SOUSA, A. O., MACMICKING, J. D. & MCKINNEY, J. D. 2004. Role of KatG catalase-peroxidase in mycobacterial pathogenesis: countering the phagocyte oxidative burst. *Mol Microbiol*, 52, 1291-302.
- NIEHAUS, A. J., MLISANA, K., GANDHI, N. R., MATHEMA, B. & BRUST, J. C. 2015. High Prevalence of inhA Promoter Mutations among Patients with Drug-Resistant Tuberculosis in KwaZulu-Natal, South Africa. *PLoS One*, 10, e0135003.
- NIKIFOROV, P. O., BLASZCZYK, M., SURADE, S., BOSHOF, H. I., SAJID, A., DELORME, V., DEBOOSERE, N., BRODIN, P., BAULARD, A. R., BARRY, C. E., 3RD, BLUNDELL, T. L. & ABELL, C. 2017. Fragment-Sized EthR Inhibitors Exhibit Exceptionally Strong Ethionamide Boosting Effect in Whole-Cell Mycobacterium tuberculosis Assays. 12, 1390-1396.
- NOORDHOEK, G. T., KAAAN, J. A., MULDER, S., WILKE, H. & KOLK, A. H. 1995. Routine application of the polymerase chain reaction for detection of Mycobacterium tuberculosis in clinical samples. *J Clin Pathol*, 48, 810-4.
- O'GARRA, A., REDFORD, P. S., MCNAB, F. W., BLOOM, C. I., WILKINSON, R. J. & BERRY, M. P. 2013. The immune response in tuberculosis. *Annu Rev Immunol*, 31, 475-527.
- PAI, M., RILEY, L. W. & COLFORD, J. M., JR. 2004. Interferon-gamma assays in the immunodiagnosis of tuberculosis: a systematic review. *Lancet Infect Dis*, 4, 761-76.

- PAI, M. Y., LOMENICK, B., HWANG, H., SCHIESTL, R., MCBRIDE, W., LOO, J. A. & HUANG, J. 2015. Drug affinity responsive target stability (DARTS) for small-molecule target identification. *Methods Mol Biol*, 1263, 287-98.
- PALENCIA, A., LI, X., BU, W., CHOI, W., DING, C. Z., EASOM, E. E., FENG, L., HERNANDEZ, V., HOUSTON, P., LIU, L., MEEWAN, M., MOHAN, M., ROCK, F. L., SEXTON, H., ZHANG, S., ZHOU, Y., WAN, B., WANG, Y., FRANZBLAU, S. G., WOOLHISER, L., GRUPPO, V., LENAERTS, A. J., O'MALLEY, T., PARISH, T., COOPER, C. B., WATERS, M. G., MA, Z., IOERGER, T. R., SACCHETTINI, J. C., RULLAS, J., ANGULO-BARTUREN, I., PEREZ-HERRAN, E., MENDOZA, A., BARROS, D., CUSACK, S., PLATTNER, J. J. & ALLEY, M. R. 2016. Discovery of Novel Oral Protein Synthesis Inhibitors of Mycobacterium tuberculosis That Target Leucyl-tRNA Synthetase. *Antimicrob Agents Chemother*, 60, 6271-80.
- PAWLOWSKI, A., JANSSON, M., SKOLD, M., ROTTENBERG, M. E. & KALLENIOUS, G. 2012. Tuberculosis and HIV co-infection. *PLoS Pathog*, 8, e1002464.
- PETHE, K., BIFANI, P., JANG, J., KANG, S., PARK, S., AHN, S., JIRICEK, J., JUNG, J., JEON, H. K., CECHETTO, J., CHRISTOPHE, T., LEE, H., KEMPF, M., JACKSON, M., LENAERTS, A. J., PHAM, H., JONES, V., SEO, M. J., KIM, Y. M., SEO, M., SEO, J. J., PARK, D., KO, Y., CHOI, I., KIM, R., KIM, S. Y., LIM, S., YIM, S. A., NAM, J., KANG, H., KWON, H., OH, C. T., CHO, Y., JANG, Y., KIM, J., CHUA, A., TAN, B. H., NANJUNDAPPA, M. B., RAO, S. P., BARNES, W. S., WINTJENS, R., WALKER, J. R., ALONSO, S., LEE, S., KIM, J., OH, S., OH, T., NEHRBASS, U., HAN, S. J., NO, Z., LEE, J., BRODIN, P., CHO, S. N., NAM, K. & KIM, J. 2013. Discovery of Q203, a potent clinical candidate for the treatment of tuberculosis. *Nat Med*, 19, 1157-60.
- PETHE, K., SEQUEIRA, P. C., AGARWALLA, S., RHEE, K., KUHEN, K., PHONG, W. Y., PATEL, V., BEER, D., WALKER, J. R., DURAISWAMY, J., JIRICEK, J., KELLER, T. H., CHATTERJEE, A., TAN, M. P., UJJINI, M., RAO, S. P., CAMACHO, L., BIFANI, P., MAK, P. A., MA, I., BARNES, S.

- W., CHEN, Z., PLOUFFE, D., THAYALAN, P., NG, S. H., AU, M., LEE, B. H., TAN, B. H., RAVINDRAN, S., NANJUNDAPPA, M., LIN, X., GOH, A., LAKSHMINARAYANA, S. B., SHOEN, C., CYNAMON, M., KREISWIRTH, B., DARTOIS, V., PETERS, E. C., GLYNNE, R., BRENNER, S. & DICK, T. 2010. A chemical genetic screen in *Mycobacterium tuberculosis* identifies carbon-source-dependent growth inhibitors devoid of in vivo efficacy. *Nat Commun*, 1, 57.
- PIETERS, J. 2008. *Mycobacterium tuberculosis* and the macrophage: maintaining a balance. *Cell Host Microbe*, 3, 399-407.
- PIETERSEN, E., IGNATIUS, E., STREICHER, E. M., MASTRAPA, B., PADANILAM, X., POORAN, A., BADRI, M., LESOSKY, M., VAN HELDEN, P., SIRGEL, F. A., WARREN, R. & DHEDA, K. 2014. Long-term outcomes of patients with extensively drug-resistant tuberculosis in South Africa: a cohort study. *Lancet*, 383, 1230-9.
- POPE, A. J., LAPOINTE, J., MENSAH, L., BENSON, N., BROWN, M. J. & MOORE, K. J. 1998a. Characterization of isoleucyl-tRNA synthetase from *Staphylococcus aureus*. I: Kinetic mechanism of the substrate activation reaction studied by transient and steady-state techniques. *J Biol Chem*, 273, 31680-90.
- POPE, A. J., MOORE, K. J., MCVEY, M., MENSAH, L., BENSON, N., OSBOURNE, N., BROOM, N., BROWN, M. J. & O'HANLON, P. 1998b. Characterization of isoleucyl-tRNA synthetase from *Staphylococcus aureus*. II. Mechanism of inhibition by reaction intermediate and pseudomonic acid analogues studied using transient and steady-state kinetics. *J Biol Chem*, 273, 31691-701.
- PULE, C. M., SAMPSON, S. L., WARREN, R. M., BLACK, P. A., VAN HELDEN, P. D., VICTOR, T. C. & LOUW, G. E. 2016. Efflux pump inhibitors: targeting mycobacterial efflux systems to enhance TB therapy. *J Antimicrob Chemother*, 71, 17-26.

- PYM, A. S., SAINT-JOANIS, B. & COLE, S. T. 2002. Effect of katG mutations on the virulence of *Mycobacterium tuberculosis* and the implication for transmission in humans. *Infect Immun*, 70, 4955-60.
- RAWAT, R., WHITTY, A. & TONGE, P. J. 2003. The isoniazid-NAD adduct is a slow, tight-binding inhibitor of InhA, the *Mycobacterium tuberculosis* enoyl reductase: adduct affinity and drug resistance. *Proc Natl Acad Sci U S A*, 100, 13881-6.
- REMUINAN, M. J., PEREZ-HERRAN, E., RULLAS, J., ALEMPARTE, C., MARTINEZ-HOYOS, M., DOW, D. J., AFARI, J., MEHTA, N., ESQUIVIAS, J., JIMENEZ, E., ORTEGA-MURO, F., FRAILE-GABALDON, M. T., SPIVEY, V. L., LOMAN, N. J., PALLAN, M. J., CONSTANTINIDOU, C., MINICK, D. J., CACHO, M., REBOLLO-LOPEZ, M. J., GONZALEZ, C., SOUSA, V., ANGULO-BARTUREN, I., MENDOZA-LOSANA, A., BARROS, D., BESRA, G. S., BALLELL, L. & CAMMACK, N. 2013. Tetrahydropyrazolo[1,5-a]pyrimidine-3-carboxamide and N-benzyl-6',7'-dihydrospiro[piperidine-4,4'-thieno[3,2-c]pyran] analogues with bactericidal efficacy against *Mycobacterium tuberculosis* targeting MmpL3. *PLoS One*, 8, e60933.
- RUDDY, M., MCHUGH, T. D., DALE, J. W., BANERJEE, D., MAGUIRE, H., WILSON, P., DROBNIIEWSKI, F., BUTCHER, P. & GILLESPIE, S. H. 2002. Estimation of the rate of unrecognized cross-contamination with *mycobacterium tuberculosis* in London microbiology laboratories. *J Clin Microbiol*, 40, 4100-4.
- SASINDRAN, S. J. & TORRELLES, J. B. 2011. *Mycobacterium Tuberculosis* Infection and Inflammation: what is Beneficial for the Host and for the Bacterium? *Front Microbiol*, 2, 2.
- SCORPIO, A. & ZHANG, Y. 1996. Mutations in pncA, a gene encoding pyrazinamidase/nicotinamidase, cause resistance to the antituberculous drug pyrazinamide in tubercle bacillus. *Nat Med*, 2, 662-7.

- SEEMANN, T. 2014. Prokka: rapid prokaryotic genome annotation. *Bioinformatics*, 30, 2068-9.
- SHI, H., CHENG, X., SZE, S. K. & YAO, S. Q. 2011. Proteome profiling reveals potential cellular targets of staurosporine using a clickable cell-permeable probe. *Chem Commun (Camb)*, 47, 11306-8.
- SHI, H., ZHANG, C. J., CHEN, G. Y. & YAO, S. Q. 2012. Cell-based proteome profiling of potential dasatinib targets by use of affinity-based probes. *J Am Chem Soc*, 134, 3001-14.
- SILVA MIRANDA, M., BREIMAN, A., ALLAIN, S., DEKNUYDT, F. & ALTARE, F. 2012. The tuberculous granuloma: an unsuccessful host defence mechanism providing a safety shelter for the bacteria? *Clin Dev Immunol*, 2012, 139127.
- SINGH LUBANA, S., ALFISHAWY, M., SINGH, N. & BRENNESESEL, D. J. 2015. First Reported Case of Methicillin-Resistant Staphylococcus aureus Vertebral Osteomyelitis with Multiple Spinal and Paraspinal Abscesses Associated with Acupuncture. *Case Rep Med*, 2015, 524241.
- SITTAMPALAM GS, C. N., BRIMACOMBE K, ET AL. 2004. *Assay guidance manual*, Eli Lilly & Company and the National Center for Advancing Translational Sciences.
- STANLEY, S. A., BARCZAK, A. K., SILVIS, M. R., LUO, S. S., SOGI, K., VOKES, M., BRAY, M. A., CARPENTER, A. E., MOORE, C. B., SIDDIQI, N., RUBIN, E. J. & HUNG, D. T. 2014. Identification of host-targeted small molecules that restrict intracellular Mycobacterium tuberculosis growth. *PLoS Pathog*, 10, e1003946.
- STRELOW, J., DEWE, W., IVERSEN, P. W., BROOKS, H. B., RADDING, J. A., MCGEE, J. & WEIDNER, J. 2004. Mechanism of Action Assays for Enzymes. In: SITTAMPALAM, G. S., COUSSENS, N. P., BRIMACOMBE, K., GROSSMAN, A., ARKIN, M., AULD, D., AUSTIN, C., BAELL, J., BEJCEK, B., CHUNG, T. D. Y., DAHLIN, J. L., DEVANARYAN, V., FOLEY, T. L., GLICKSMAN, M., HALL, M. D., HASS, J. V., INGLESE, J., IVERSEN, P. W., KAHL, S. D., KALES,

- S. C., LAL-NAG, M., LI, Z., MCGEE, J., MCMANUS, O., RISS, T., TRASK, O. J., JR., WEIDNER, J. R., XIA, M. & XU, X. (eds.) *Assay Guidance Manual*. Bethesda (MD).
- SUTHERLAND, R., BOON, R. J., GRIFFIN, K. E., MASTERS, P. J., SLOCOMBE, B. & WHITE, A. R. 1985. Antibacterial activity of mupirocin (pseudomonic acid), a new antibiotic for topical use. *Antimicrob Agents Chemother*, 27, 495-8.
- TAHLAN, K., WILSON, R., KASTRINSKY, D. B., ARORA, K., NAIR, V., FISCHER, E., BARNES, S. W., WALKER, J. R., ALLAND, D., BARRY, C. E., 3RD & BOSHOF, H. I. 2012. SQ109 targets MmpL3, a membrane transporter of trehalose monomycolate involved in mycolic acid donation to the cell wall core of *Mycobacterium tuberculosis*. *Antimicrob Agents Chemother*, 56, 1797-809.
- TERSTAPPEN, G. C., SCHLUPEN, C., RAGGIASCHI, R. & GAVIRAGHI, G. 2007. Target deconvolution strategies in drug discovery. *Nat Rev Drug Discov*, 6, 891-903.
- TIMMINS, G. S. & DERETIC, V. 2006. Mechanisms of action of isoniazid. *Mol Microbiol*, 62, 1220-7.
- TITOV, D. V. & LIU, J. O. 2012. Identification and validation of protein targets of bioactive small molecules. *Bioorg Med Chem*, 20, 1902-9.
- VANNELLI, T. A., DYKMAN, A. & ORTIZ DE MONTELLANO, P. R. 2002. The antituberculosis drug ethionamide is activated by a flavoprotein monooxygenase. *J Biol Chem*, 277, 12824-9.
- VELAYATI, A. A., FARNIA, P. & MASJEDI, M. R. 2013. The totally drug resistant tuberculosis (TDR-TB). *Int J Clin Exp Med*, 6, 307-9.
- VENTOLA, C. L. 2015. The antibiotic resistance crisis: part 1: causes and threats. *P T*, 40, 277-83.

- VILCHEZE, C., HARTMAN, T., WEINRICK, B. & JACOBS, W. R., JR. 2013. Mycobacterium tuberculosis is extraordinarily sensitive to killing by a vitamin C-induced Fenton reaction. *Nat Commun*, 4, 1881.
- WANG, L., TURNER, M. O., ELWOOD, R. K., SCHULZER, M. & FITZGERALD, J. M. 2002. A meta-analysis of the effect of Bacille Calmette Guerin vaccination on tuberculin skin test measurements. *Thorax*, 57, 804-9.
- WARING, M. J. 2010. Lipophilicity in drug discovery. *Expert Opin Drug Discov*, 5, 235-48.
- WARRINGTON, R. 2012. Drug allergy: causes and desensitization. *Hum Vaccin Immunother*, 8, 1513-24.
- WHO 2015. WHO report on tuberculosis
- WOHLKONIG, A., REMAUT, H., MOUNE, M., TANINA, A., MEYER, F., DESROSES, M., STEYAERT, J., WILLAND, N., BAULARD, A. R. & WINTJENS, R. 2017. Structural analysis of the interaction between spiroisoxazoline SMART-420 and the Mycobacterium tuberculosis repressor EthR2. *Biochem Biophys Res Commun*, 487, 403-408.
- YANAGISAWA, T., LEE, J. T., WU, H. C. & KAWAKAMI, M. 1994. Relationship of protein structure of isoleucyl-tRNA synthetase with pseudomonic acid resistance of Escherichia coli. A proposed mode of action of pseudomonic acid as an inhibitor of isoleucyl-tRNA synthetase. *J Biol Chem*, 269, 24304-9.
- ZHANG, J., YANG, P. L. & GRAY, N. S. 2009. Targeting cancer with small molecule kinase inhibitors. *Nat Rev Cancer*, 9, 28-39.
- ZHANG, J. H., CHUNG, T. D. & OLDENBURG, K. R. 1999. A Simple Statistical Parameter for Use in Evaluation and Validation of High Throughput Screening Assays. *J Biomol Screen*, 4, 67-73.
- ZHANG, Y., HEYM, B., ALLEN, B., YOUNG, D. & COLE, S. 1992. The catalase-peroxidase gene and isoniazid resistance of Mycobacterium tuberculosis. *Nature*, 358, 591-3.

- ZHAO, H., PALENCIA, A., SEIRADAKE, E., GHAEMI, Z., CUSACK, S., LUTHEY-SCHULTEN, Z. & MARTINIS, S. 2015. Analysis of the Resistance Mechanism of a Benzoxaborole Inhibitor Reveals Insight into the Leucyl-tRNA Synthetase Editing Mechanism. *ACS Chem Biol*, 10, 2277-85.
- ZHOU, B., HE, Y., ZHANG, X., XU, J., LUO, Y., WANG, Y., FRANZBLAU, S. G., YANG, Z., CHAN, R. J., LIU, Y., ZHENG, J. & ZHANG, Z. Y. 2010. Targeting mycobacterium protein tyrosine phosphatase B for antituberculosis agents. *Proc Natl Acad Sci U S A*, 107, 4573-8.
- ZIMHONY, O., COX, J. S., WELCH, J. T., VILCHEZE, C. & JACOBS, W. R., JR. 2000. Pyrazinamide inhibits the eukaryotic-like fatty acid synthetase I (FASI) of *Mycobacterium tuberculosis*. *Nat Med*, 6, 1043-7.
- ZUMLA, A., MAEURER, M., HOST-DIRECTED THERAPIES, N., CHAKAYA, J., HOELSCHER, M., NTOUMI, F., RUSTOMJEE, R., VILAPLANA, C., YEBOAH-MANU, D., RASOLOF, V., MUNDERI, P., SINGH, N., AKLILLU, E., PADAYATCHI, N., MACETE, E., KAPATA, N., MULENGA, M., KIBIKI, G., MFINANGA, S., NYIRENDA, T., MABOKO, L., GARCIA-BASTEIRO, A., RAKOTOSAMIMANANA, N., BATES, M., MWABA, P., REITHER, K., GAGNEUX, S., EDWARDS, S., MFINANGA, E., ABDULLA, S., CARDONA, P. J., RUSSELL, J. B., GANT, V., NOURSADEGHI, M., ELKINGTON, P., BONNET, M., MENENDEZ, C., DIEYE, T. N., DIARRA, B., MAIGA, A., ASEFFA, A., PARIDA, S., WEJSE, C., PETERSEN, E., KALEEBU, P., OLIVER, M., CRAIG, G., CORRAH, T., TIENTCHEU, L., ANTONIO, M., RAO, M., MCHUGH, T. D., SHEIKH, A., IPPOLITO, G., RAMJEE, G., KAUFMANN, S. H., CHURCHYARD, G., STEYN, A., GROBUSCH, M., SANNE, I., MARTINSON, N., MADANSEIN, R., WILKINSON, R. J., MAYOSI, B., SCHITO, M. & WALLIS, R. S. 2015. Towards host-directed therapies for tuberculosis. *Nat Rev Drug Discov*, 14, 511-2.

SUPPLEMENTARY INFORMATION

(Please see email for instructions)